University of São Paulo
Institute of Astronomy, Geophysics and Atmospheric Science
Department of Geophysics

Julia Carolina Rivadeneyra Vera

Determination of the Fault Plane and Rupture Size of the 2013 Santa Cruz earthquake, Bolivia, 5.2 Mw, by Relative Location of the Aftershocks

(Determinação do Plano de Falha e Tamanho da Ruptura do Sismo de Santa Cruz, Bolívia, 5.2 Mw, mediante Localização Relativa das réplicas)

"Versão corrigida. O original encontra-se disponível na Unidade"

São Paulo

2016

Julia Carolina Rivadeneyra Vera

Determination of the Fault Plane and Rupture Size of the 2013 Santa Cruz earthquake, Bolivia, 5.2 Mw, by Relative Location of the Aftershocks

(Determinação do Plano de Falha e Tamanho da Ruptura do Sismo de Santa Cruz, Bolívia, 5.2 Mw, mediante Localização Relativa das réplicas)

Dissertation presented at the Institute of Astronomy, Geophysics and Atmospheric Sciences at the University of São Paulo as a partial requirement for obtaining the title of Master of Science.

Area of concentration: Geophysics
Advisor: PhD. Marcelo Assumpção

São Paulo

2016

To my mother who is the biggest support in my life

Acknowledgements

I would like to thank my advisor: PhD Marcelo Assumpção, for all the support and patience that I got from him and for teach me all that I know about seismology. Thanks for guide me in the way of the science, and for not giving me the answers to everything, instead to do I find them for myself.

I thank the San Calixto Observatory (OSC), specially to Estela Minaya, Percy Aliaga and Guido Ávila to share the data recorded of the Santa Cruz de la Sierra events.

Thank to the team of the Seismological Center at University of São Paulo, for all the support and recommendations in the develop for this work, for your friendship and for having the patience to teach me Portuguese. I would like to especially thank to Caio Ciardelli for allowing me to use his code to develop this work.

Also I want to thank all the staff of Department of Geophysics for their kindness and help when I needed it. I am thankful to my colleagues for the afternoons coffee and to make more pleasant the days in the institute.

None of this would be possible without the encouragement of my beloved Mom, she taught me that nothing is impossible and with dedication and work the dreams can come true. Despite the distance she always was present, thanks Mom for all your support and love. Thanks all my family to be always aware of me. Special thanks to my cousin Claudia, more than cousin she is like a sister, thanks for be present even though the difference in time.

My life in Brazil would not have been the same without all the friends that I met, and those who already knew from Lima, I want not put names to not forget anyone, all of you are special because make that every moment is better. To my Brazilian friends: thank

for understand my “portuñol”, I want to say that I have learned more Portuguese talking with you than in language classes. Thanks to Peruvian friends who I met in São Paulo, you did a little piece of Peru was in the USP. Thanks friends because of you I was in many countries without leaving Brazil.

I do not wanna stop thanking to my friends from Peru, who were always present despite the distance, and they always have the formula to make me laugh, despite how difficult it could be the day.

I would thank the CAPES scholarship, this work would not have been possible without its help.

"Anyone who has never made a mistake
has never tried anything new"

Albert Einstein (1879-1955)

"Science never solves a problem
without creating ten more"

George Bernard Shaw (1856-1950)

Abstract

The Central Andes of southern Bolivia is a highly seismic region with many active faults, that could generate earthquakes up to 8.9 Mw. In 2013, an earthquake of 5.2 Mw occurred in Santa Cruz de la Sierra, in the sub-Andean belt, close to the Mandeyapecua fault, one of the most important reverse faults in Bolivia. Five larger aftershocks were reported by the International Seismological Centre (ISC) and 33 smaller aftershocks were recorded by the San Calixto Observatory (OSC) in the two months after the mainshock. Distances between epicenters of the aftershocks and the mainshock were up to 36 km, which is larger than expected for an earthquake of this magnitude. Using data from South American regional stations and the relative location technique with Rayleigh waves, the epicenters of the five larger aftershocks of the Santa Cruz series were determined in relation to the mainshock. This method enabled to achieve epicentral locations with uncertainties smaller than one km. Additionally, using data of three Bolivian stations (MOC, SIV and LPAZ) eight smaller aftershocks, recorded by the OSC, were relocated through correlation of P and S waves. The results show a NNW-SSE trend of epicenters and suggest an E dipping plane. The maximum distance between the aftershocks is 14 km, that is not consistent with the expected subsurface rupture length, in accordance with the magnitude of the mainshock. The events are located away from the Mandeyapecua fault and show an opposite dip, demonstrating that these events were generated by another fault in the area, that had not been well studied yet.

Keywords: Relative Locations, Mandeyapecua fault

Resumo

Os Andes Centrais do Sul da Bolívia é uma região altamente sísmica com muitas falhas ativas que poderiam gerar sismos de até 8.9 Mw. Em 2013, um terremoto de magnitude 5.2 Mw ocorreu em Santa Cruz de la Sierra, no cinturão sub Andino, próximo da falha Mandeyapecua, uma das mais importantes falhas inversas da Bolívia. As cinco réplicas maiores foram reportadas pelo ISC (International Seismological Centre) e as 33 réplicas menores foram registradas pelo OSC (Observatorio San Calixto) nos dois meses posteriores ao sismo principal. As distâncias entre os eventos foram de até 36 km, maior que o esperado para um sismo de 5.2 Mw. Usando dados das estações regionais da América do Sul e a técnica da localização relativa com ondas Rayleigh, os epicentros das cinco réplicas maiores dos eventos de Santa Cruz foram determinados em relação ao evento principal. Esse método permite obter localizações epicentrais com incertezas menores do que um km. Adicionalmente, usando os dados de três estações da Bolívia(MOC, SIV e LPAZ), oito réplicas menores registradas pelo OSC, foram relocalizadas através da correlação das ondas P e S. Os resultados mostram uma orientação NNW-SSE dos epicentros e sugerem um plano de mergulho para o leste. A máxima distância entre as réplicas é de 14 km, que 'e maior do que o tamanho de ruptura esperado na subsuperfície, concordo com a magnitude do evento principal. Os eventos estão localizados afastados da falha Mandeyapecua e mostram um mergulho oposto, demostrando que os eventos foram generados por outras falhas presentes na área e que ainda não tem sido bem estudadas.

Palavras chave: Localização relativa, Falha Mandeyapecua

Resumen

Los Andes Centrales del sur de Bolivia es una región altamente sísmica con varias fallas activas que pueden generar sismos de hasta 8.9 Mw. En el año 2012, ocurrió un terremoto de 5.2 Mw en la región de Santa Cruz de la Sierra, en el cinturón sub Andino, en una área próxima de donde se ubica la falla Mandeyapecua, una de las fallas inversas más importantes de Bolivia. El ISC (International Seismological Centre) reportó cinco réplicas, las cuales fueron llamadas de "mayores" en los dos meses posteriores al evento principal, mientras que el OSC (Observatorio San Calixto) registró 33 réplicas menores. La máxima distancia entre los eventos es de 36 km, mayor de lo esperado para un sismo de 5.2 Mw. Usando datos de las estaciones regionales de América del Sur y la técnica de localización relativa con ondas Rayleigh, los epicentros de las cinco réplicas mayores fueron determinados en relación al evento principal. Este método permite obtener localizaciones epicentrales con incertidumbres menores a un km. Adicionalmente, haciendo uso de tres estaciones de Bolivia (MOC, SIV, LPAZ), ocho réplicas menores registradas por el OSC, fueron relocalizadas a través de la correlación de las ondas P y S. Los resultados muestran una orientación NNW-SSE de los epicentros y sugiere un buzamiento para el este. La distancia máxima entre las réplicas es de 14 km, este valor no es consistente con el tamaño de ruptura esperado en la subsuperficie, de acuerdo con la magnitud del evento principal. Los epicentros de los eventos relocalizados se encuentran alejados de la falla Mandeyapecua y muestran un buzamiento opuesto a esta, demostrando que los eventos fueron generados por otras fallas presentes en esta área y que todavía no han sido estudiadas en detalle.

Palabras llave: Localización relativa, Falla Mandeyapecua

List of Figures

List of Tables

Contents

Chapter 1

Introduction

The Central Andes of Bolivia are the widest part of the Andean chain (300-600 km). Significant upper-crustal shortening in this area ended before 10 Ma, extending the active deformation eastwards into the Subandean zone, which is located in the transition from the high elevations of the Central Andean Plateu to the foreland plains through synclinal basins separated by thrust-faulted anticlines (Ward et al., 2013). The eastern area is characterized by soft folds and reverse faults with N-S orientation, one of the most important being the Mandeyapecua fault. It has an extension of 486 km (Lavenu et al., 2000), and is capable of generating an earthquake up to 8.9 Mw (Brooks et al., 2011).

On 2013/10/15, an 5.2 Mw earthquake occurred in the Subandean belt, in the Department of *Santa Cruz de la Sierra*; here, this event will be called Santa Cruz de la Sierra earthquake. The International Seismological Centre (ISC) reported five large aftershocks (3.2 - 5.0 mb), and the San Calixto Observatory (OSC) reported 33 smaller aftershocks (2.0 - 4.5 ML).

The eastern area of the Central Andes of Bolivia is affected with shallow earthquakes ($\leq$ 70 km of depth) greater than 5.0 mb at least once every year (International Seismological Centre, 2013b), and the department of Santa Cruz de la Sierra presents high seismic hazard (Observatorio San Calixto, 2012). Nevertheless there is not enough studies about the geometry of the active faults, in order to get more accurate information of these active faults and for tectonic studies it is necessary to have a high epicentral precision of the events.

In areas with dense seismic networks, epicenters can be accurately located (Cleveland and Ammon, 2013). However, the lack of stations in the Central Andes and the use of

1-D Earth models make it difficult to locate epicenters with small uncertainties. The large uncertainties of regional epicenters prevent the study of fault geometry.

Here we used two techniques of relative location to better estimate rupture size and fault orientation. We used correlated Rayleigh-wave arrival times to relocate the five larger aftershocks with a better accuracy. The advantage of using surface waves is that time shifts can be measured with a precision better than one second, and the low propagation velocities of surface waves provides a substantial sensitivity to location (Cleveland and Ammon, 2013).

We also relocated eight of the 33 smaller aftershocks recorded by the OSC, using P- and S-waves correlated arrivals and Hypocenter software (Lienert, 1994). Even though the uncertainty is greater, we achieved good results to estimate the rupture size and orientation of the fault that generated these events.

1.1 Objective

The objective is to determine the fault plane orientation of the Santa Cruz de la Sierra earthquake of 2013, and to estimate its rupture size.

To achieve this goal, we used two techniques:

- Relative location of the five larger aftershocks reported by the ISC, by Rayleigh waves correlation, using the relative times of the 20 seconds component of the wavetrain.
- Relative location of the eight smaller aftershocks recorded by the OSC using correlation of P- and S-waves arrivals.

Chapter 2

2013 Seismic Sequence

2.1 Mainshock

On 15th October of 2013 a 5.2 Mw earthquake occurred at 20:13:19 UTC (16:13:19 local time) in the Cordillera Province, Department of Santa Cruz de la Sierra, Bolivia. The fault plane solutions are detailed in Table 2.1, and the parameters of the event in Table 2.2. Figure 2.1 shows the location of the epicenter and the crustal seismicity in the Central Andes of Bolivia, with earthquakes greater than 5.0 mb since 1960 until 2015.

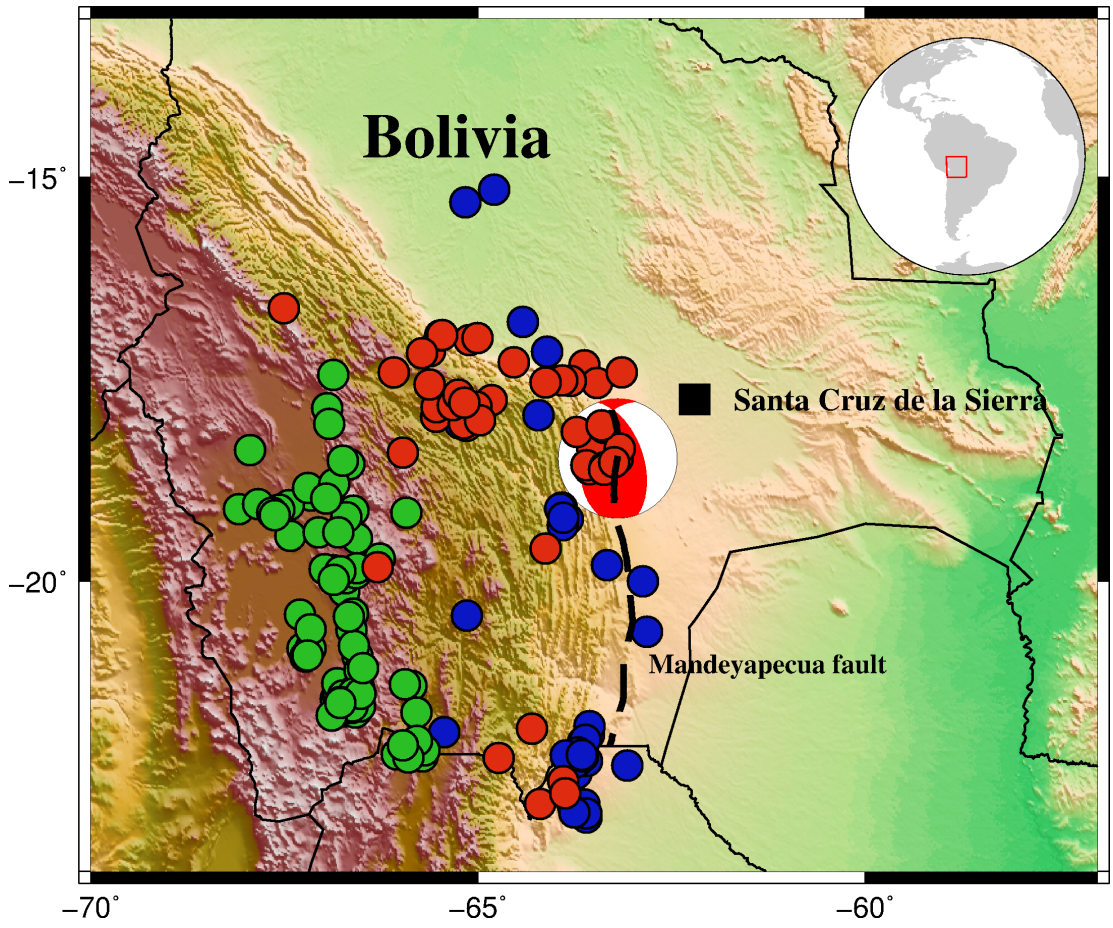

Figure 2.1: Bolivian seismicity from 1960 to 2015 from the ISC catalog (International Seismological Centre, 2013a). Earthquakes with magnitudes greater than 5.0 mb. Earthquakes shallower than 70 km (red circles), between 70 and 300 km (green circles) and deeper than 300 km (blue circles). The beach ball represents the focal mechanism of Santa Cruz de la Sierra earthquake. Black square is Santa Cruz de la Sierra city, and black dashed line is the Mandeyapecua fault (Brooks et al., 2011).

Table 2.1 - Fault plane solution from GCMT

Fault plane solutions	**Strike**	**Dip**	**Rake**
Nodal plane 1	198 °	41 °	120 °
Nodal plane 2	341 °	56 °	67°

The largest intensity was VII in the Modified Mercalli Intensity Scale (MM), in the Indigenous Community of Cotoca. In the area, most houses are built with adobe, because of this several walls and ceilings fell down and cracks were observed; also buildings of good construction, made of bricks and cement, presented damage. The the lowest intensity

was of IV MM, in Montero, where was felt indoors and outdoors, windows and doors were disturbed; and walls made cracking sound. Figure 2.2 shows the isoseismal map (Observatorio San Calixto, 2012).

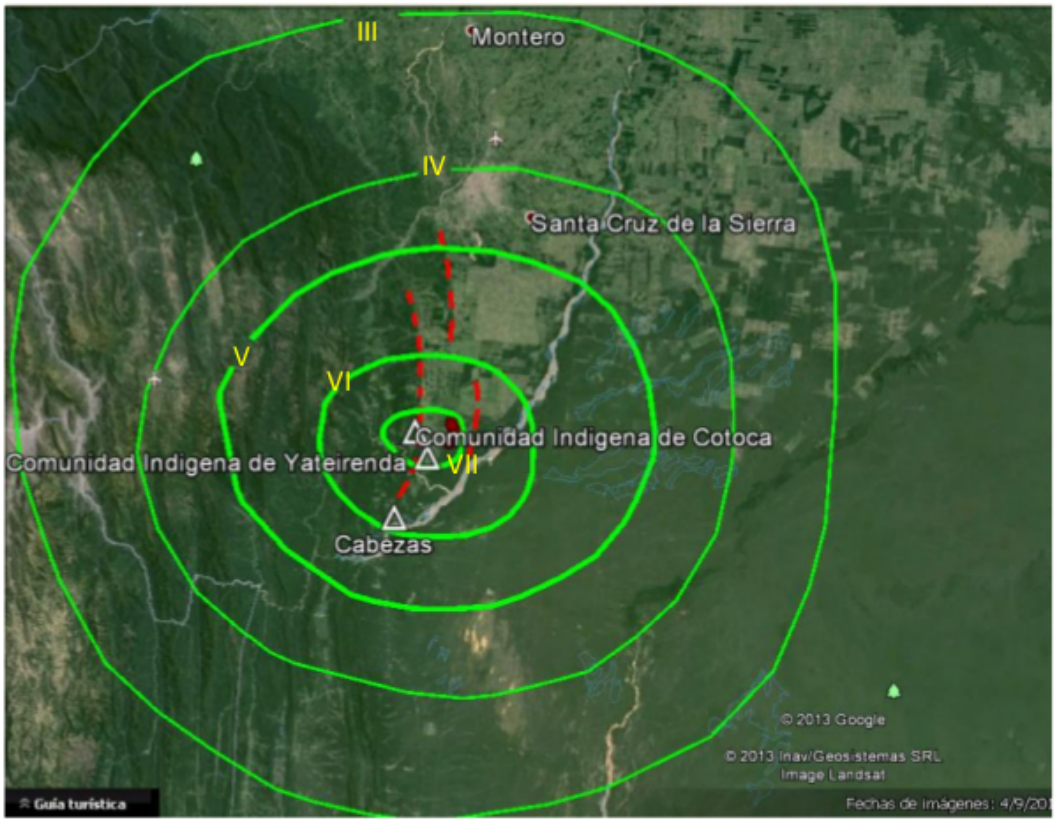

Figure 2.2: Isoseismal map of the Santa Cruz de la Sierra earthquake (green lines). Reverse faults (red dashed lines) (Observatorio San Calixto, 2013).

The International Seismological Centre (2013b) reported epicenters for the mainshock given by different agencies; obtained mainly from traditional linearized inversion methods using 1-D IASPEI or ak135 travel-time tables. However, these algorithms do not consider 3-D Earth velocity variations at local and regional distances, and does not account for the geological complexity of the crust and upper mantle (Bondár and Storchak, 2011). When 1-D models are used with teleseismic phases, errors up to 20 or 30 km are possible (Bondár et al., 2004).

For this reason a regional seismic travel time (RSTT) model was developed by Myers et al. (2010), from a 1-D Earth model, through a tessellation of nodes spacing approximately 1° with a velocity profile at each node. Interpolation of the velocity profiles generates a 3-D crustal model overlies a laterally varying upper mantle, reducing the travel time

prediction error. They developed this 3-D model that consist in an average crustal velocity, mantle velocity at the Moho, and the mantle velocity gradient at each node. First, they refine the model using a tomographic formulation in Eurasia and North Africa and tested with earthquakes which present accurate location with a local networks; each event was located using only Pn arrival times, and event depths were fixed. Epicenter error was improved from 17.3 km with the ak135 model to 9.3 km with the RSST model, and the area of epicenter uncertainty ellipses were reduced in 68%.

To improve the epicenter of the mainshock we used the *iLoc* program developed by Bondár and Storchak (2011), that is an update of the current algorithm used by the ISC. The *iLoc* takes into account for correlated error structure, and uses all IASPEI standard phases with a valid ak135 traveltime prediction to obtain more accurate event locations. This new method works best only with first-arriving phases, because it treats all phases as equal. We performed three tests:

- For stations up to 90°, and using ak135 model;
- For stations up to 90°, corrected with RSTT model up to 15°;
- For stations up to 15°, corrected with RSTT

Figure 2.3 shows the stations up to 15° utilized to do the mainshock relocation. Table 2.2 and Figure 2.4 show the results.

Figure 2.3: Santa Cruz de la Sierra earthquake (red star) and stations (green triangle) up to a distance of 15° utilized to do the relocation with the iLoc program. Arrival times were taken from ISC catalog (International Seismological Centre, 2013b).

Table 2.2 - Epicenters of the mainshock from different agencies, and the relocation with iLoc code

Author	**Time UTC**	**RMS residual** (sec)	**Latitude** (°S)	**Longitude** (°W)	**Error ellipse (km)**		**Azimuth** (°)	**Depth** (km)
					Smaj	**Smin**		
NEIC	20:13:19.00	NA	18.494	63.196	NA	NA	NA	33.0f
IDC	20:13:16.08	1.02	18.490	63.220	13.4	11.6	41	NA
OSC	20:13:24.70	0.90	18.442	63.203	6.2	3.8	0	35.1
iLoc [1]	20:13:19.63	1.57	18.527	63.244	7.4	9.6	49	24.0f
iLoc [2]	20:13:19.53	1.74	18.544	63.315	7.4	9.7	49	24.0f
iLoc [3]	20:13:20.46	1.40	18.555	63.349	11.8	11.0	65	24.0f

[1] iLoc with stations up to 90° and 1-D Earth model.

[2] iLoc with stations up to 90° and stations corrected with a RSTT model up to 15°.

[3] iLoc with stations up to 15° corrected with the RSTT model.

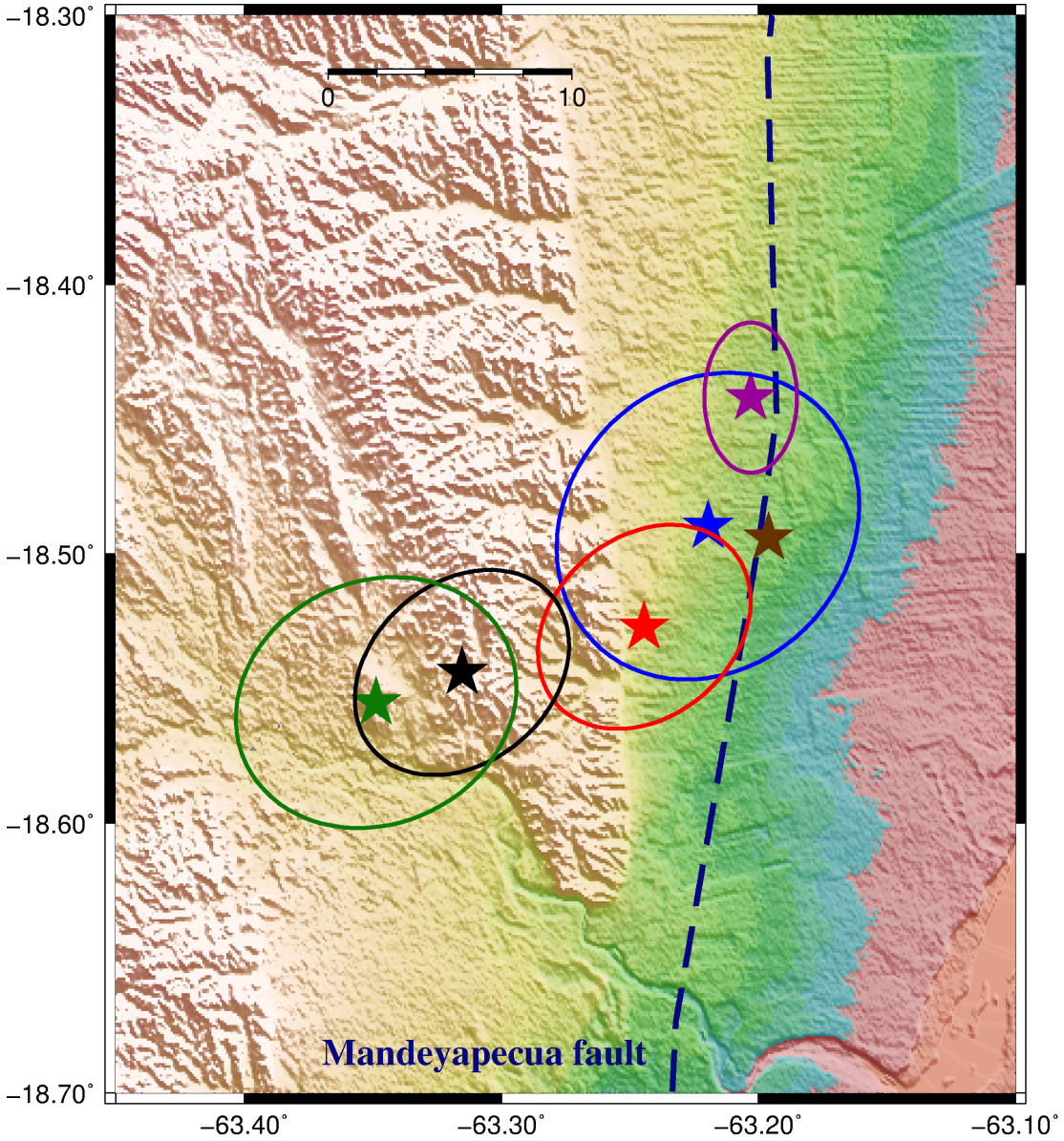

Figure 2.4: Epicenters given by different agencies and their error ellipses: NEIC (brown star) has no error ellipse, IDC (blue star), OSC (purple star). Mainshock relocation: iLoc relocation with stations up to 90° and 1-D Earth model (red star), iLoc relocation with station up to 90°, corrected with RSTT up to 15° (black star), and iLoc relocation only with stations corrected with RSTT up to 15° (green star).

To prove that *iLoc* algorithm and the RSTT model are useful to improve location of earthquakes in the Central Andes area, we relocated an earthquake of 6.3 Mw, occurred on 27th February in the Province of Salta in Argentina, this event has an accuracy location given by INPRES, that is a federal agency of the Argentine government that operates the national network of seismic stations in Argentina (Sanchéz et al., 2013). We performed the same tests that we did in the relocation of Santa Cruz de la Sierra earthquake, obtained good results that are shown in Figure 2.5.

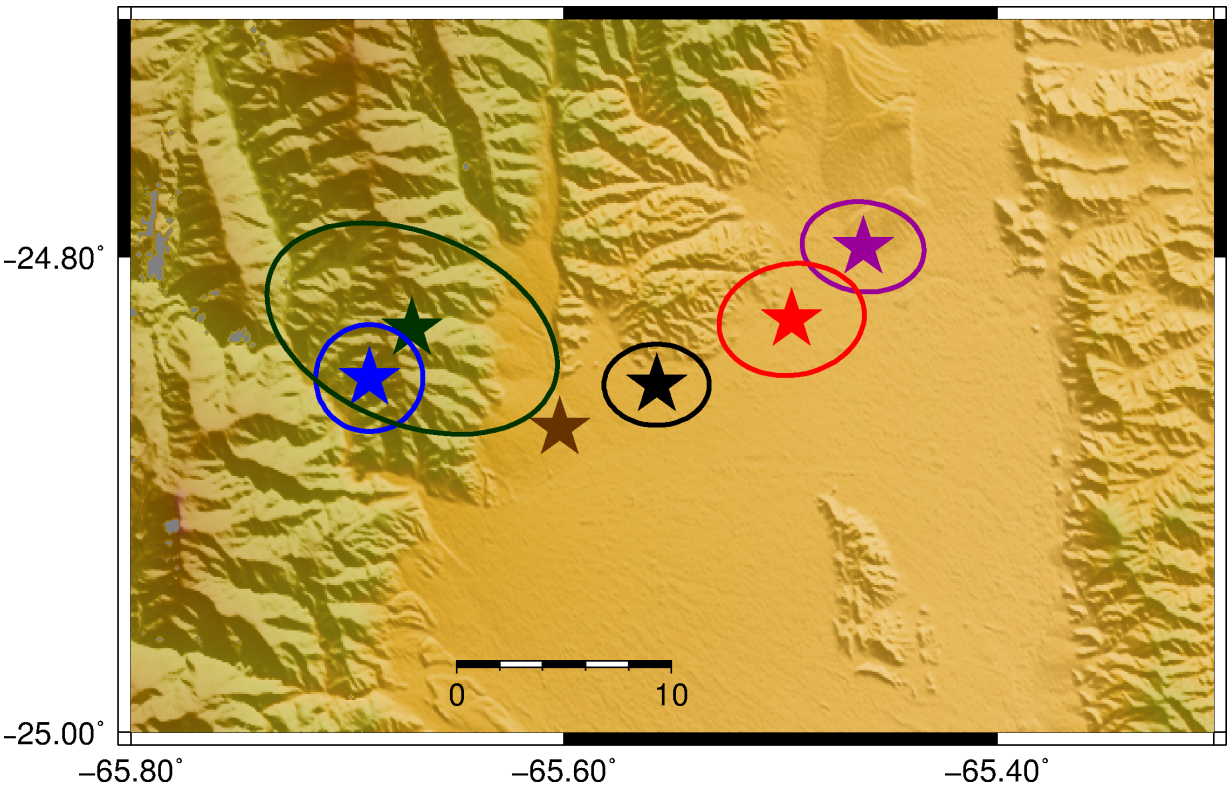

Figure 2.5: Epicenters given by different agencies and their error ellipses: NEIC (brown star) has no error ellipse, INPRES (blue star), ISC (purple star). Mainshock relocation: iLoc relocation with stations up to 90° and 1-D Earth model (red star), iLoc relocation with station up to 90°, corrected with RSTT up to 15° (black star), and iLoc relocation only with stations corrected with RSTT up to 15° (green star).

2.2 Aftershocks

2.2.1 Aftershocks reported by International Seismological Centre (ISC)

We searched events in the two months after the mainshock, within a radius of 50 km around the epicenter, and a depth less than 60 km. Five events were reported by the (International Seismological Centre, 2013b) with magnitudes between 3.2 - 5.0 mb . We call these events as "larger aftershocks" (Table 2.3 and Figure 2.6).

Table 2.3 - Larger aftershocks reported by the ISC

Event	**Date**	**Time UTC**	**Longitude (°W)**	**Latitude (°S)**	**Depth (km)**	**Magnitude (mb)**
A1	2013-10-15	20:15:28	63.174	18.371	21.0	5.0
A2	2013-10-15	22:00:29	62.920	18.420	10.0	4.4
A3	2013-10-16	08:31:31	63.340	18.232	59.0	3.6
A4	2013-10-21	19:54:01	63.270	18.490	36.0	4.7
A5	2013-11-17	06:18:23	63.258	18.398	47.0	3.2

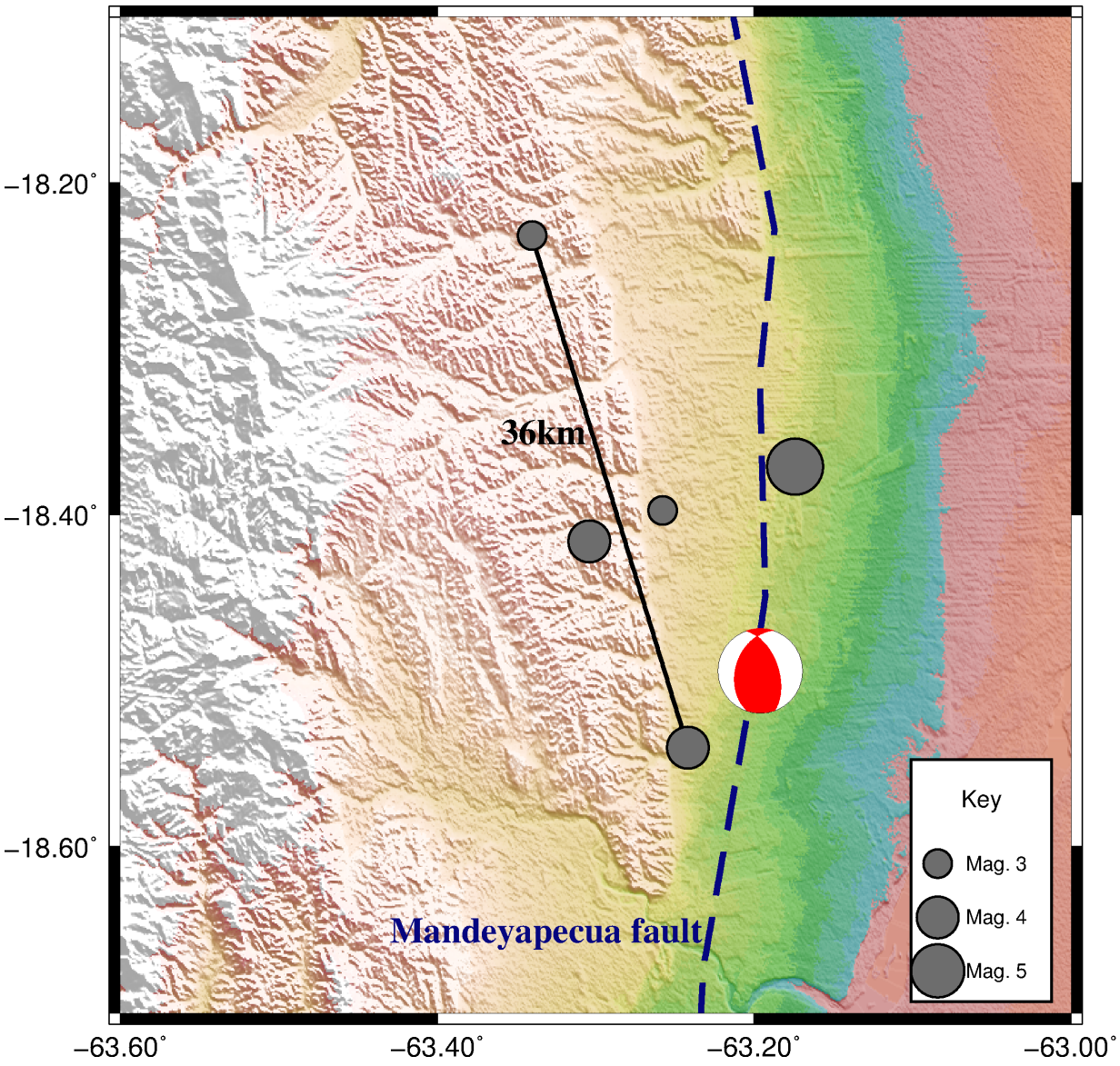

Figure 2.6: Mainshock reported by NEIC (beach ball) and aftershocks reported by the ISC (grey circles). The depth of these events are between 10 and 59 km. Maximum distance between aftershocks are up to 36 km, which is greater than expected for an earthquake of 5.2 Mw.

Wells and Coppersmith (1994) developed empirical relationships among moment magnitude (M), surface rupture length (SRL), subsurface rupture length (RLD), downdip rupture width, rupture area, and maximum and average displacement for worldwide earthquakes. The statistical tests showed a strong correlation between magnitude and various rupture parameters (r=0.89-0.95), with lower standard deviation (σ=0.12-0.28) and high significance level (95%) suggesting that the use of these relationships to estimate magnitudes or rupture parameters is highly reliable.

To estimated subsurface rupture length, they performed regressions between magnitude

and spatial pattern of early aftershocks, that occurred within a few days for more than 150 global earthquakes; also considering all types of tectonic environments. Figure 2.7 shows the regression of subsurface rupture length on magnitude (M).

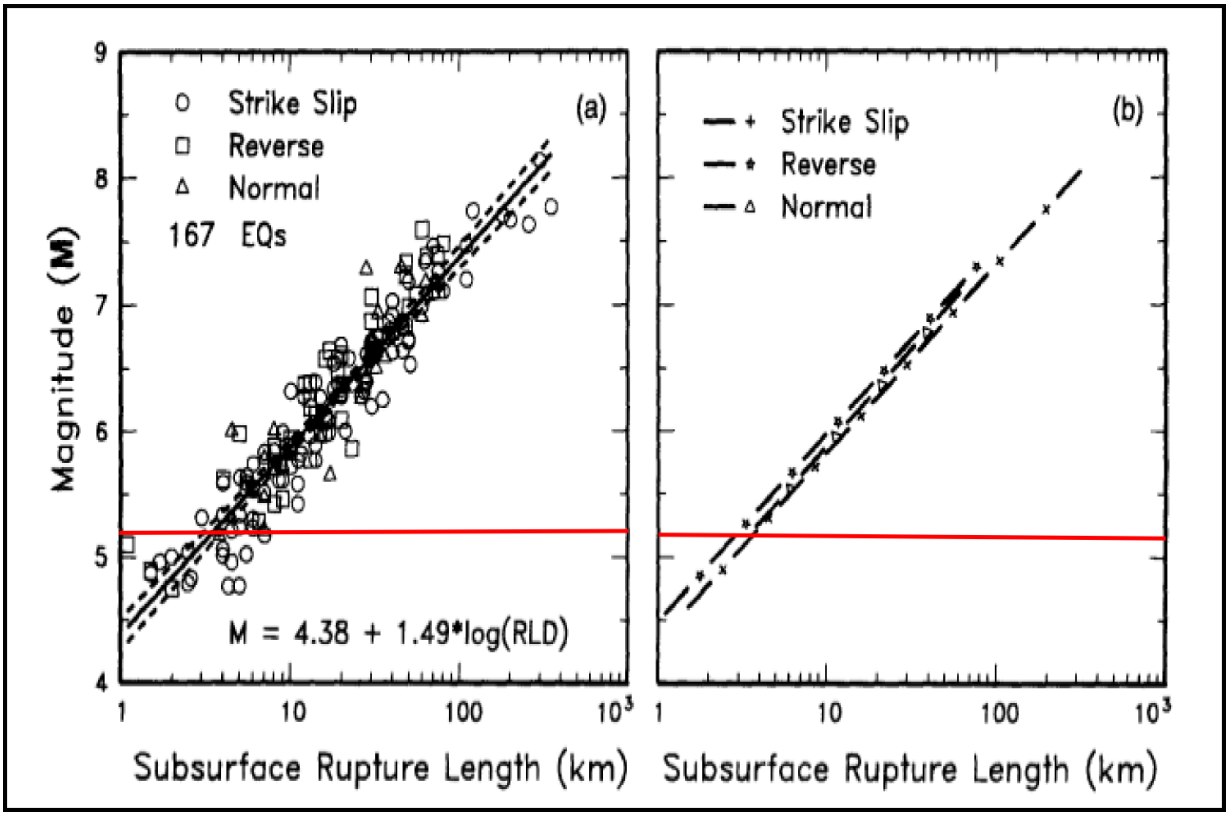

Figure 2.7: Red line indicates Santa Cruz de la Sierra earthquake magnitude. (a) Regression of subsurface rupture length on magnitude (M). Regression line shown for all-slip-type relationship. Dashed line indicates 95% confidence interval. (b) Regressions lines for strike-slip relationships. Length of regression lines shows the range of data for each relationship (Wells and Coppersmith, 1994).

According to the fault plane solution given by GCMT, Santa Cruz de la Sierra earthquake was caused by a reverse fault, then we used the relationship between moment magnitude (M) and subsurface rupture length (RLD) for events caused by reverse faults (equation 2.1) to assess the relationship stated above for the Santa Cruz de la Sierra earthquake and its aftershocks.

Equation 2.1 was developed by regression of 50 global events caused by reverse faults. The correlation coefficient (r) was of 0.93, and the standard deviation (σ) of 0.16. This equation is valid in a magnitude range (M) of 4.8-7.6 (Wells and Coppersmith, 1994).

$$log(RLD) = -2.42(\pm 0.21) + 0.58(\pm 0.03) * M \tag{2.1}$$

Using Equation 2.1, for an event of 5.2 Mw, the length of the subsurface rupture is approximately 4 km, with a minimum and maximum value of between 2 and 10 km respectively; therefore the events should have a maximum distance between them within this range. But, as can be observed in Figure 2.6, the distances were up to 36 km; inconsistent with Equation 2.1; indicating a large error in the epicentral location, or that these events are not aftershocks of the Santa Cruz de la Sierra earthquake.

2.2.2 Aftershocks recorded by San Calixto Observatory (OSC)

The San Calixto Observatory (OSC) from Bolivia, which has as one of its main activities the monitoring and vigilance of the seismic activity, registered 28 shallow foreshocks and 33 aftershocks until the 30th October of 2013. The aftershocks had magnitudes between 2.0 and 4.5 ML and all of them occurred in the crust (23-59 km), and will be called "smaller aftershocks". (Figure 2.8). Distances observed among these aftershocks are close to 14 km, more in agreement with the expected value for an earthquake of 5.2 Mw. However, we cannot observe a clear trend in the location or in the epicentral migracion respect the time.

Table 2.4 - Aftershocks registered by San Calixto Observatory

Event	**Date**	**Time UTC**	**Longitude (°W)**	**Latitude (°S)**	**Depth (km)**	**Magnitude (ML)**
1	2013-10-15	20:38:51	63.1540	18.5120	44.0	2.90
2	2013-10-15	20:42:43	62.1660	18.5160	46.0	2.95
3	2013-10-15	21:26:07	63.1940	18.4570	45.0	2.76
4	2013-10-15	21:41:12	63.1630	18.4730	23.0	2.78
5	2013-10-15	21:59:31	63.1910	18.4730	55.0	4.00
6	2013-10-15	22:26:43	63.1940	18.4520	53.0	2.61
7	2013-10-15	22:52:33	62.1820	18.5200	56.0	2.21
8	2013-10-15	22:57:27	63.1680	18.5440	53.0	2.00
9	2013-10-15	23:00:15	63.1660	18.4970	43.0	2.63
10	2013-10-15	23:19:24	63.1760	18.4580	57.0	3.09
11	2013-10-15	23:32:57	63.1630	18.4900	40.0	2.56
12	2013-10-16	00:20:53	62.2120	18.4630	47.0	2.50
13	2013-10-16	00:34:34	63.1600	18.5000	45.0	2.46
14	2013-10-16	00:42:26	63.1840	18.5070	52.0	2.28
15	2013-10-16	00:50:31	63.1760	18.4790	49.0	2.98
16	2013-10-16	02:44:47	63.1580	18.4640	51.0	2.67
17	2013-10-16	02:54:23	62.1730	18.4870	29.0	2.99
18	2013-10-16	02:59:40	63.1620	18.4700	54.0	2.55
19	2013-10-16	03:53:35	63.1740	18.5230	50.0	3.42
20	2013-10-16	04:01:53	63.1440	18.4940	46.0	3.37
21	2013-10-16	06:13:16	63.1780	18.4470	55.0	2.74
22	2013-10-16	06:54:21	62.1460	18.5280	41.0	2.84
23	2013-10-16	08:06:52	63.1850	18.4580	52.0	2.36
24	2013-10-16	08:31:22	63.1420	18.4720	34.0	3.71
25	2013-10-16	08:48:43	63.1960	18.4610	58.0	3.02
26	2013-10-16	09:50:42	63.1890	18.4460	43.0	2.37
27	2013-10-16	10:38:00	62.1780	18.4800	51.0	3.11
28	2013-10-16	11:41:35	63.1330	18.5100	56.0	2.59
29	2013-10-16	12:53:04	63.1710	18.4740	40.0	3.21
30	2013-10-16	13:34:53	63.1750	18.5120	48.0	3.41
31	2013-10-21	19:53:57	63.1700	18.5300	59.0	4.57
32	2013-10-22	08:09:53	62.1600	18.5600	59.0	3.00
33	2013-10-22	13:35:50	63.1500	18.5700	45.0	2.74

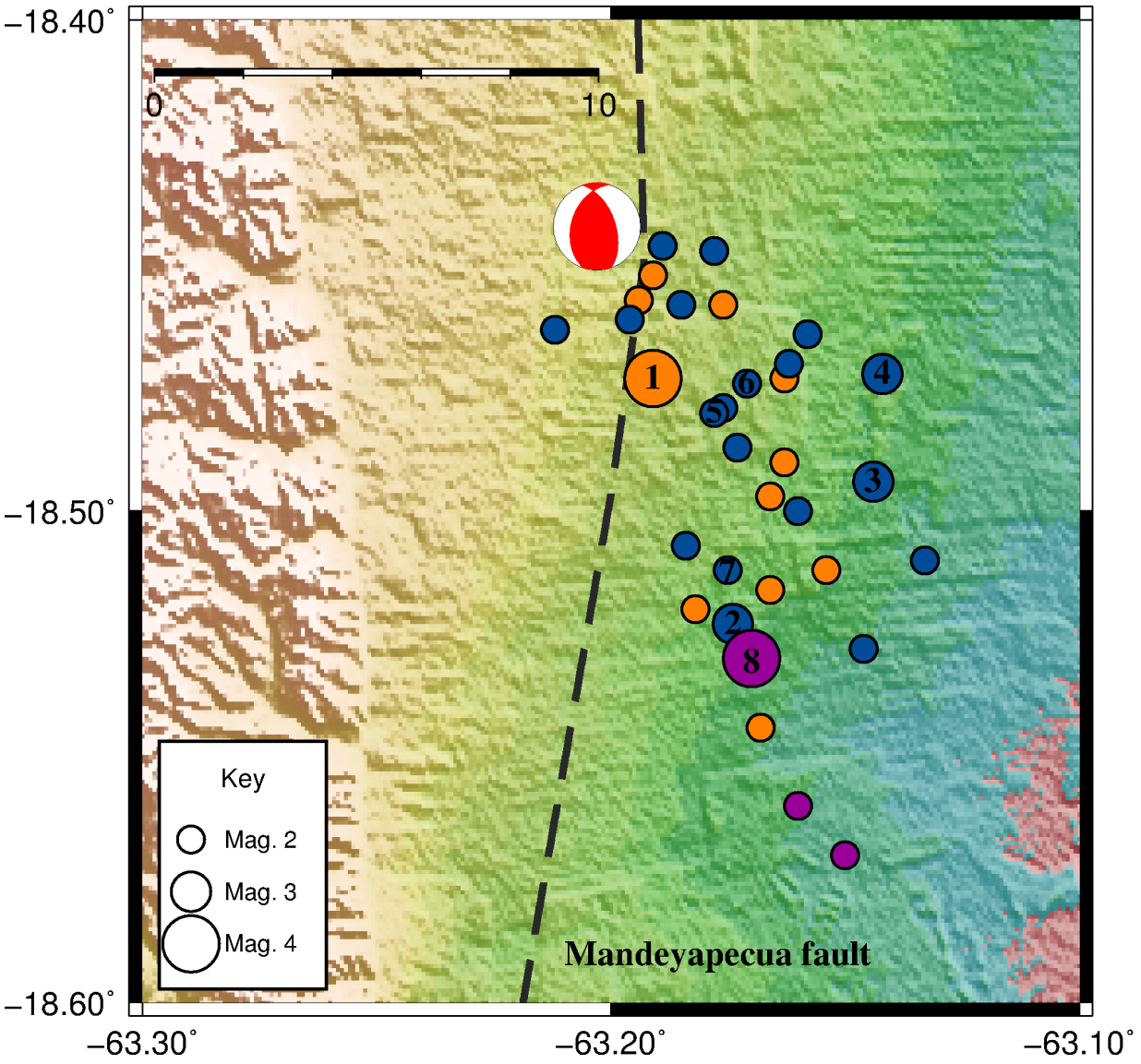

Figure 2.8: Mainshock (beach ball) and aftershocks reported by San Calixto Observatory. Aftershocks occurred one day after the mainshock (orange circles), aftershocks occurred two days after the mainshock (blue circles), and aftershocks occurred two weeks after the mainshock (purple circles). It can be observed that the distance between the mainshock an the aftershock are approximately 14 km, more in agreement with the expected value for an earthquake of 5.2 Mw.

Chapter 3

Geological Setting

3.1 Geology of the area

The Central Andes of Bolivia define an active Cordillera-type orogen, and has been considered as a young orogenic belt due to of their high elevation and topography, rugged peaks little affected by erosion, and broad internally drained areas of low relief (McQuarrie et al., 2005). They are located above a 30° east-dipping portion of the Nazca plate and represent the widest part of the Andean chain (300 - 600 km). Its formation occurred during the Cenozoic with the slow subduction of the oceanic Nazca plate under the continental South American plate and the underthrusting Brazilian shield (Beck and Zandt, 2002). These processes have produced large intraplate deformations in a broad part of the continent, resulting in different styles of crustal deformation.

The main characteristics of the Bolivian Central Andes are:

- The presence of a wide and thick (6 to 15 km) Tertiary sedimentary basin, which forms a high plateu, the Altiplano, and have and average elevation of 3800 meters.
- The elbow shape of the mountain range, which is referred to as the Bolivian Orocline.
- Active Cenozoic and Quaternary volcanic arc.
- A thick crust, between 55 and 70 km.
- A high amount of topographic relief within and across the range.

The Central Andes of Bolivia consist of four morphostructural units: the Western Cordillera, the Altiplano, the Eastern Cordillera, and the Subandean zone as shown Figure

3.1. This last unit has a break in its orientation, known as the Bolivian Orocline or Santa Cruz elbow; to the north the strike is N-W whereas to the south is roughly N-S (Rocha and Cristallini, 2015).

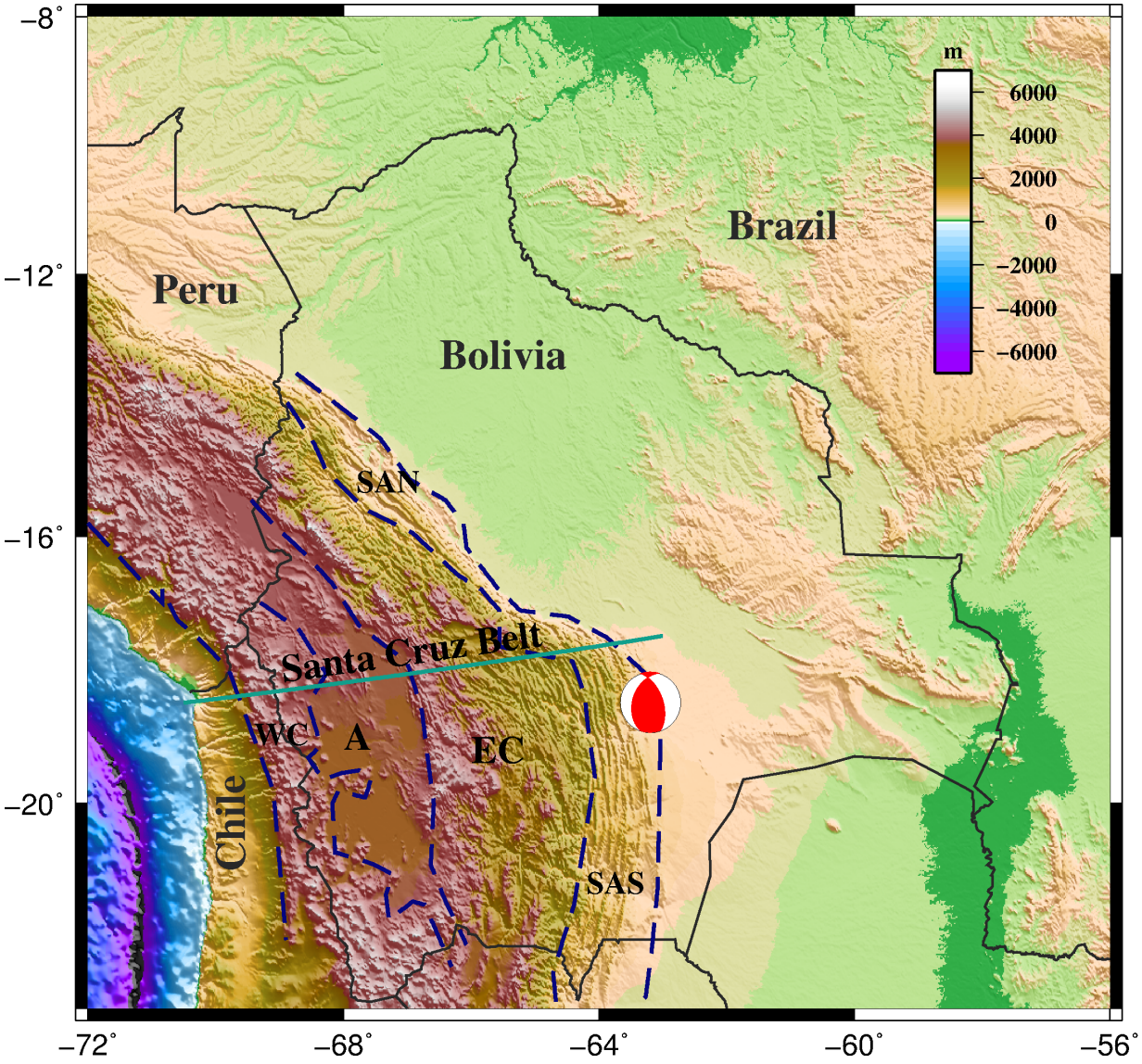

Figure 3.1: Mainshock (red star). WC: Western Cordillera; A: Altiplano; EC: Eastern Cordillera; IA: Interandean Zone; SAN: Northern Subandean Zone; SAS: Southern Subandean Zone; Ch: Chaco Plain; CB: Brazilian Craton (Rocha and Cristallini, 2015).

The Central Andes have a long history of subduction and volcanic arc activity. The horizontal subduction increases intraplate friction, favoring the continental shortening and build-up of the Andes. However, both processes are not necessary contemporaneous, because many complex dynamics are involved in the development of the Andes. The growth of the Andes would be marked by two periods (Martinod et al., 2010):

- A build-up period that started in the Upper Cretaceous and finished in the Miocene, where the continental lithosphere was thickened.

- The Late Miocene, when it reaches its modern elevations, and would in turn transmit compression to the lowlands in the east.

The topographic growth of compressional mountain belts and associated plateaus has been considered as a function of a increasing lithospheric thickness in response to orogenic deformation. The deformation of the Andes is proposed to have initiated by 60 Ma along the western margin of the Altiplano, jumping to the eastern plateau margin at the Eastern Cordillera by 45 Ma and finally to the modern deformation front in the Subandean zone by 15 Ma (Eichlberger et al., 2015).

The area where the Santa Cruz events occurred is located in the southern Subandean zone, which is the transition from the high elevations of the Central Andean Plateu to the foreland plains (Beck and Zandt, 2002). It accommodates the transition through synclinal basins separated by thrust-faulted anticlines (Ward et al., 2013).

The Eocene deformation of the Central Andes affected some regions of the foreland basin, the compression of the Cordillera began in the Oligocene, between 25 and 29 Ma and continued until about 10-6 Ma. The foreland basin shifted eastward, building the Subandean zone (Gregory-Wodzicky, 1999)

The statigraphic column for the southern Subandean zone is approximately 10 km thick, and it involves rocks with ages between the Silurian and Cenozoic. It is characterized by narrow, outcropping, largely continuous anticlines (Rocha and Cristallini, 2015). These sedimentary rocks present a low average crustal velocities of 5.9 km/s (Wigger et al., 1994); and values of 40 km to 42 km for crustal thicknesses (Beck and Zandt, 2002). Figure 3.2 shows the geological map of Bolivia.

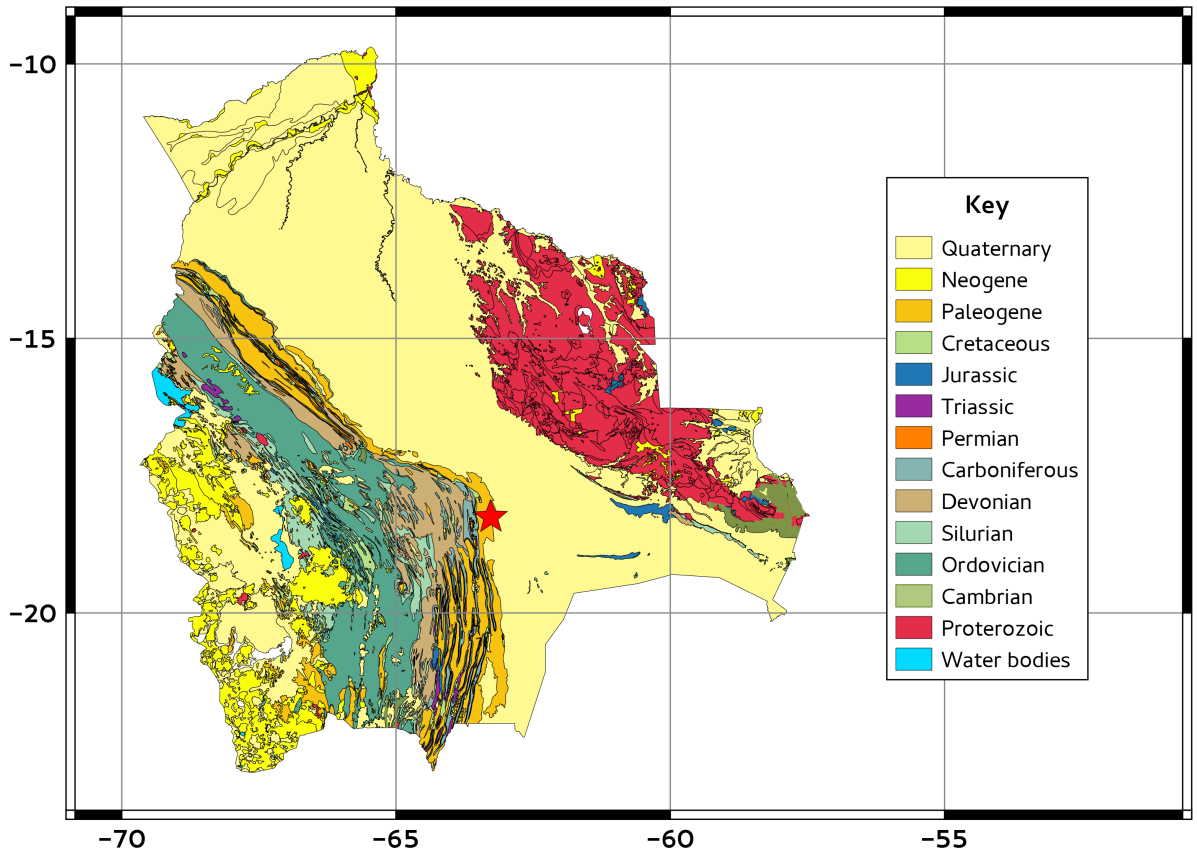

Figure 3.2: Geological map of Bolivia. The Subandean zone contains rocks mostly from the Paleogene Age (Servicio Nacional de Geología y Técnico de Minas, 2000b).

Foreland regions above subduction in the Andes are characterized by thin-skinned fold and thrust structures topographically expressed as a series of subparallel ridges. Folding has small wavelenghts of 5-10 km and generally faults are steep (45° - 60°) (Devlin et al., 2011). Figure 3.3 shows the Bolivian faults and lineaments compiled by the Servicio Nacional de Geología y Técnico de Minas (2000a), which is a government institution of Bolivia.

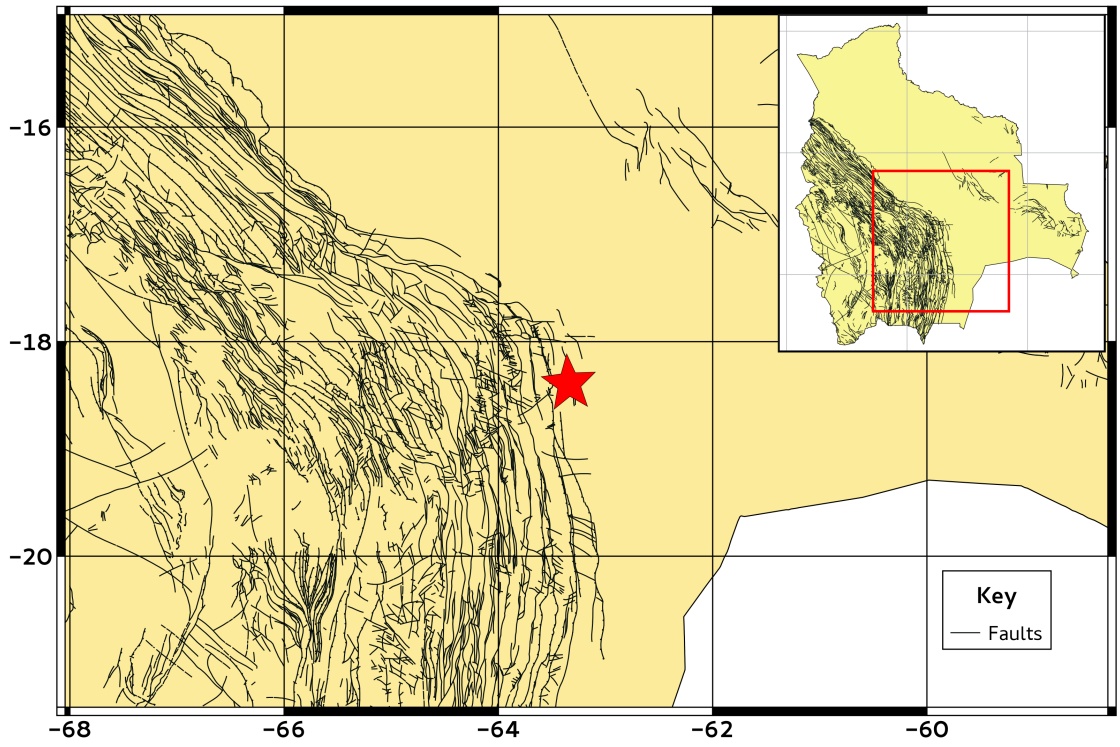

Figure 3.3: Mainshock (red star). Bolivian faults in the area where the Santa Cruz de la Sierra events occurred. There are many faults that show N-S trend.

In Bolivia there are a total of 14 major Quaternary faults, listed in Table 3.1 (Lavenu et al., 2000). The eastern area is characterized by reverse faults with N-S orientation, and soft folds. One of the most important is the reverse Mandeyapecua fault, that has an extension of 486 km (Lavenu et al., 2000).

The Mandeyapecua fault is the structure with the easternmost surface expression of the southern Subandean zone fold belt. Its surface expression is divided into five topographic segments exhibiting relief profiles characterized by central maximum tapering toward zero valued inflection points that should indicate persistent rupture segmentation. A single earthquake of 8.7 -8.9 Mw could rupture the entire fault. It is likely that enough slip has accumulated since 1886 for an event of 7 Mw (Brooks et al., 2011).

Table 3.1 - Major Quaternary Bolivian faults

Name	**Fault Geometry**			**Type**	**Slip Rate**	**Most recent Movement**
	Lenght	**Strike**	**Dip**			
Achacachi	29.9 km	-57.4°	Unknown	Normal	Unknown	Quaternary (<1.6 Ma)
Peñas	53.6 km	-46.3°	70°NE	Normal	Unknown	<1.5 ka)
Kenko	11.4 km	-35.7°	75°SE	Normal-sinistral	<0.2 mm/year	Quaternary (<1.6 Ma)
LLojeta	12.7 km	-50.2°	75°NE	Normal-dextral	Unknown	Quaternary (<1.6 Ma)
Amachuma	40.0 km	-24.6°	70°E	Normal-sinistral	<0.2 mm/year	Quaternary (<1.6 Ma)
Quebrada	7.7 km	-70.2°	85°S	Normal-dextral	Unknown	Quaternary (<1.6 Ma)
Escoma	26.6 km	-43.2°	Unknown (W)	Normal	Unknown	Quaternary (<1.6 Ma)
Viacha	16.7 km	31.5°	Unknown (SE)	Normal	Unknown	Quaternary (<1.6 Ma)
Ayo Ayo	14.6 km	-53.6°	70°N	Normal-dextral	Unknown	Quaternary (<1.6 Ma)
Cuenca de Charaña	26.7 km	-37.3°	Unknown (E)	Normal	Unknown	Quaternary (<1.6 Ma)
Tunari	81.0 km	-72.0°	60°S	Normal-dextral	Unknown	Quaternary (<1.6 Ma)
Tarija	54.4 km	22.6°	70°W	Normal	Unknown	Quaternary (<1.6 Ma)
Beni	91.1 km	4.5°	unknown	Normal	Unknown	Quaternary (<1.6 Ma)
Mandeyapecua	486.6 km	-6.7°	60°W	Reverse	Unknown	Quaternary (<1.6 Ma)

3.2 Seismicity of Bolivian Sub-Andes

The subduction of the Nazca plate beneath the South American plate has caused the rise of the Andes mountains. Also, it could generate earthquakes of large magnitude along the west side of the Andes; however in the east side the seismic potential is not well known (Brooks et al., 2011).

The seismic activity in Bolivia is moderate compared to the high activity in Peru and Chile. However, there are some events with intermediate depth in the west region, deep events in the southern part, and shallow earthquakes with small magnitude (less than 5.6 Mw) in the Subandean zone. Intraplate seismic activity in Bolivia in mainly located in the central region (16°S and 19°S, 63°W and 67°W) which includes the Eastern Cordillera and the Subandean zone (Vega and Buforn, 1991).

The seismicity in Bolivia has been studied by the Observatorio San Calixto (2012), recognizing two seismogenic sources in the area:

1. The crust, associated with continental deformation: This group includes earthquakes with depth until 70 km (shallow earthquakes), which is the maximum crustal thickness in Bolivia. The potentially active faults are related to this source, being likely responsible for seismic activity in the Holocene and in the Quaternary period.

2. The subduction zone: this group includes the earthquakes that could have a magnitude up to 8.0 Mw, but they do not cause damage and are felt slightly in the epicentral area, due to their great depth. The seismogenic activity of this source is not continuous because there are not many earthquakes between 350 and 500 km depth (intermediate earthquakes), the activity becomes manifest again in depths between 500 and 700 km (deep earthquakes).

The Observatorio San Calixto (2013) has studied earthquakes in the Department of Santa Cruz de la Sierra since 1929, and has a record of historic earthquakes since 1625. This area is located in the Chaco Beniano plain, in the easternmost portion of the Bolivian Andes, being a large floodplain and it is part of the Subandenan deformation belt. Further, most of the earthquakes in this area are shallow (crustal source) as shown in Figure 3.4. Figure 2.1 shows the Bolivian seismicity of shallow earthquakes ($\leq$ 70 km) greater than 5.0 mb.

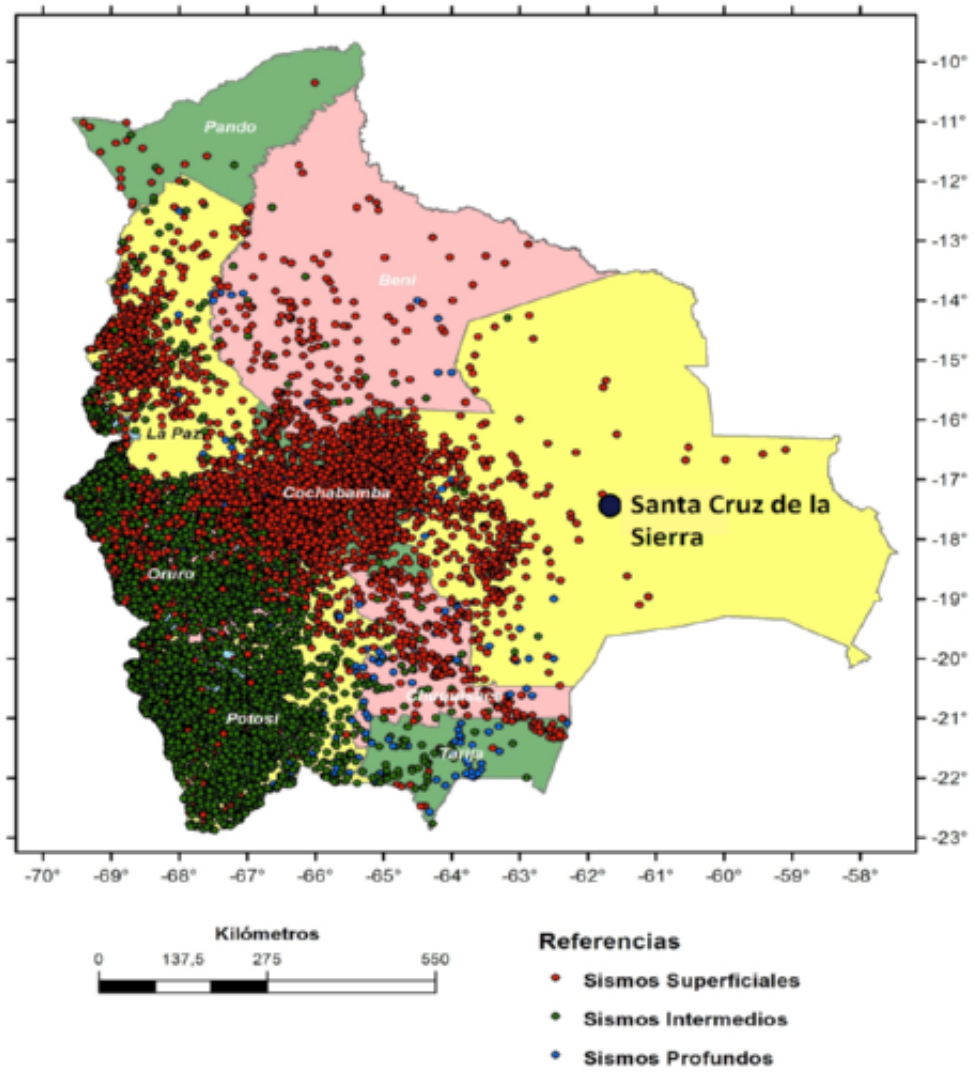

Figure 3.4: Santa Cruz de la Sierra earthquake (blue circle). Bolivian Seismicity since 1625 until 2010. The shallow earthquakes are represented by red circles ($\leq$ 70 km), the intermediate earthquakes by green circles (70-300 km) and the deep earthquakes by blue circles ($\geq$700 km). In the west most events have intermediate depth, while in the east the most are shallow (Observatorio San Calixto, 2012).

The historic seismicity of Bolivia affected the towns of Warnes (1929), La Florida (1949), Postervalle (1957), and Pasorapa (1958); with an intensity in the Mercalli Modified Scale of IV, V, VII and VI respectively. Most are located in the Department of Santa Cruz de la Sierra (Observatorio San Calixto, 2012), as shown Figure 3.5.

Figure 3.5: Purple stars show the location of the towns affected by the historic seismicity of Bolivia. These events are located close to the Santa Cruz de la Sierra earthquake (beach ball).

Between 15°S and 19°S, near the cities of Cochabamba and Santa Cruz de la Sierra, along the Subandean zone, the topography changes influence the averaging P axis orientation. Figure 3.6 shows the rotation of dominant focal mechanism orientation in the Eastern Cordillera and Subandean zone, suggesting that structural trends and strike of the mountain influence the compressional axis orientation in this region (Devlin et al., 2011). The strike-slip events in the area (green focal mechanism) could reflect E-W or N-S structures, but Funning et al. (2005) favor the N-S interpretation for Aiquile event, occurred in 1998 based on INSAR data.

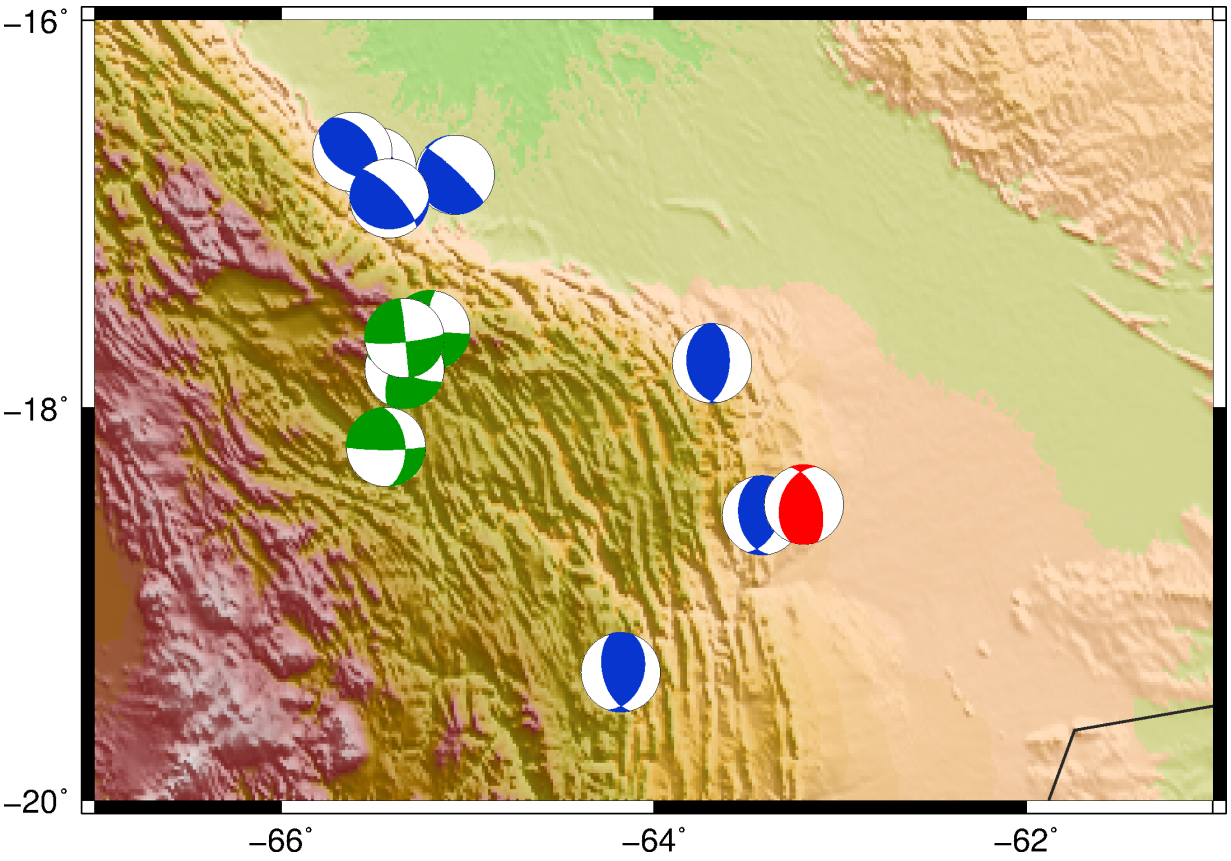

Figure 3.6: Santa Cruz de la Sierra earthquake (red focal mechanism). Strike-slip events (green focal mechanisms).In the northern area the events show a WNW-ESE trend, while in the southern area it can be observed a N-S trend.

Vega and Buforn (1991) also studied the focal mechanisms of 10 Bolivian earthquakes of magnitudes between 4.9 and 5.6 Mw. Their results can be grouped in two types; one with pure reverse faulting indicate a E-W horizontal compressional stress in the south Subandean zone, and the other with azimuth WNW-ESE in the north Subandean zone.

The results of Vega and Buforn (1991) and Devlin et al. (2011) shows that the maximun stress axis (P-axis) is practically horizontal (dipping less than 5°) oriented in a mean N56°E direction. This can be interpreted as a result of intraplate compression of the crust, caused by the deformation that originates the subduction of the Nazca plate between the Bolivian Altiplano and the Brazilian lithosphere. Also, this features result in E-W shortening of the crust.

The high seismogenic potential in the Subandean zone is attributable to the combination of (Brooks et al., 2011):

- Increase in accretionary flux and material properties (stratigraphic architecture and

thermal properties) that have governed the growth of the contractional wedge.

- Depth of the transition to velocity strengthening behavior

3.3 Seismic Hazard in Bolivia

The Observatorio San Calixto (2012) conducted a study of seismic hazard, based on statistical, probabilistic and deterministic evaluations of the national catalog since 1625 until 2010. The catalog contains information about both historic earthquakes (1625-1913) and instrumental earthquakes (1913-2010). Besides, they also considered paleoseismicity data.

Figure 3.7 shows the result of the seismic hazard. The area with highest seismic risk is where Mandeyapecua reverse fault is located. They concluded that areas with higher seismic risk are those where are located the major Quaternary faults.

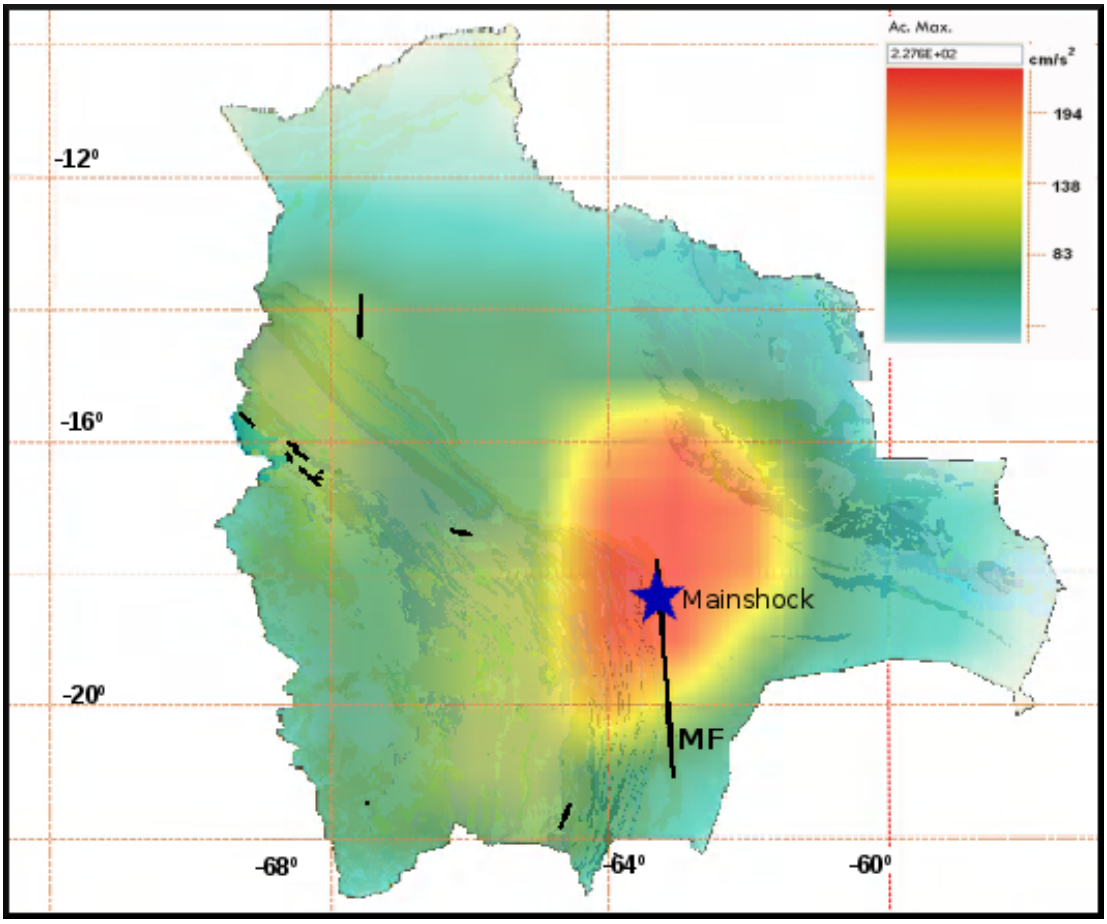

Figure 3.7: Hot colors show areas with higher seismic risk. Black lines represent Quaternary faults. Blue star is the epicenter of Santa Cruz de la Sierra earthquake. The area near the Mandeyapecua fault (MF), area where the events occurred, presents the highest acceleration and seismic risk (Observatorio San Calixto, 2012).

Chapter 4

Relative Location with Rayleigh Waves

Precision in the epicentral location is important to determine fault orientation, detect epicenter migration and develop regional velocity models. However, the determination of epicenters using regional and teleseismic stations has uncertainties over 20 km, due to noise in the seismograms, lateral velocity variations, and regional stations with sparse distribution. In order to obtain uncertainties lesser than 5 km, it is necessary at least 10 stations closer than 250 km, an azimuthal gap less than 110°, a secondary azimuthal gap less than 160° and at least one station within 30 km from the epicenter (Bondár et al., 2004). In the Central Andes these conditions are seldom met, so it is necessary to use alternative techniques to improve the earthquakes location.

A relative location technique uses a reference event, preferably with a well know epicenter, to get stations corrections which are used to locate other events. Rayleigh waves are generally the clearest waves in noisy seismograms, due to having amplitudes larger than body waves, and commonly are used for relative locations. Rayleigh waves are recorded in the vertical and radial components of seismograms, and for regional distances, between 300 and 2000 km, are easily recognized. Also the waveform similarity between events is high when they have similar paths and similar focal mechanisms (Chiu and Snyder, 2014). The window of group velocity of the Rayleigh wave is generally from 3.0 to 3.6 km/s, and for continental lithospheric paths are the dominant phase (Gallegos et al., 2014).

The low propagation velocity of Rayleigh waves provides a substantial sensitivity for relative location, especially when correlation is used to pick accurate relative arrival times. The precision of wave correlation for periods of 20 seconds is better than one second, which corresponds to a distance error less than 3 km.

4.1 Data

To do a relative location of the aftershocks using surface waves it is better to use the nearest stations, preferentially those located within a distance of 2000 km, where the surface waves are dominant. We used data from South American stations listed in Table 4.1 and shown in Figure 4.1.

Table 4.1 - Stations used for relative location with Rayleigh waves

Network	**Station**	**Localization**			**Epicentral distance**
		Longitude	**Latitude**	**Country**	
BL	AQDB	55.70°W	20.48°S	Brazil	816.88 km
	BSCB	44.76°W	21.00°S	Brazil	1950.62 km
	CLDB	55.80°W	10.87°S	Brazil	1159.75 km
	CNLB	50.85°W	29.31°S	Brazil	1734.23 km
	CPSB	53.49°W	30.51°S	Brazil	1647.59 km
	ITAB	52.34°W	27.31°S	Brazil	1490.63 km
	PEXB	48.30°W	12.11°S	Brazil	1747.729 km
	PLTB	53.65°W	31.75°S	Brazil	1759.598 km
BR	ARAG	51.81°W	15.71°S	Brazil	1249.950 km
G	SPB	47.43°W	23.59°S	Brazil	1732.17 km
	PEL	70.67°W	33.14°S	Chile	1786.394 km
GT	CPUP	57.33°W	26.33°S	Paraguay	1056.82 km
	PLCA	70.55°W	40.73°S	Chile	2563.62 km
	LPAZ*	68.13°W	16.29°S	Bolivia	581.65 km
II	NNA	76.84°W	11.99°S	Peru	1632.17 km
IU	LVC	68.91°W	22.61°S	Chile	750.22 km
	OTAV	78.45°W	0.24°N	Ecuador	2660.31 km
	PAYG	90.29 °W	0.67°S	Ecuador	3556.26 km
	SAML	63.18°W	8.95°S	Brazil	1056.07 km

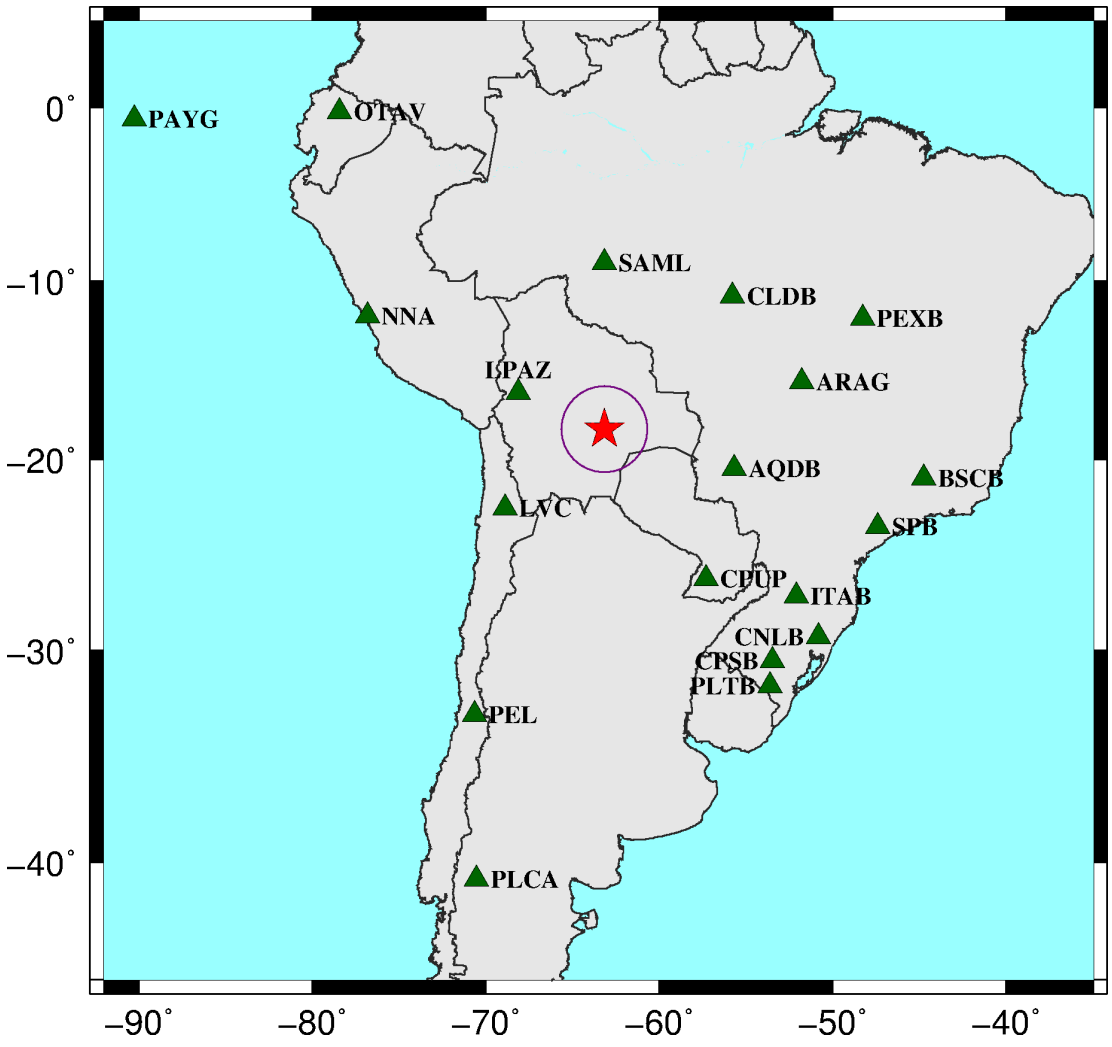

Figure 4.1: Santa Cruz de la Sierra earthquake (red star) and stations (triangles) used to do the relative location with surface waves. The purple circle has a radius of 250 km around the Santa Cruz de la Sierra earthquake, the closest station is located more than 250 km away from Santa Cruz de la Sierra earthquake.

4.2 Methodology

For this work we only used the vertical component of seismograms. The data was processed by the multiple-filtering match techniques of Hermman and Ammon (2002), which permits to select filter parameters, interactive identification of modes, choice of phase match filtering, and save the results along of the process. The filter analysis was made between periods of 10 and 70 seconds, and a velocity range from 2 km/s to 4.8 km/s. The technique of match-filtering uses a Gaussian filter which has a central frequency and a band-width defined by the alpha parameter (α). As α increases, the filter gets more selective; but this tends to make the filtered signal look like as a sinusoid (single frequency)

with longer duration, worsening the arrival time resolution of the envelope. The best value of α depends on the distance between the events and the station. The values recommended by Hermman and Ammon (2002) for this parameter are shown in Table 4.2.

Table 4.2 - Best values of the parameter alpha (α)

Distance	α
1000 km	25
2000 km	50
4000 km	100
8000 km	200

The seismograms were match-filtered twice in order to obtain a better signal of Rayleigh waves. Figure 4.2 shows the dispersion curve of the Rayleigh wave, in each filter, for A4 (2.3) at CPUP station.

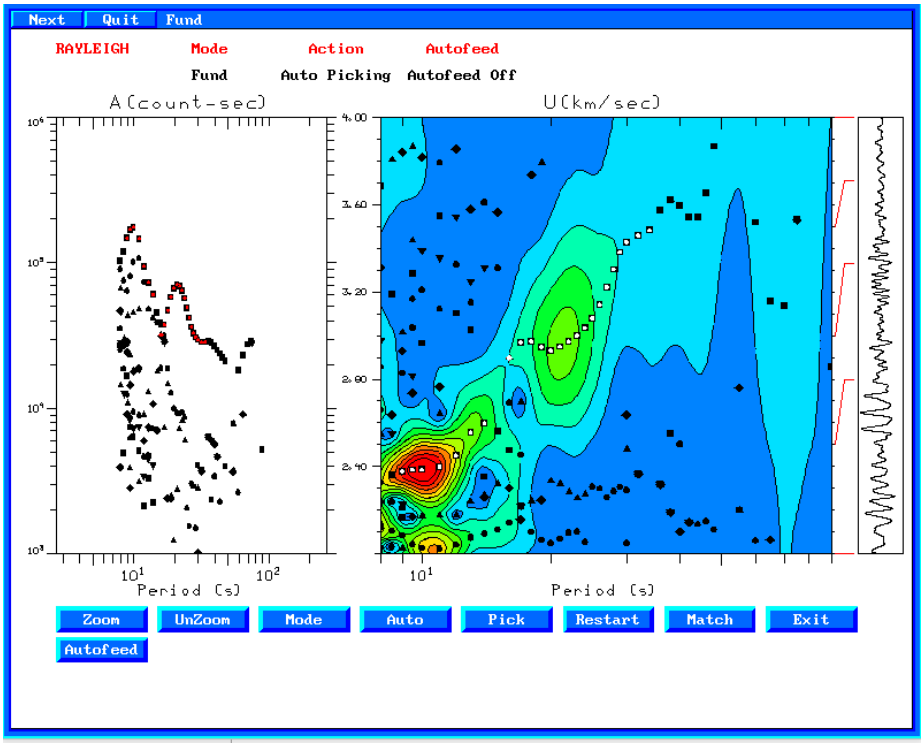

(a)

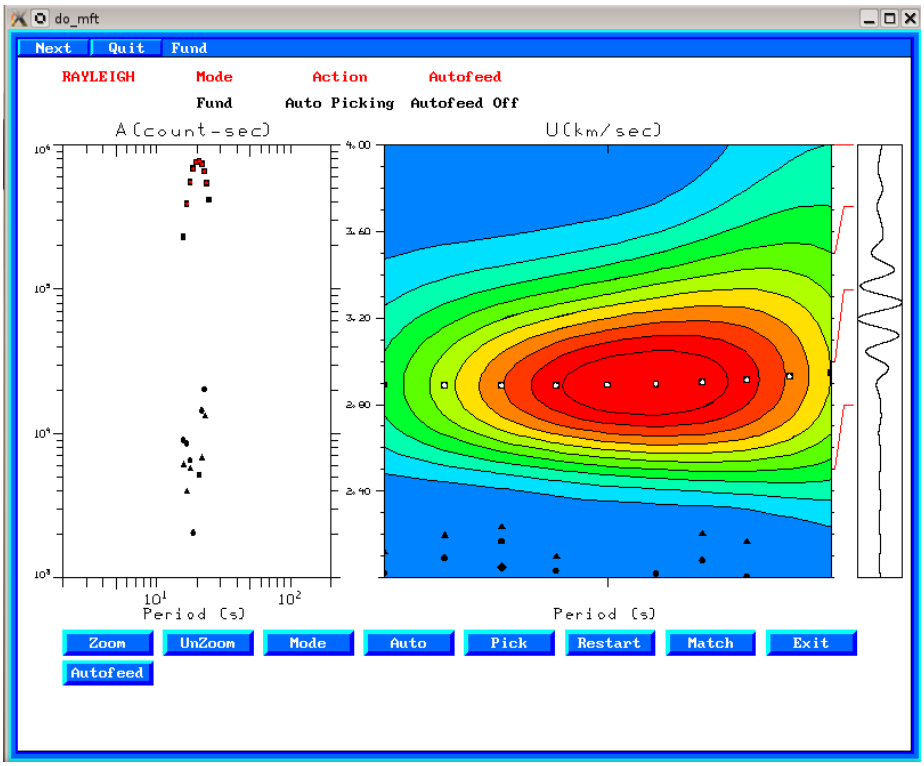

(b)

Figure 4.2: Filtering of the A4 seismogram by the multiple-filtering technique at CPUP station. (a) First match-filter between 10-70 seconds. The trace on the right is the original seismogram. (b) Second match-filter between 15 and 25 seconds. The trace on the right is the output of the match-filter used in (a). The red areas represent the maximum energy.

The multiple-filtering technique isolates the Rayleigh waves from the other phases present in the seismograms, as shown in Figure 4.3.

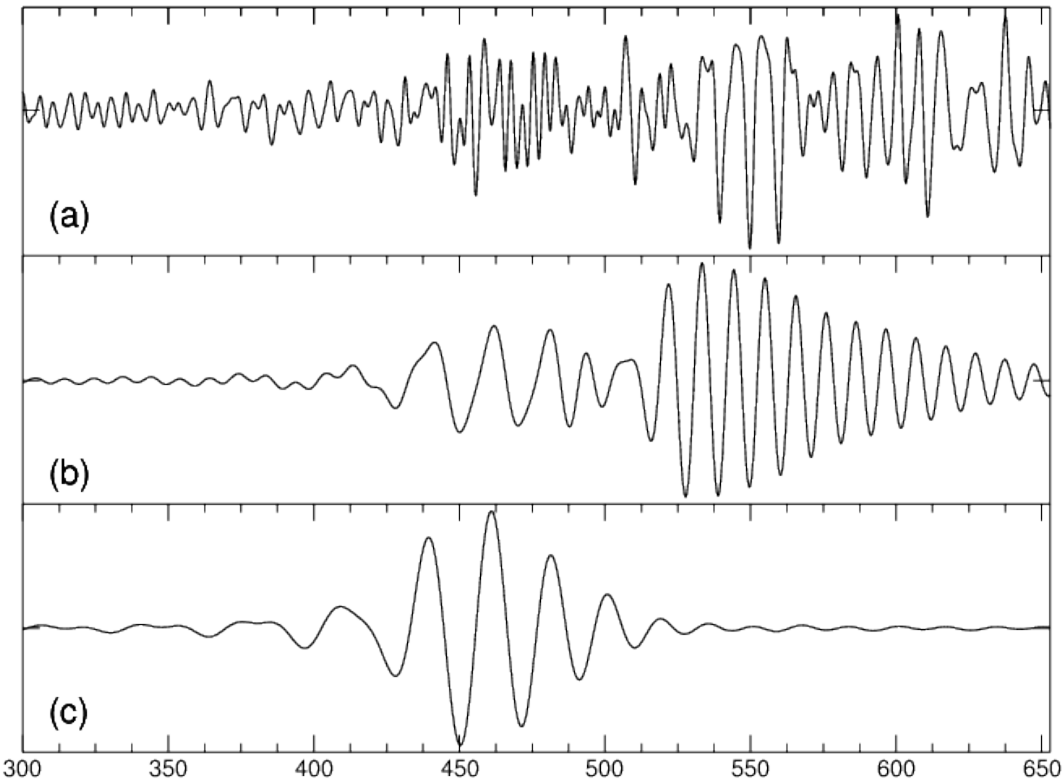

Figure 4.3: (a) Original seismogram of Aftershock 4 (A4) at CPUP station before filtering. (b) Seismogram of A4 at CPUP station after match-filtering between 10 sec and 70 sec. (c) Seismogram of A4 at CPUP station after match-filtering between 15 sec and 25 sec. The Rayleigh waves were isolated from the other phases.

In order to do the relative location of the five largest aftershocks, we used as reference event the mainshock relocated with *iLoc* program using stations up to 90°, corrected with RSTT model up to 15° (black star in Figure 2.4).

We identified the frequency which presents the most energy density in the dispersion curve, and the one that is present in all seismograms. For all of them the peak energy was around of 0.05 Hz (20 seconds), and this frequency was defined to do the waveform correlation.

A code developed by the Seismology Center of the University of Sao Paulo (Ciardelli and Assumpcao, 2015) was used to correlate automatically the waves. It is first necessary to choose an event as reference and define the parameters: phase, filter corner-frequencies, time window, and maximum lag. The values used to do the correlation are specified in Table 4.3.

Table 4.3 - Parameters used in the Rayleigh wave correlation

Parameter	**Value**
Phase	Rayleigh
Component	Vertical (Z)
Filter corner	0.04-0.06 (Hz)
Time window	40 seconds
Maximum lag	3 seconds

The code calculates the highest correlation between the target and reference event in the time window specified, and updating the header of the seismogram. Table 4.4 shows the correlation coefficients of all aftershocks with the mainshock at each station.

Table 4.4 - Correlation coefficients of Rayleigh waves

Station	**A1**	**A2**	**A3**	**A4**	**A5**
AQDB	1.00	1.00	1.00	1.00	1.00
BSCB	1.00	1.00	1.00	1.00	1.00
CLDB	1.00	1.00	1.00	1.00	1.00
CNLB	NA	1.00	1.00	1.00	1.00
CPSB	NA	1.00	1.00	1.00	NA
ITAB	NA	1.00	1.00	0.99	1.00
PEXB	1.00	1.00	1.00	1.00	NA
PLTB	NA	1.00	NA	1.00	1.00
ARAG	1.00	1.00	1.00	1.00	1.00
PEL	NA	NA	NA	1.00	1.00
SPB	1.00	1.00	1.00	1.00	1.00
CPUP	1.00	1.00	1.00	1.00	1.00
LPAZ	1.00	1.00	1.00	1.00	1.00
PLCA	1.00	1.00	1.00	1.00	1.00
NNA	1.00	1.00	1.00	1.00	1.00
LVC	0.98	1.00	1.00	1.00	1.00
SAML	0.98	1.00	NA	1.00	NA
OTAV	NA	1.00	NA	1.00	1.00
PAYG	NA	1.00	NA	1.00	1.00

Figure 4.4 shows the correlated Rayleigh wave at CPUP station, after applying a band-pass filter to isolate the period of 20 seconds. We can observe a high similarity of waveform that allows the relative arrival-time difference to be picked with an accuracy better than 0.5 seconds.

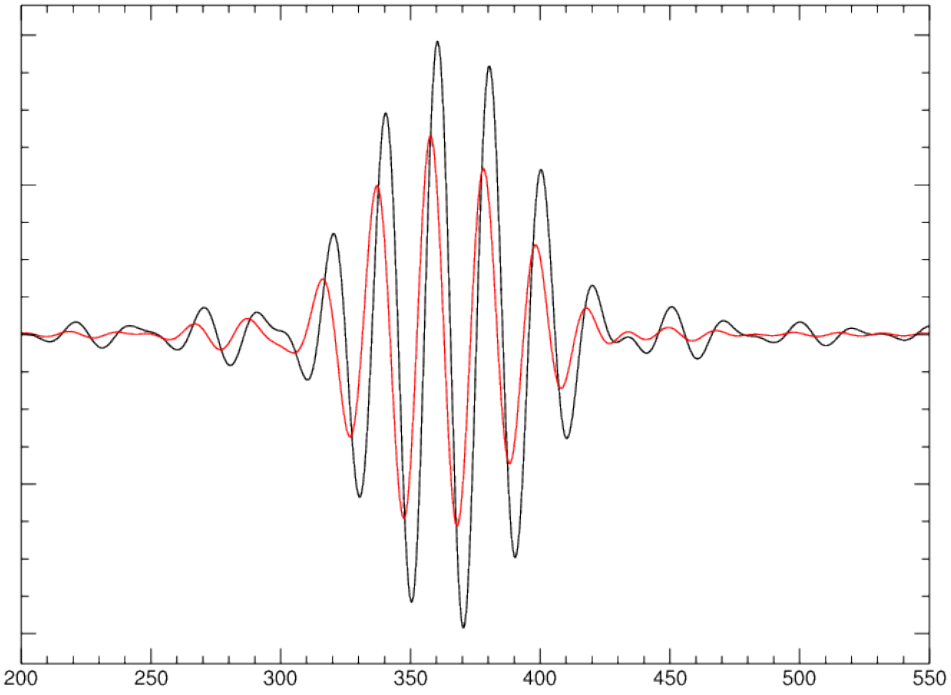

Figure 4.4: Correlation of Rayleigh waves at CPUP Station, for a period around of 20 seconds. Seismograms are aligned by the event origin time. Black seismogram is the reference event and red seismogram is the target event A4 (Table 2.3). The travel time difference between the two Rayleigh waves is of 2.7 seconds.

After the waveform correlation, we found the difference between the traveltime of the Rayleigh waves of the target and reference event for the period at 20 seconds (0.05 Hz). The difference in the time shifts (the target event relative to reference event) can be represented as a cosine function of the azimuths (Cleveland and Ammon, 2013). Figure 4.5 shows the basis of this technique.

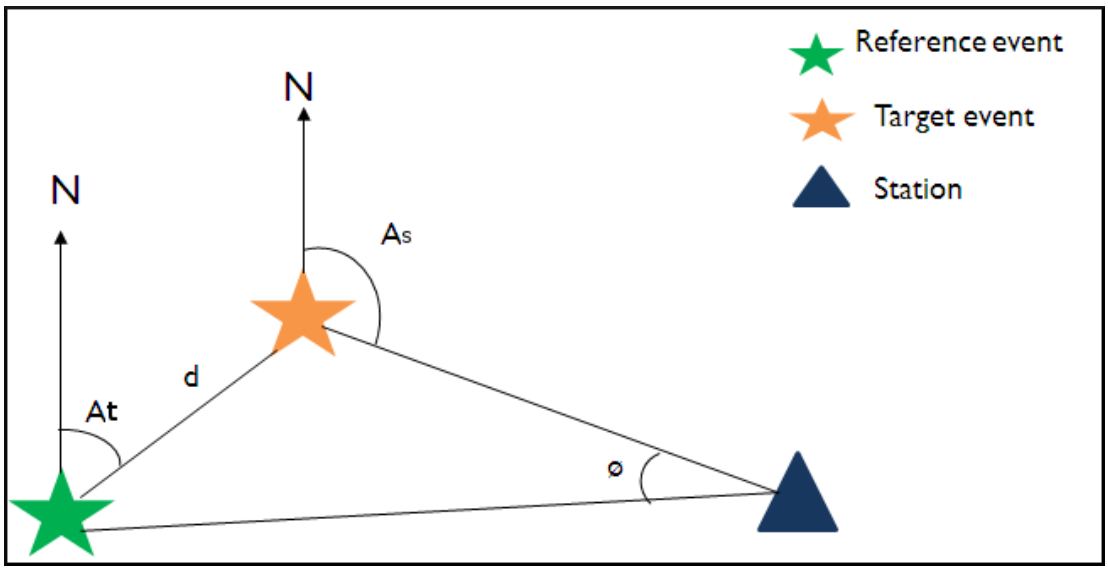

Figure 4.5: Relative location technique, considering that the distance (d) between the target and reference event is much smaller than the distance to the station. ($\phi \simeq 0$).

Considering that the distance between the station and the events is much greater than the distance between the events, it can be assumed that the angle ϕ is close to zero, and the ray paths of the two events are parallel. Then the difference in travel time between the reference and the target event could be represented by the Equation 4.1 (Cleveland and Ammon, 2013).

$$T_t - T_r = A_0 - \frac{d * cos(A_s - A_t)}{V_{ap}} \tag{4.1}$$

where:

- T_t is the travel time of the Rayleigh wave of the target event.
- T_r is the Rayleigh travel time of the reference event.
- A_0 is the correction for the target event origin time.
- A_s is the station azimuth in relation to the reference event.
- A_t is the azimuth of the target in relation to the reference event.
- V_{ap} is the apparent velocity of the Rayleigh wave (i.e., phase velocity).
- d is the distance between the target event and the reference event.

With Equation 4.1, it is possible to calculate unknown parameters like A_0, d and A_t, through the theoretical curve of time differences (T_t-T_r) versus station azimuth (A_s). For this purpose, we used a phase velocity of 3,4 km/s as determined by Ward et al. (2013) in a tomography study of the Central Andes, in their study they constructed Rayleigh-wave phase velocity maps in the period range of 8-40 seconds. Figure 4.6 shows the phase velocity of the Rayleigh waves in this area. Also we estimate errors using Monte Carlo simulations.

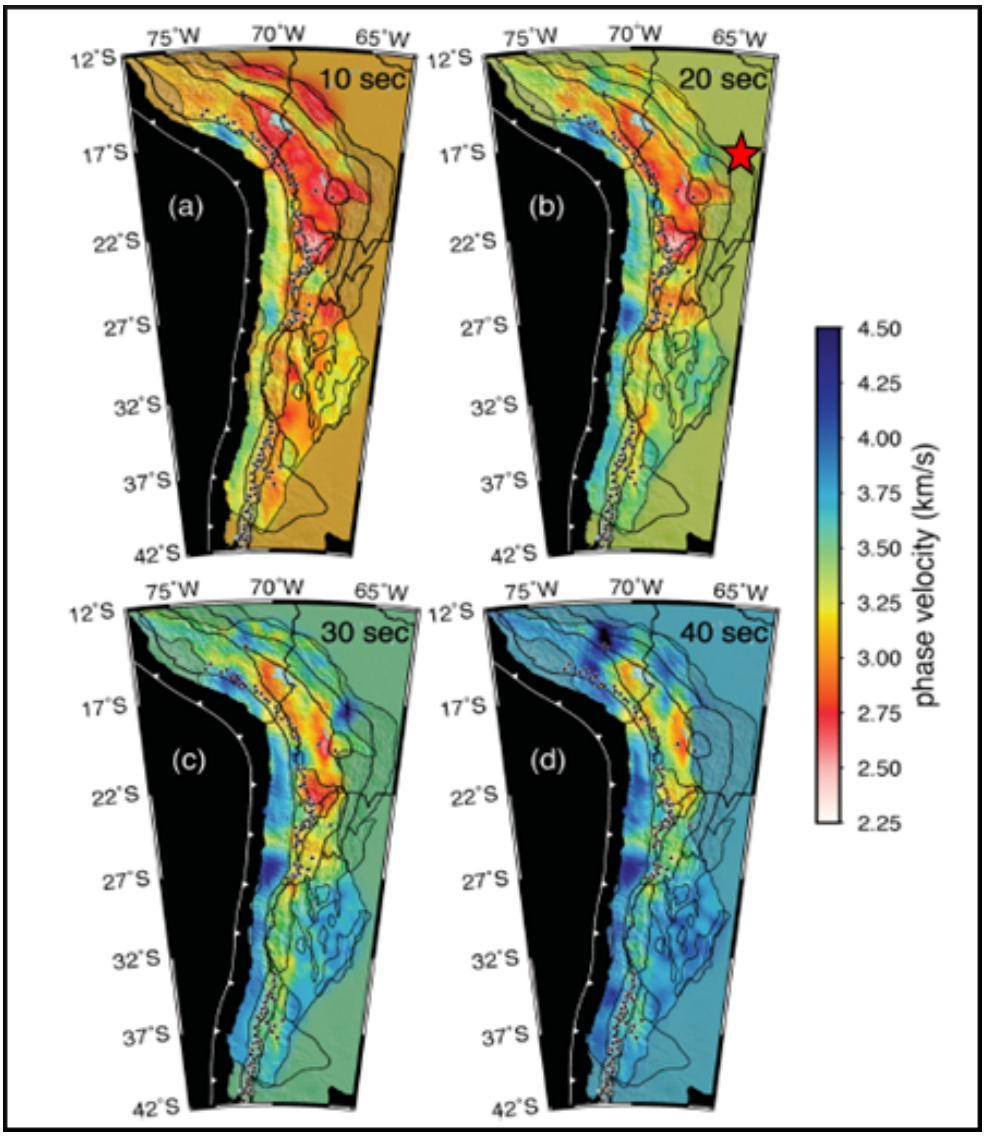

Figure 4.6: Rayleigh wave phase velocity maps for 10, 20, 30 and 40 seconds. We used the period of 20 seconds to perform the relative location. The red star shows the epicenter of Santa Cruz de la Sierra earthquake. Taken from Ward et al. (2013).

4.3 Results

Figures 4.7, 4.8, 4.9, 4.10, 4.11 show the fitted curve of the equation 4.1 for relative location of each aftershock.

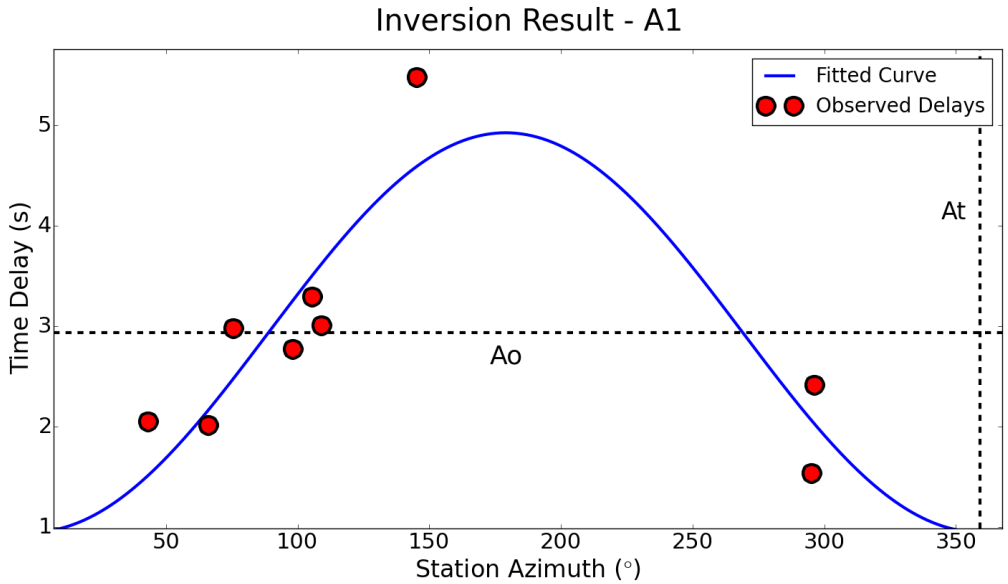

Figure 4.7: Fitted curve for the relative location of the aftershock 1. Only a few stations were used in the relocation, because this aftershock occurred two minutes after the mainshock and the signal of both events are mixed in many seismograms. The RMS residual is 0.52 sec.

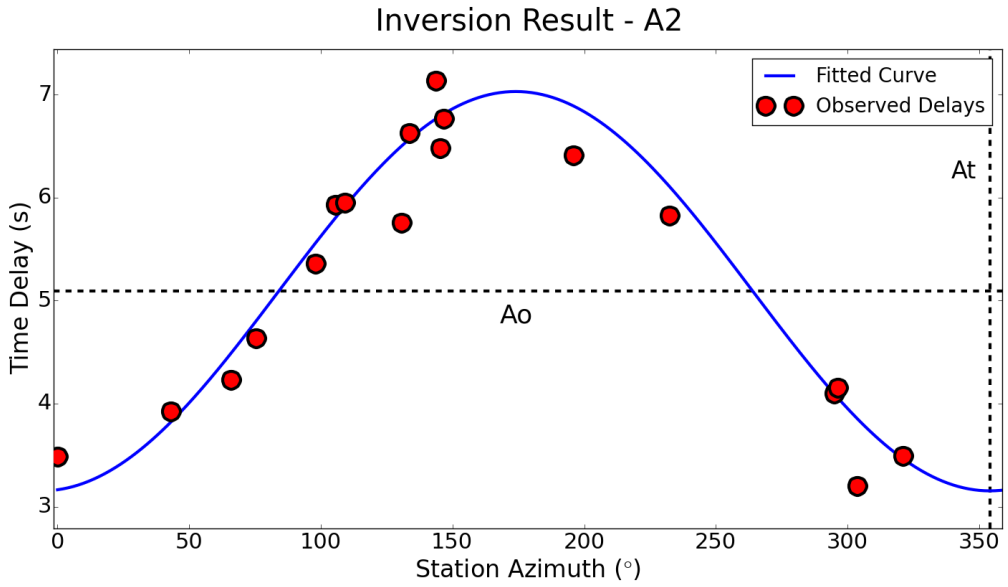

Figure 4.8: Fitted curve for the relative location of the aftershock 2. Good fit with small uncertainties (RMS residual= 0.32 sec).

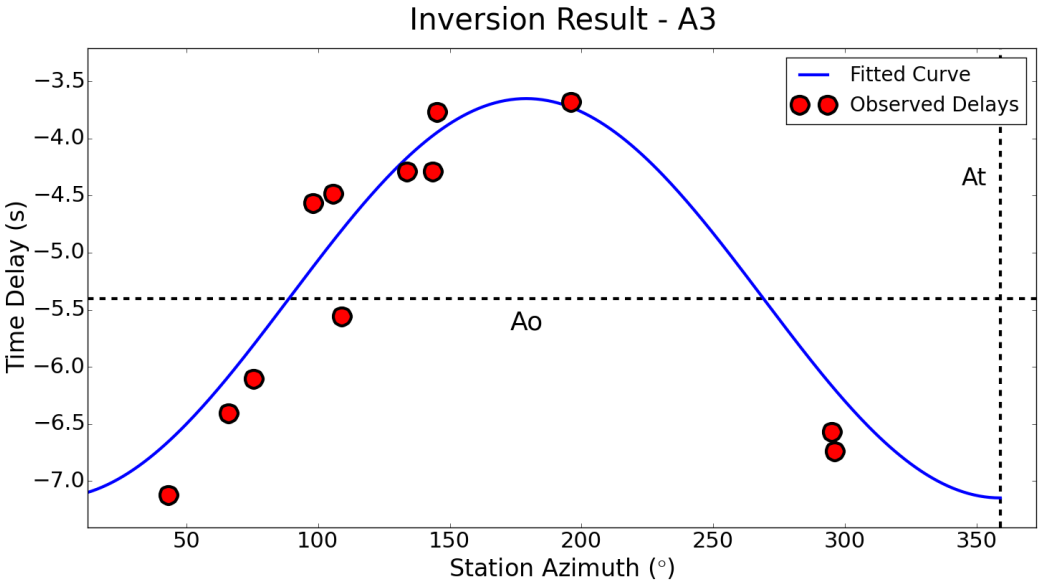

Figure 4.9: Fitted curve for the relative location os the aftershock 3. The RMS residual is 0.46 sec.

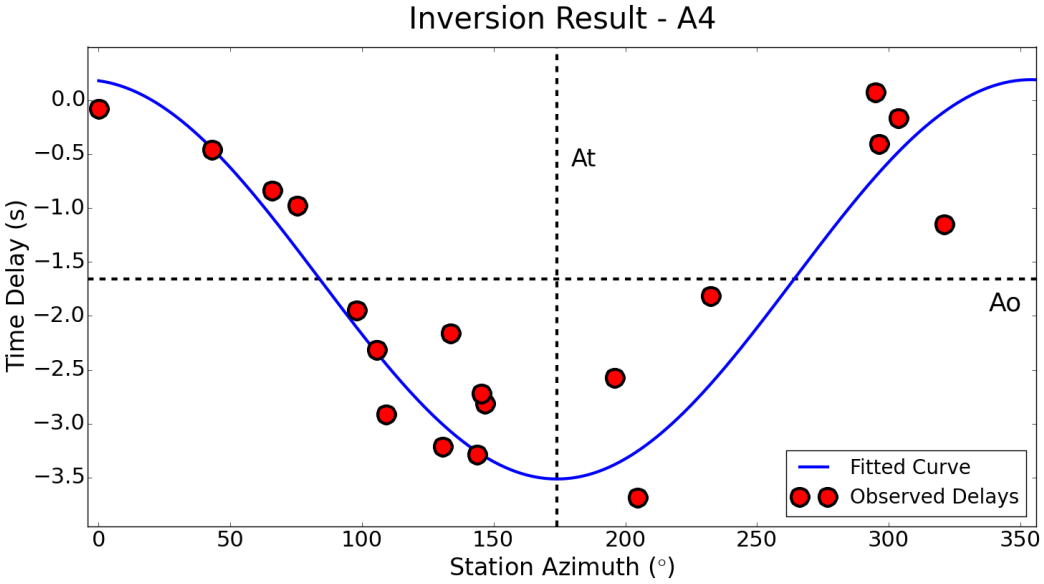

Figure 4.10: Fitted curve for the relative location of the aftershock 4. The RMS residual is 0.53 sec

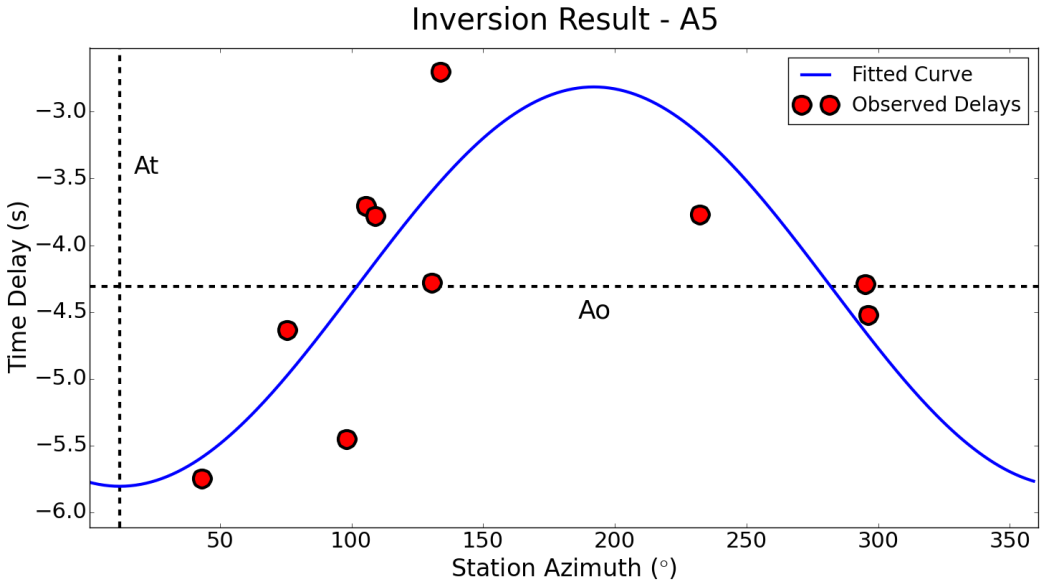

Figure 4.11: Fitted curve for the relative location of aftershock 5. Delay times does not fit very well with the curve, because this aftershock has a low magnitude and presents a low signal-noise ratio. The RMS residual is 0.70 sec.

The fitted curves of the Rayleigh-waves delays, for some aftershocks, are not well constrained because of low magnitude and poor signal-noise ratio. The best fittings were for large aftershocks.

In the case of aftershock A1, despite its large magnitude, it occurred two minutes after the mainshock. Because of that, the seismograms of all stations present overlapping signals, and it was difficult to isolate the Rayleigh waves of the event in most of them.

In all the inversions, the RMS residual is lesser than one second, an the uncertainties of the relative location are about 1 km. The maximum uncertainty was found in the inversion of the aftershock A1; because we used fewer stations than the others aftershocks, and there is a lack of stations with azimuths between 150° and 250°.

Table 4.5 shows the values obtained after the relative location and their respective uncertainties.

Table 4.5 - Result of the Rayleigh-wave relative location

Event	**Date**	**Time UTC**	**Magnitude (mb)**	**Parameters**				**Localization**		
				RMS	A_0 **(sec)**	**d (km)**	A_t **(°)**	**Long. (°W)**	**Lat. (°S)**	**Depth (∗)**
A1	2013-10-15	20:15:51	5.0	0.52 (sec)	2.94±0.30	6.96±2.024	359±23.5	63.317 ±0.020	18.481 ±0.007	21.0 km
A2	2013-10-15	22:00:32	4.4	0.32 (sec)	5.09±0.25	6.78±0.48	354±9.4	63.322 ±0.009	18.483 ±0.006	10.0 km
A3	2013-10-16	08:31:25	3.6	0.46 (sec)	-5.56±0.26	5.97±0.645	352±8.2	63.323 ±0.006	18.491 ±0.006	59.0 km
A4	2013-10-21	19:53:57	4.7	0.53 (sec)	-1.66±0.24	6.48±0.45	174±7.6	63.309 ±0.008	18.602 ±0.004	36.0 km
A5	2013-11-17	06:18:19	3.2	0.70 (sec)	-4.41±0.19	5.24±0.97	16±24.5	63.302 ±0.013	18.499 ±0.007	47.0 km

(∗) Depths were fixed at the original ISC value.

Figure 4.12 shows the final localization of the relocated events, where we can observe the N-S trend of the aftershocks relocated, agree with the fault plane solution given by GCMT (Table 2.1). Also, the maximum distance between events is of 14 km and does not agree with the expected subsurface rupture length according to Wells and Coppersmith (1994).

After the relative location, all the aftershocks placed closer to the mainshock. The aftershock A3 was the event which experimented greater displacement, moving approximately 28 km after the relative location. The final location of all events suggests that these event are aftershocks of Santa Cruz de la Sierra earthquake.

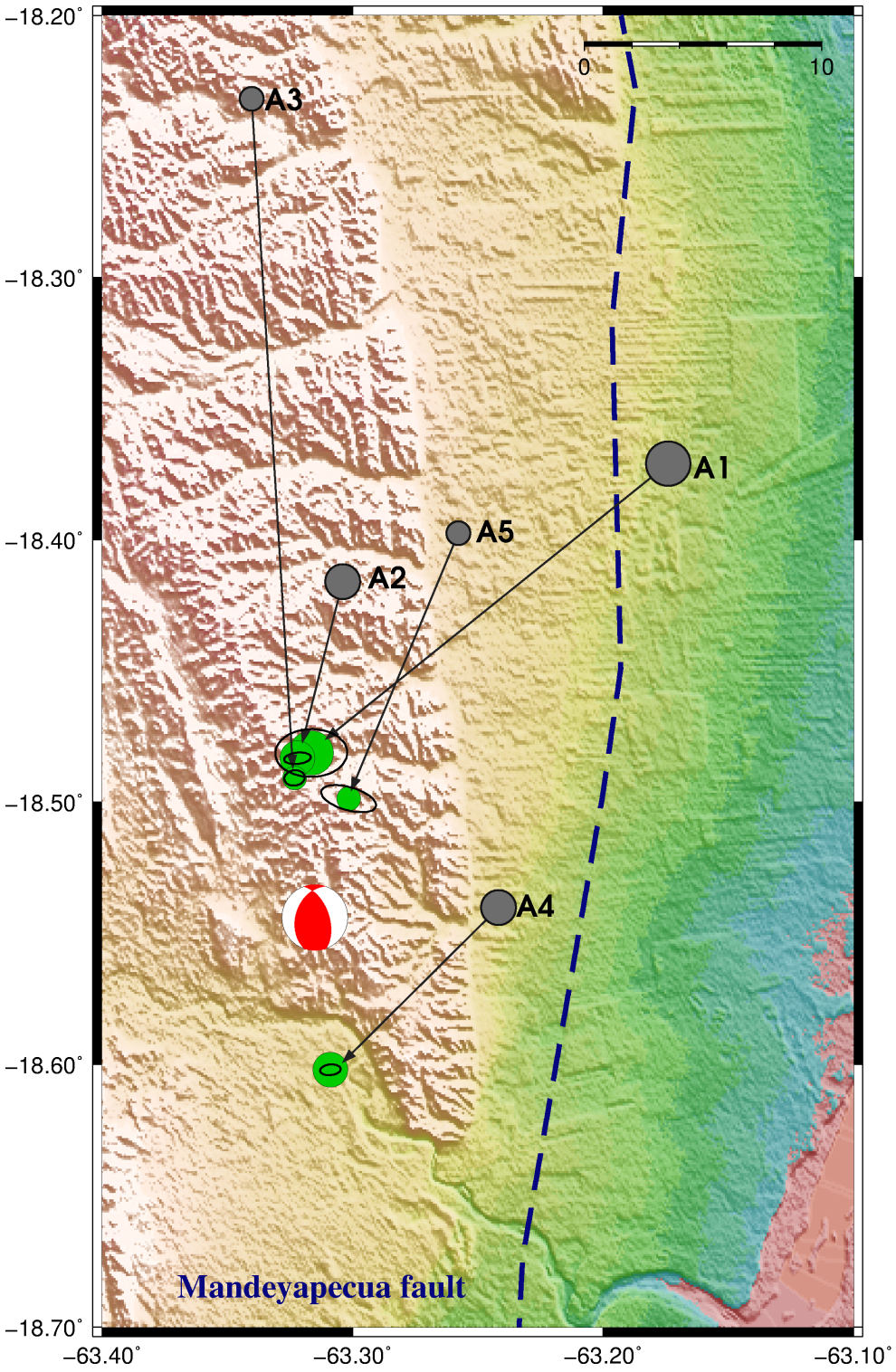

Figure 4.12: Beach ball is the mainshock used as reference event and nodal plane solutions given by GCMT catalog. Grey circles are the aftershocks before the relative location. Green circles indicate epicenters and magnitude of relocated aftershocks; black ellipse are error according to Table 4.5. Maximum distance between the aftershocks is 14 km and does not agree with the expected rupture fault length according to (Wells and Coppersmith, 1994). The location of the events shows a N-S trend, in agreement to the orientation of the nodal planes of the focal mechanism solution (Table 2.1).

Chapter 5

Relocation Using P- and S-Wave Correlated Arrivals

It was not possible to correlate the Rayleigh waves for the smaller aftershocks recorded by the San Calixto Observatory (OSC) because they did not present clear Rayleigh waves at 20 seconds period. Nevertheless, the surface waves provided a better sensitive in the location of earthquakes than the body waves (Cleveland and Ammon, 2013), if the P- and S-wave arrivals are well determined, and using a suitable velocity model we can achieve good results in the location.

5.1 Data

We selected eight aftershocks (Table5.1 and Figure 5.1) of the 33 recorded by the San Calixto Observatory (OSC), those present good signal-noise ratio. Three of these events, aftershocks 1, 4 and 8, were also registered by the ISC and were listed as A2, A3 and A4, respectively in Table 2.3.

Table 5.1 - Eight smallest aftershocks used to relative location

Event	**Date**	**Time UTC**	**Longitude (°W)**	**Latitude (°S)**	**Depth (km)**	**Magnitude (ML)**
1 (A2)	2013-10-15	21:59:31	63.1910	18.4730	55.0	4.00
2	2013-10-16	03:53:35	63.1740	18.5230	50.0	3.42
3	2013-10-16	04:01:53	63.1440	18.4940	46.0	3.37
4 (A3)	2013-10-16	08:31:22	63.1420	18.4720	34.0	3.71
5	2013-10-16	10:38:00	62.1780	18.4800	51.0	3.11
6	2013-10-16	12:53:04	63.1710	18.4740	40.0	3.21
7	2013-10-16	13:34:53	63.1750	18.5120	48.0	3.41
8 (A4)	2013-10-21	19:53:57	63.1700	18.5300	59.0	4.57

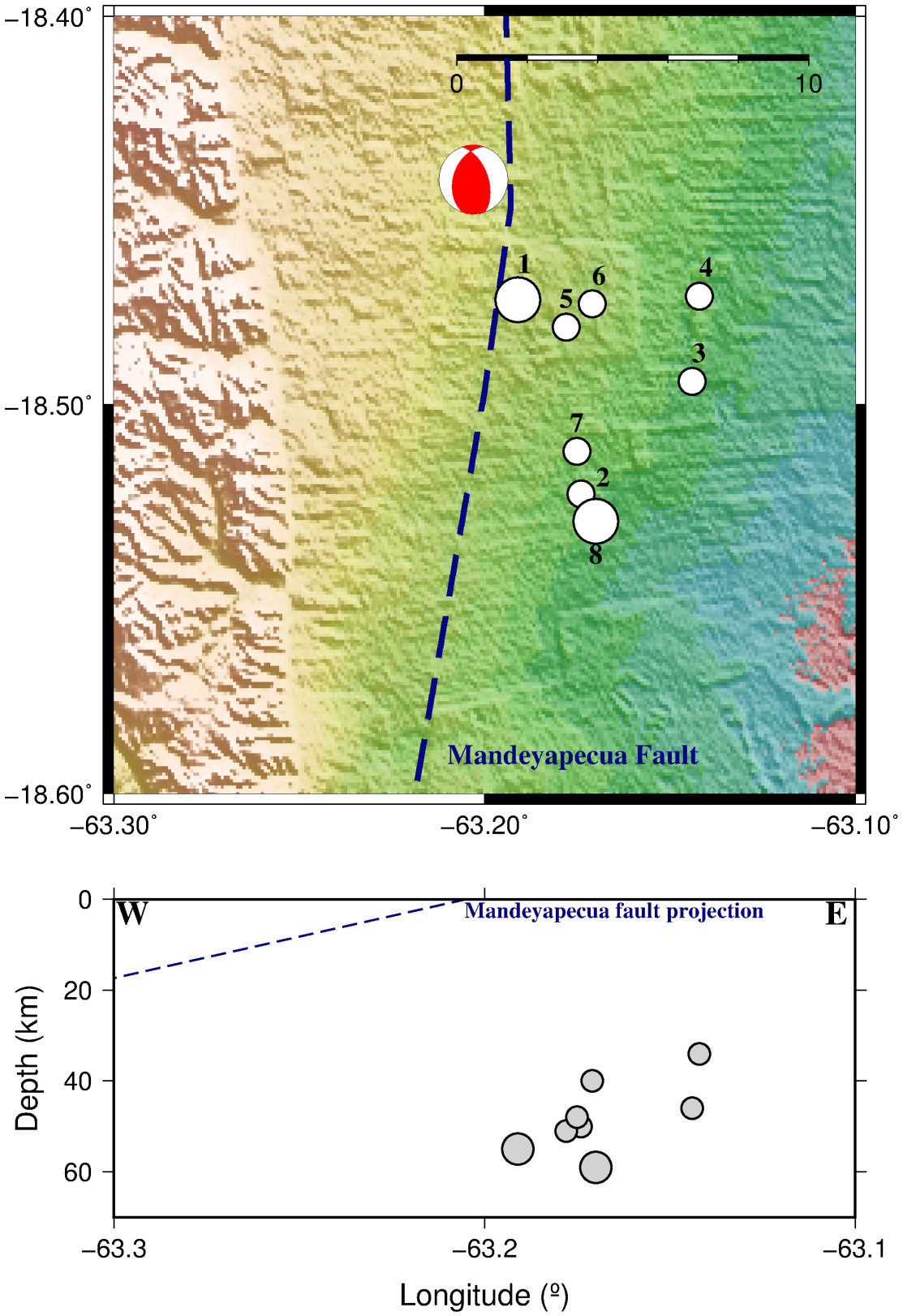

Figure 5.1: Beach ball represents the mainshock reported by San Calixto Observatory (OSC) and white circles are the eight aftershocks registered by OSC and selected for relative location. The profile depth suggest a W dipping, however the hypocenters are away from the Mandeyapecua fault projection (Lavenu et al., 2000).

The data used to relocate the eight aftershocks recorded by San Calixto Observatory (OSC) by correlation of the P and S wave was from three stations of the national network of Bolivia, including LPAZ station. Table 5.2 and Figure 5.2 show the information of these stations.

Table 5.2 - Stations used to relative location with P- and S-wave correlated arrivals

Network	**Stations**	**Localization**			**Epicentral**
		Longitude	**Latitude**	**Country**	**distance**
GT	LPAZ	68.13°W	16.29°S	Bolivia	581.45 km
BO	MOC	65.64°W	21.25°S	Bolivia	400.59 km
	SIV	61.07°W	15.99°S	Bolivia	355.35 km

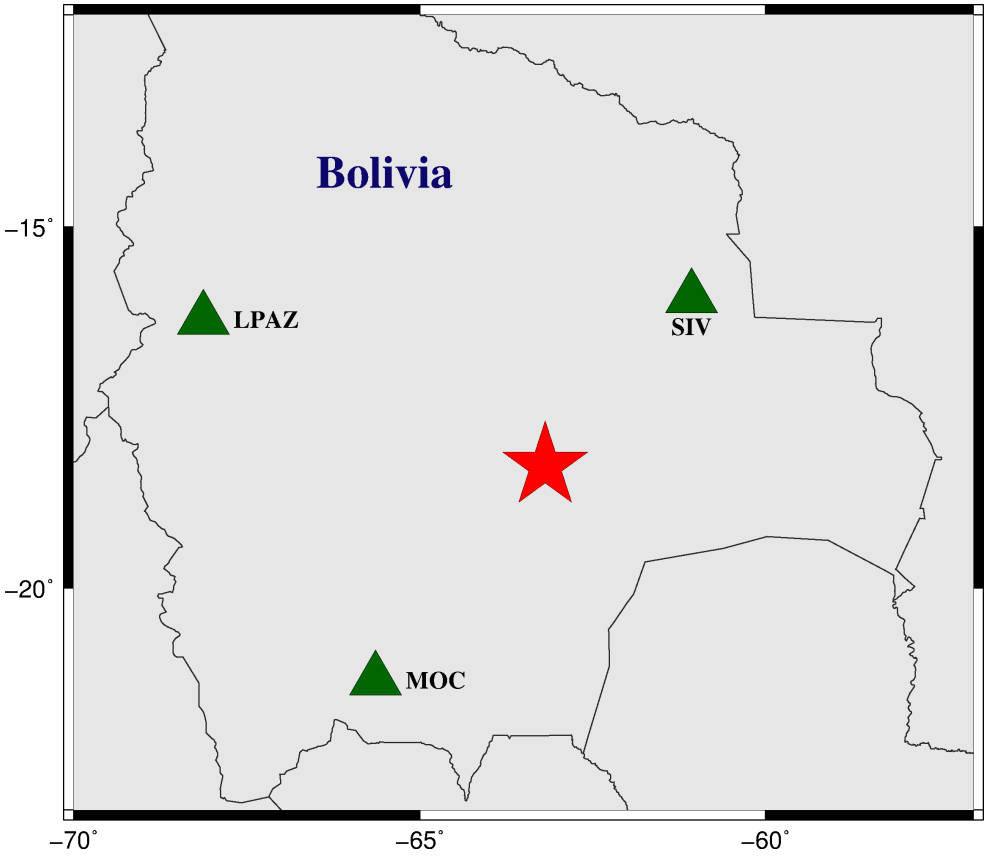

Figure 5.2: Santa Cruz de la Sierra earthquake (red star) and stations (triangles) used in the relative location. MOC and SIV are stations of the Bolivian network; also we used LPAZ station of the international network.

5.2 Methodology

We determined the arrival time of the P wave in the vertical component of the seismograms, and the arrival of S wave in the transverse components. In order to recognize the P- and S-wave arrivals we filtered the signal, using the same filter for each station and phase, as shown Table 5.3. At MOC station it was not possible to recognize the S-wave arrival, due to the low signal-noise ratio; thus, this phase was not used in the relocation.

Table 5.3 - Filters

Phase	**SIV**	**MOC**	**LPAZ**
P	1-2 Hz	2-4 Hz	2-4 Hz
S	1-2 Hz	NA	1-2 Hz

In this case, we did not use the mainshock as reference event because its waveform was very different from that of the aftershocks. In order to do a correlation and relative location we used the aftershock A4, relocated with Rayleigh wave correlation, as reference event (Table 4.5 Figure 4.12). This event was also registered by the San Calixto Observatory and is listed as event 8 in Table 5.1.

The correlation of the P- and S-wave arrivals was performed manually, in order to improve the accuracy of arrival times in both phases. Figure 5.3 shows the P- and S-wave correlated arrivals for LPAZ station.

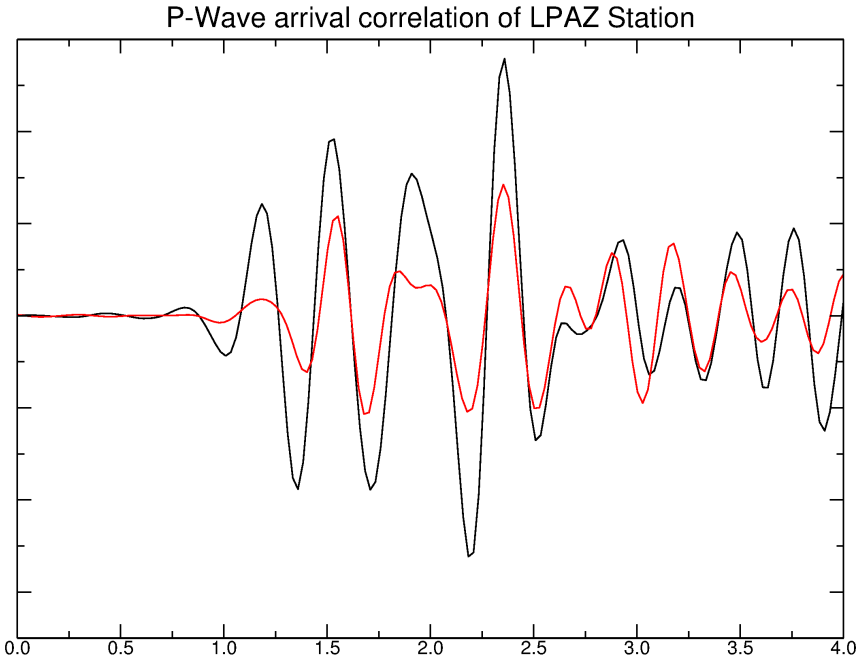

(a)

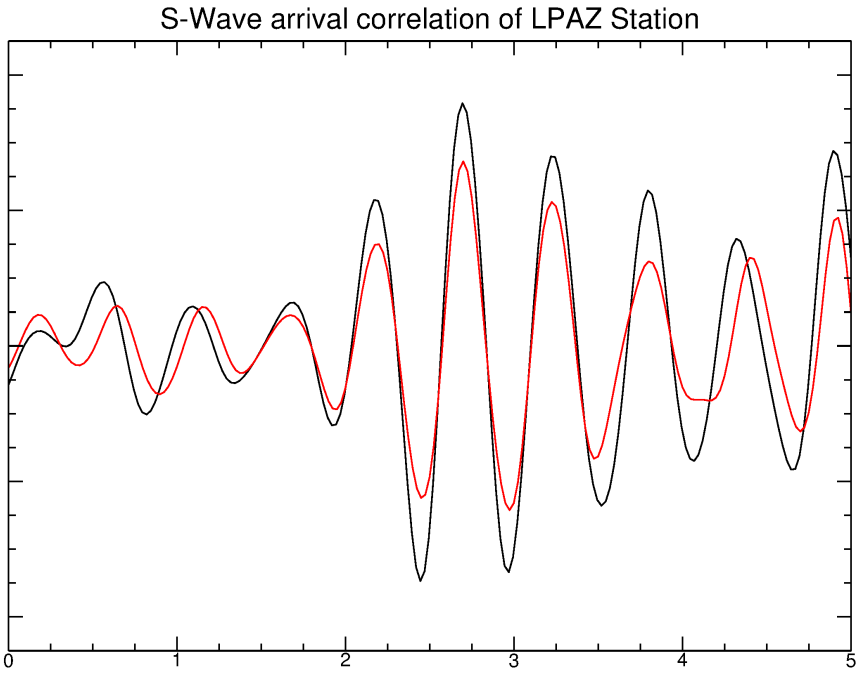

(b)

Figure 5.3: Correlated P- and S-wave arrivals at LPAZ station. Black seismograms are the reference event (8 in Table 5.5) and red seismograms are the target event (7 in Table 5.5). (a) P-wave correlation and (b) S-wave correlation. Both phases present high correlation.

To relocate the epicenters of the aftershocks we use the Hypocenter software that was developed by Lienert (1994). This software is a Fortran Program for locating local, regional and global earthquakes. The last release is capable of locating local events using a layered velocity model, or global events using IASP91, which is a parameterised velocity model that was constructed to be a summary of the travel time characteristics of the main seismic phases (Kennett and Engdahl, 1991).

In the Hypocenter program we used a regional distance indicator and fixed the depth of the reference event at 15 km; because we had not certainty of the depth of the events, but we know that the events occurred in the upper crust according to International Seismological Centre (2013b). We used the layered velocity model for the crust and upper mantle developed by Masson et al. (2000) and (Beck and Zandt, 2002) for the Bolivian Central Andes, shown in Table 5.4.

Masson et al. (2000) used arrival times of P and S waves of 280 local earthquakes from local earthquakes recorded by a temporary seismic network installed crossing the whole Andean chain, to obtain a local earthquake tomography, and the P- and S-wave velocity models. In the final model, the standard deviation within each layer is about 0.20 km/s for P wave. Also the final model shows layers of 30 km, and according to (Rocha and Cristallini, 2015) in the subandean zone there is a sediment layer of 10 km.

To consider the sediment layer, we used the P-wave velocity models for the crust developed by (Beck and Zandt, 2002). They determined their models from receiver function of 12 teleseismic earthquakes and five deep regional earthquakes recorded on the portable seismic networks to investigate the crustal structure in the central Andes from 1994 to 1995, for stations in the lower elevations of the Eastern Cordillera, sub-Andean zone and Chaco.

Table 5.4 - Velocity model used to relocate events

Layer	**Depth**	**Average Vp (km/s)**
1	0	5.00
2	10	6.20
3	30	6.84
4	60	8.06

5.3 Results

The relocated epicenters and depths of the aftershocks using the P- and S-wave correlated arrivals are shown in Table 5.5, which also includes relocated depth.

Figure 5.4 presents the relocation of aftershocks recorded by the OSC, using P- and S-wave correlated arrivals. The results show a N-S trend, and a maximum distance between them up to 14 km. Two of the seven events relocated using P- and S-wave arrivals (1 and 4) were also registered by the ISC and relocated using correlated Rayleigh waves (A2 and A3), showing differences in the epicentral location of one km between both relocation methods; demonstrating that our results are reliable.

After the relocation the shift of the depths of all events was significant, all depths are located shallower than 21 km. Also, we can observe that the initial trend in the depth profile was W dipping (Figure 5.1), and after the relative location the depth profile suggests an E dipping, and the hypocenters are away of the Mandeyapecua fault projection. Figure 5.5 shows the depth profile of the relocated events and the uncertainties obtained.

Table 5.5 - Result of the location by correlation of P- and S-wave arrivals

Event	**Date**	**Time UTC**	**Magnitude ML**	**Longitude (°W)**	**Latitude (°S)**	**Depth (km)**	**Error X (km)**	**Error Y (km)**	**Error Z (km)**	**RMS (sec)**
1 (A2)	2013-10-15	22:59:31	4.0	63.321	18.476	12.3	2.0 km	3.7 km	7.3 km	0.126
2	2013-10-16	03:53:35	3.4	63.289	18.595	20.2	1.7 km	3.1 km	6.0 km	0.073
3	2013-10-16	04:01:53	3.4	63.283	18.522	11.9	2.2 km	4.0 km	7.9 km	0.145
4 (A3)	2013-10-16	08:31:22	3.7	63.323	18.479	7.5	1.5 km	2.6 km	3.4 km	0.013
5	2013-10-16	10:38:00	3.1	63.278	18.553	15.4	1.6 km	2.7 km	5.5 km	0.041
6	2013-10-16	12:53:04	3.2	63.293	18.520	16.0	2.1 km	3.6 km	7.3 km	0.126
7	2013-10-21	13:34:53	3.4	63.292	18.606	20.7	2.0 km	3.4 km	6.9 km	0.112
(∗)8 (A4)	10-22-2013	19:53:57	4.6	63.309	18.602	15.0	1.1 km	1.6 km	0 km	0.001

(∗) = Reference event, epicenter from Table 4.5.

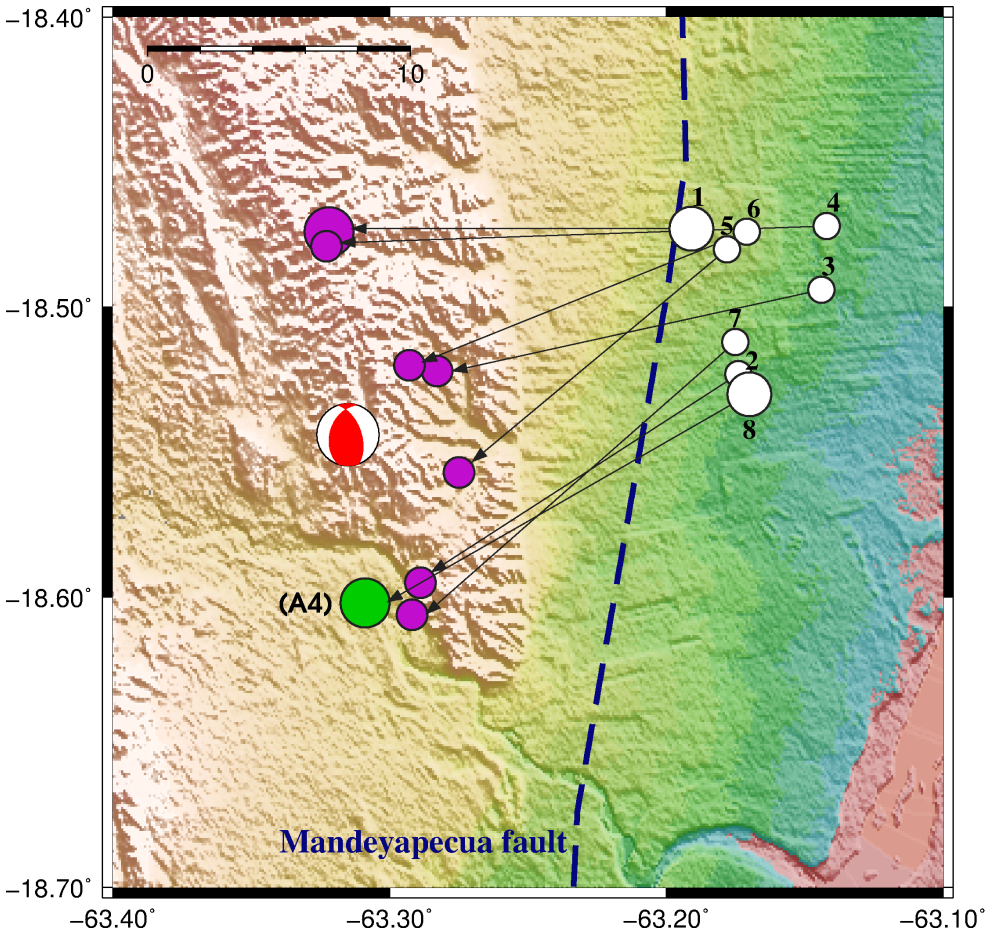

Figure 5.4: Beach ball represents the mainshock used as reference event in the relative location with Rayleigh waves. Green circle is the aftershock (A4) relocated with Rayleigh wave and used as reference event in the location of the other seven OSC aftershocks. White circles are the initial location of the aftershocks given by OSC and purple circles are the relocated events. Maximum distance between the relocated targets is 14 km and does not agree with the expected subsurface rupture fault length according to Wells and Coppersmith (1994).

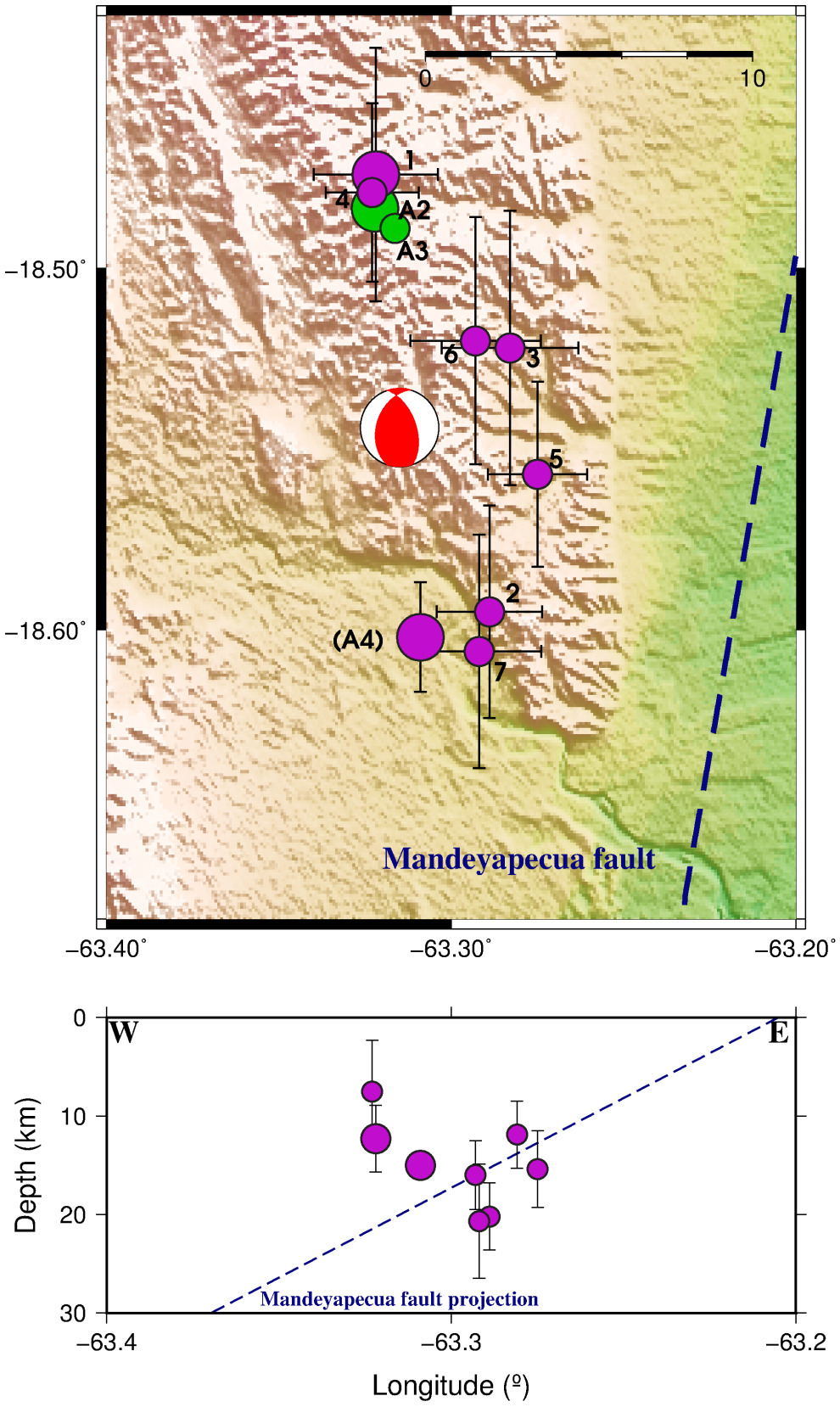

Figure 5.5: Beach ball represents the mainshock used as reference event in relocation with Rayleigh waves. Green circles are the epicenters of A2 and A3 relocated with Rayleigh waves and are the same events named as aftershocks 1 and 4 by OSC (Table 5.5). Aftershocks relocated through correlation of P- and S-wave arrivals (purple circles). Depth profile of the smaller relocated aftershocks shows an E dipping trend.

Chapter 6

Discussion

Distances between the aftershocks relocated using Rayleigh waves, are up to 14 km. The uncertainties of all the parameters calculated by this technique are low, of the order of ± 1 km, which makes the 14 km rupture length a reliable measure. Maximum distance between the relocated aftershocks by P- and S-wave correlated arrivals is also 14 km, with uncertainties of the order of ± 4 km. This value is larger than the expected subsurface rupture length (RLD) proposed by Wells and Coppersmith (1994), which is RLD=2 to 10 km for an earthquake of 5.2 Mw.

Taking into account a magnitude uncertainty of the mainshock of 0.1 Mw, the maximum size of the subsurface rupture for a 5.3 Mw earthquake, according to Wells and Coppersmith (1994) would be 11 km. This value is still less than the rupture length we estimated with the relative location of the aftershocks.

All aftershocks, after the relocation, are placed within a range of 14 km, which would correspond to an earthquake of 6.1 ±0.6 Mw according to Wells and Coppersmith (1994). The variation of the magnitude between the value reported by the ISC (5.2 Mw) and the value obtained by the relationship of subsurface rupture length and magnitude (6.1 ±0.6 Mw), proposed by (Wells and Coppersmith, 1994), is large.

In the relative location using P and S waves it was possible to determine the depth of the events, which indicates a possible E dipping rupture plane, opposite to the W dipping of the events before to the relative location. Although the trend of the dip is not well constrained, the NNW-SSE orientation of the aftershocks agrees with the E dipping plane of the fault plane solution (plane 2 in Table 2.1).

The two events that were registered also by ISC (A2 and A3) and by OSC (event 1 and 4), and were relocated by Rayleigh wave correlation and body wave correlation respectively, show a difference of 1 km in their epicentral location between both techniques, which is within the uncertainties of methods; demonstrating that both methods are reliable.

The shift in the depth of the smaller aftershocks relocated is large, 40 km in average. It is because we fixed the depth of the reference event at 15 km, despite the depths reported by the OSC were close to 60 km of all events. We selected 15 km as reference event depth due to the Santa Cruz de la Sierra earthquake occurred in the upper crust. The depth reported by NEIC (2.2) for the mainshock was of 35 km, which was also fixed.

Based on the location of the aftershocks (Figure 5.5), it seems that the mainshock released all stresses in the central part of the rupture, while the aftershocks occurred at the edges. Considering 14 km as a size of the subsurface rupture, we estimated the stress drop for Santa Cruz de la Sierra earthquake using the theoretical equation below for a circular fault (e.g. Allmann and Shearer, 2009).

$$\triangle\sigma = \frac{7}{16} \times (\frac{M_0}{r^3}) \tag{6.1}$$

where:

- M_0: Seismic moment
- r: Source radius, we used 7 km.

The calculated stress drop is about 0.1 MPa.

Allmann and Shearer (2009) estimated the stress drop of about 2000 global events, finding an overall average of 4 MPa that does not vary with moment or magnitude i the range 5.2 to 8.3 Mw. Also they concluded that the median stress drop varies with the tectonic environment, being higher than the average for intraplate earthquakes. On the other hand, the few Bolivian sub-Andean events analyzed by Allmann and Shearer (2009) seem to have slightly lower stress drops (about 2 MPa)than the global average.

The value of stress drop which we estimated (0.1 MPa) is much lower than the global average (4 MPa) and also lower than the value observed previously in the Bolivian sub-Andean zone (2 MPa), which shows that the Santa Cruz de la Sierra earthquake is an anomalous event.

The relocation of the earthquake of Salta Province in Argentina, using *iLoc* program with P-wave arrivals of stations up 90° and correction with RSTT model for stations up to 15° , shows good results regarding to well known epicenter location given by the Argentinean National Network (INPRES). This demonstrate that the epicenter location obtained with this method is reliable.

The location of the Santa Cruz de la Sierra earthquake with *iLoc* program and RSTT model and the relative location of all aftershocks place all the events away from the Mandeyapecua fault. Besides, the relocated aftershocks recorded by the OSC show an E dipping fault, opposite to the W dip of Mandeyapecua fault. Then, we can conclude that these events were not generated by this fault and must have occurred on some other fault that has not been well studied yet. Unfortunately we can not suggest one fault or lineament of the Figure 3.3, because that map is referential and has not a good accuracy of the fault locations.

The isoseismal map performed by the OSC (2.2) shows that the place where the greatest intensity of the Santa Cruz de la Sierra earthquake was felt is located away of the Mandeyapecua fault, being consistent with the results achieved with the mainshock relocation using *iLoc* algorithm and the RSTT model.

Chapter 7

Conclusion

The relative location of the five larger aftershocks using Rayleigh waves and the eight smaller events using P and S waves show the same result: a NNW-SSE trend, in agreement with the East dipping nodal plane of the focal mechanism shown by the GCMT catalog.

Distances between the aftershocks, in both techniques of relative location, are up to 14km. This value is larger than expected with the relationship between magnitude and subsurface rupture length proposed by Wells and Coppersmith (1994), for an earthquake of 5.2 Mw magnitude.

Relocation with Rayleigh waves is a useful technique, and epicenter uncertainties better than 1 km can be achieved. While relocation with correlated P- and S-wave at regional distances showed accuracies better than 4 km.

The depth profile of the smaller aftershocks shows an E dipping fault, demonstrating that the nodal plane of the events is the number 2 shown in Table 2.1 (Strike 341, east dipping plane). This confirms the focal mechanism proposed by the GMCT agency (Table 2.1).

The absolute epicenters of the mainshock, determined with the 3-D RSTT model, and the located aftershocks are far of the Mandeyapecua fault, and show a probable E dipping trend. With this information we conclude that the W-dipping Mandeyapecua fault did not cause these events. In this area there are many other faults, which have not been well studied yet, and it is likely that one of those faults may have generated the Santa Cruz de la Sierra earthquake and its aftershocks.

In the future, it is recommendable to continue studying the fault geometry of the events in order to improve the seismotectonic knowledge of the eastern area of the Central Andes of Bolivia. As we observed in the seimicity map, one earthquake of 5.0 mb occurred at least once each year, studying these events it could improve the information that already exist about the active faults in the area.

If we have a better knowledge about the active faults and their activity, it is possible improve the map of seismic hazard of Bolivia, this tool may be helpful for the Bolivian population, as they may better prepare for future events and minimize possible damage in the cities or communities close to the active faults, with implications for seismic hazard estimates. .

Bibliography

Allmann, B. and Shearer, M. (2009). Global variations of stress drop for moderate to large earthquakes. *Journal of Geophysical Research*, 114:BO1310.

Beck, S. and Zandt, G. (2002). The nature of orogenic crust in Central Andes. *Journal of Geophysical Research*, 107.

Bondár, I., Myers, S., Engdahl, R., and Bergman, A. (2004). Epicentre accuracy based on seismic network criteria. *Geophysical. J. Int*, 156:483–496.

Bondár, I. and Storchak, D. (2011). Improved location procedures at the International Seismological Centre. *Geophysical Journal International*, 186:1220–1244.

Brooks, B., Bevis, M., Whipple, K., Arrowsmith, R., Foster, J.and Zapata, T., Kendrick, E., Minaya, E., Echalar, A., Blanco, M., Euillades, P., Sandoval, M., and Smalley, R. (2011). Orogenic-wedge deformation and potential for great earthquakes in the central Andean backarc. *Nature Geoscience*, 4.

Chiu, F. and Snyder, B. (2014). Regional seismic wave propagation (Lg and Sn phases) in the Amerasia Basin and high Artic. *Polar Science*.

Ciardelli, C. and Assumpcao, M. (2015). Relative epicentral location with cross-correlation of surface waves: application to studies of faulting evolution in four Brazilian earthquake sequences. *XV SNET*.

Cleveland, M. and Ammon, C. (2013). Precise relative earthquake location using surface waves. *Journal of Geophysical Research: Solid Earth*, 118:2893–2904.

Devlin, S., Isacks, B., Pritchard, M., Bamharth, W., and Lohman, R. (2011). Dephts and focal mechanisms of crustal eathquakes in the Central Andes determined from telesismic waveform analysis ans inSaR. *Tectonics*, 31:1–33.

Eichlberger, N., McQuarrie, N., Ryan, J., bobak, K., Beck, S., and Zandt, G. (2015). Evolution of crustal thickening in the central Andes, Bolivia. *Earth and Planetary Science Letters*, 45:191–203.

Funning, G., Barke, R., Lamb, S., Minaya, E., Parsons, B., and Wright, T. (2005). The 1998 Aiquile, Bolivia earthquake; A seismically active fault revealed with inSAR. *Earth and Planetry Science Letters*, 232:39–49.

Gallegos, A., Ranasinghe, N., and Sandovl, E. (2014). Lg attenuation in the central and eastern United states as revealed by the Earthscope Transportable Array. *Earth and Planetary Science*, 402:187–196.

Gregory-Wodzicky, K. (1999). Uplift history of the Central and Northern Andes: A review. *Geological Society of America Bulletin*.

Hermman, R. and Ammon, C. (2002). Computer program in seismology: Surface Waves, Receiver Functions and Crustal Structure. Technical report, Department of Earth and Atmospheric Sciences, Saint Louis University.

International Seismological Centre (2013a). EHB Bulletin, http://www.isc.ac.uk. Technical report, Internatl. Seis. Cent., Thatcham, United Kingdom.

International Seismological Centre (2013b). Reference Event Bulletin, http://www.isc.ac.uk. Technical report, Internatl. Seis. Cent., Thatcham, United Kingdom.

Kennett, B. and Engdahl, E. (1991). Traveltimes for global earthquake location and phase identification. *Geophysical Journal International*, 105:429–465.

Lavenu, A., Thiele, R., Machette, M., Dart, R., Bradley, L., and Haller, K. (2000). Maps and Database of Quaternary Faults in Bolivia and Chile. Technical report, U.S.Geological Survey.

Lienert, B. (1994). Hypocenter 3.2, A Computer Program for Locating Earthquakes Locally, Regionally and Globally. Technical report, Hawaii Institute of Geophysics and Planetology.

Martinod, J., Husson, L., Roperch, P., Guillaume, B., and Espurt, N. (2010). Horizontal subduction zones, convergence velocity and the building of the Andes. *Earth and Planetary Science Letters*, 299:299–309.

Masson, F., Dorbath, D., Martinez, C., and Carlier, G. (2000). Local Earthquake tomography of the Andes at 20S: Implications for the structure and building of the mountain range. *Journal of South American Earth Science*, 3:3–19.

McQuarrie, N., Horton, B., Zandt, G., Beck, S., and DeCelles, P. (2005). Lithospheric evolution of the Andean fold-thrust belt, Bolivia, and the origin of the Central Andean plateu. *Tectonophysics*, 399:15–37.

Myers, S., Begnaud, M., Ballard, S., Pasyanos, M., Phillips, W., Ramirez, A., Antolik, M., Hutchenson, K., Dwyer, J., Rowe, C., and Wagner, G. (2010). A Crust and Upper-Mantle Model of Eurasia and North Africa for Pn Travel-Time Calculation. *Bulletin of the Seismological Society of America*, 100:640–656.

Observatorio San Calixto (2012). Amenaza Sísmica y Volcánica en Bolivia. Technical report, Observatorio San Calixto.

Observatorio San Calixto (2013). Actividad Sśmica en la Provincia Cordillera - Departamento de Santa Cruz. Technical report, Observatorio San Calixto.

Rocha, E. and Cristallini, E. (2015). Controls on structural styles along the deformation front of the Subandean zone of southern Bolivia. *Journal of Structural Geology*, 73:83–96.

Sanchéz, G., Recio, R., Marcuzzi, O., Moreno, M., Araujo, M., Navarro, C., Suárez, J., Havskov, J., and Ottemoller, L. (2013). The Argentinean National Network of Seismic and Strong-Motion Stations. *Seismological Research Letters*, 84(5):729–736.

Servicio Nacional de Geología y Técnico de Minas (2000a). Mapa de Fallas Geológicas de Bolivia. Technical report, Servicio Nacional de Geología y Técnico de Minas SERGEOTECMIN.

Servicio Nacional de Geología y Técnico de Minas (2000b). Mapa Geológico de Bolivia. Technical report, Servicio Nacional de Geología y Técnico de Minas SERGEOTECMIN.

Vega, A. and Buforn, E. (1991). Focal Mechanism of Intraplate Earthquakes in Boliva, South America. *Pure and Applied Geophysics*, 136(4).

Ward, K., Porter, R., Zandt, G., Beck, S., Wagner, L., Minaya, E., and Tavera, H. (2013). Ambient noise tomography across the Central Andes. *Geophysical Journal International*, 194:1559–1573.

Wells, D. and Coppersmith, K. (1994). New Empirical Relationships among Magnitude, Rupture Length, Rupture Width, Rupture Area, and Surface Discplacement. *Bulletin of Seismological Society of America*, 84:972–1002.

Wigger, P., Schmitz, M., Araneda, M., Asch, G., Baldzuhn, S., Giese, P., Heinsohn, W., Martinez, E., and Ricaldi, E. (1994). Variation in the Crustas Structure of the Southerns Central Andes Deduced from Seismic Refraction Investigations. *Tectonics of the Southern Central Andes*, pages 22–48.

Appendix

Appendix A

Match-filtering of the larger aftershocks

A.1 AQDB Station

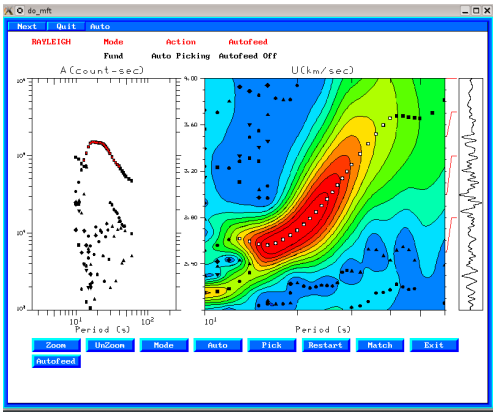

Figure A.1: Mainshock

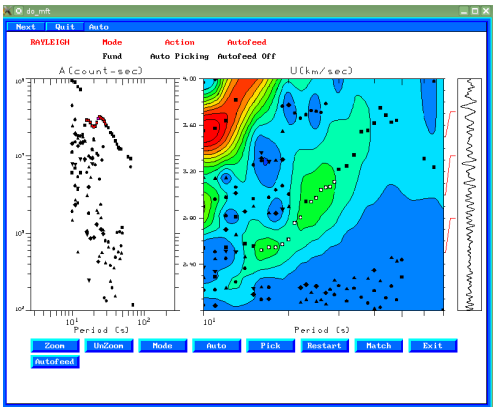

Figure A.2: Aftershock 1

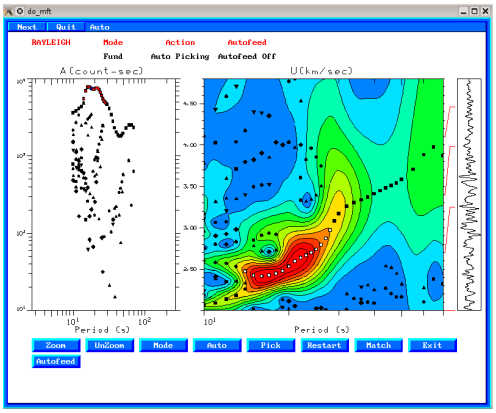

Figure A.3: Aftershock 2

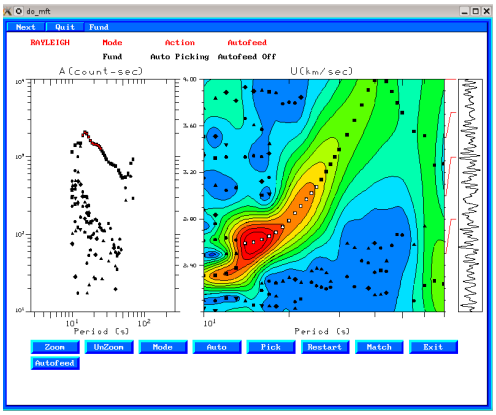

Figure A.4: Aftershock 3

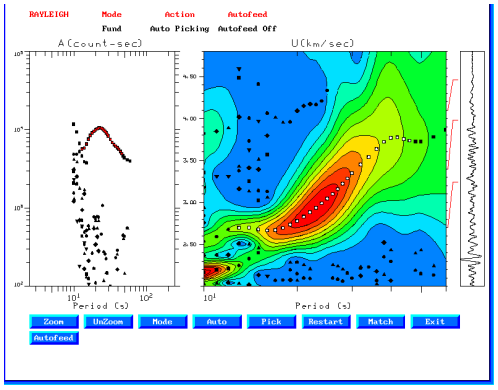

Figure A.5: Aftershock 4

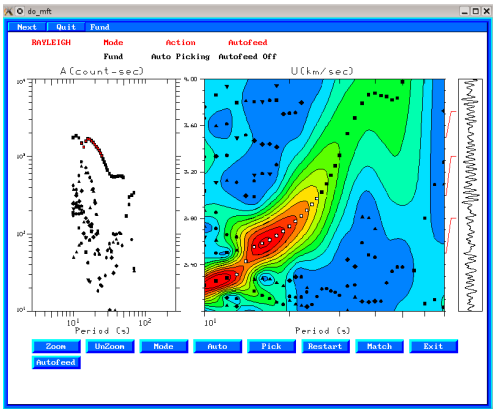

Figure A.6: Aftershock 5

A.2 BSCB Station

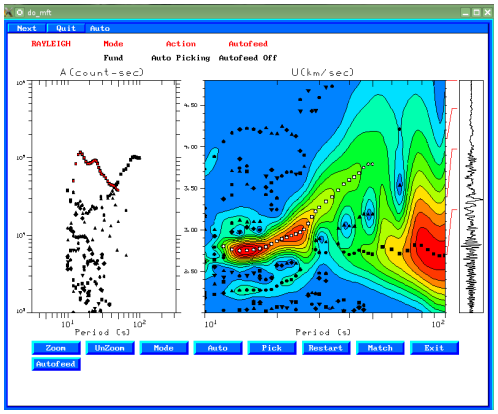

Figure A.7: Mainshock

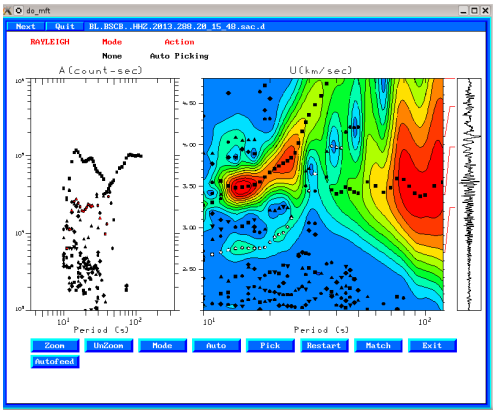

Figure A.8: Aftershock 1

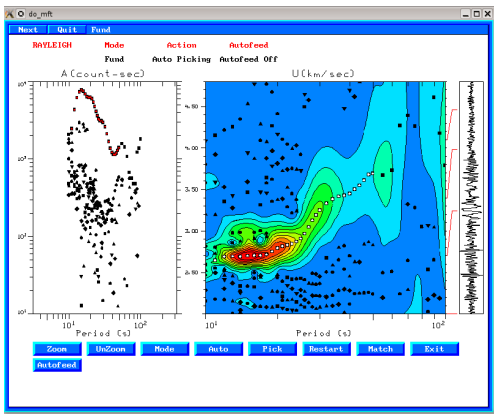

Figure A.9: Aftershock 2

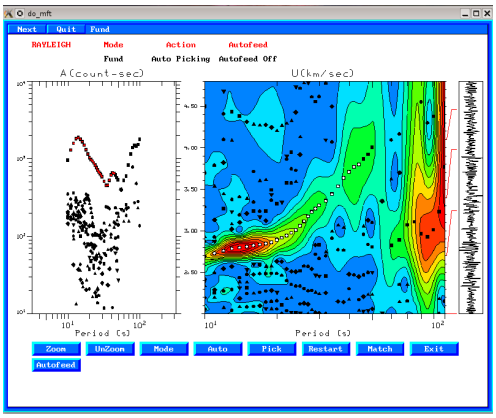

Figure A.10: Aftershock 3

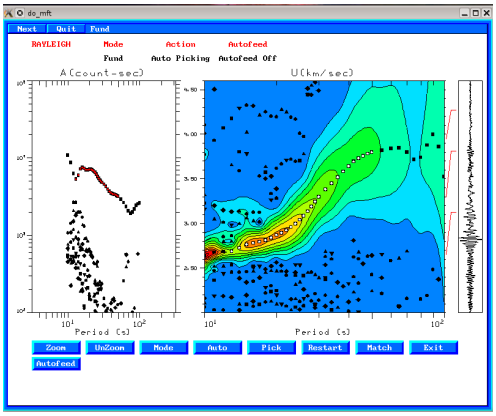

Figure A.11: Aftershock 4

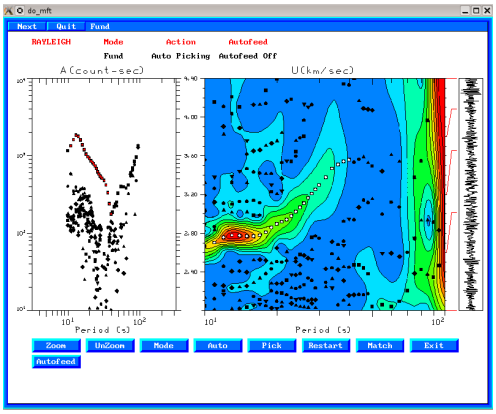

Figure A.12: Aftershock 5

A.3 CLDB Station

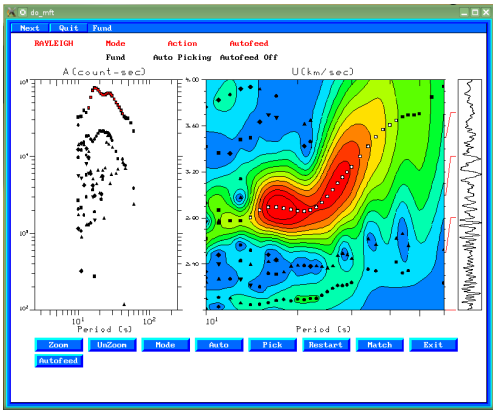

Figure A.13: Mainshock

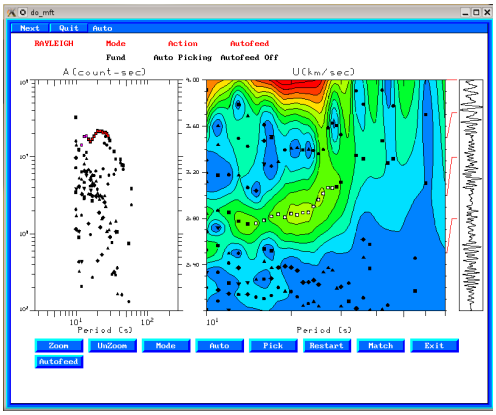

Figure A.14: Aftershock 1

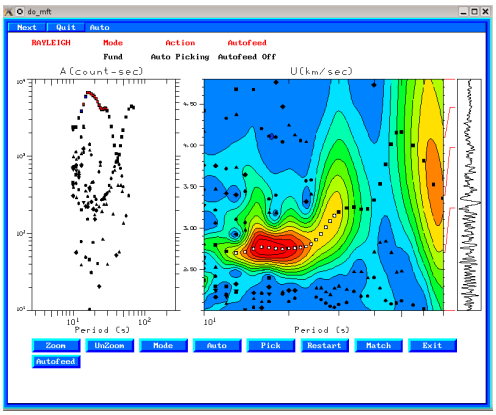

Figure A.15: Aftershock 2

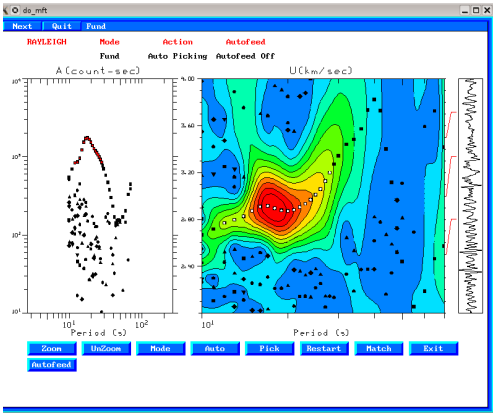

Figure A.16: Aftershock 3

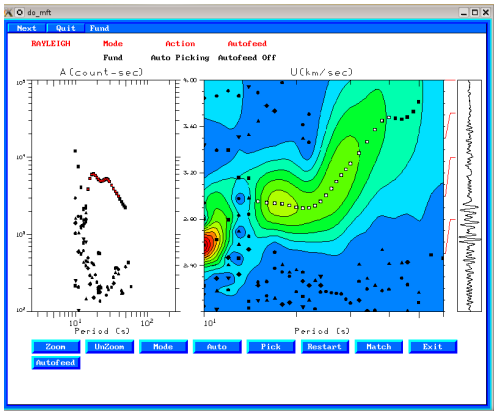

Figure A.17: Aftershock 4

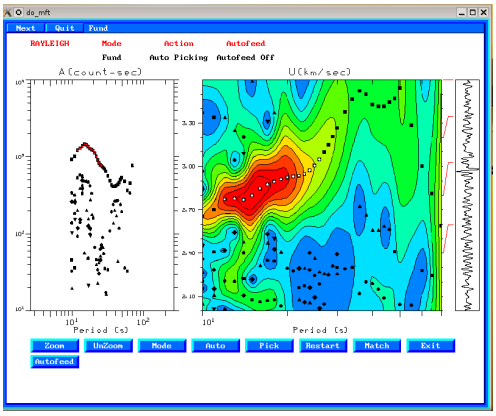

Figure A.18: Aftershock 5

A.4 CNLB Station

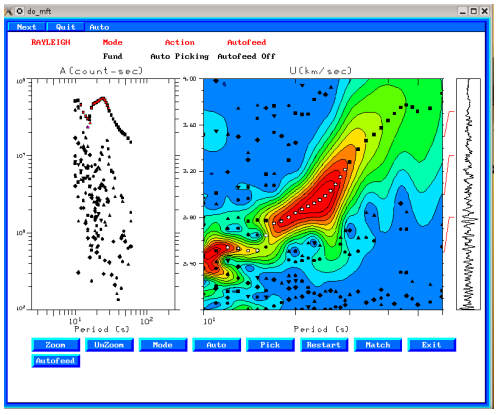

Figure A.19: Mainshock

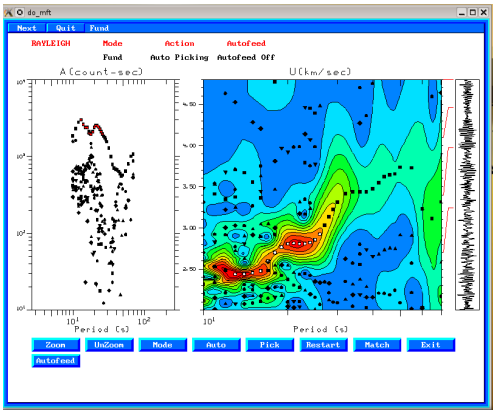

Figure A.20: Aftershock 2

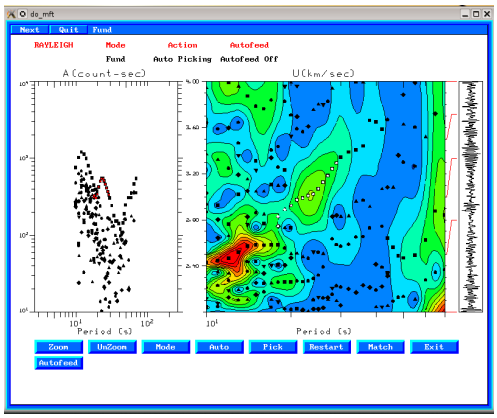

Figure A.21: Aftershock 3

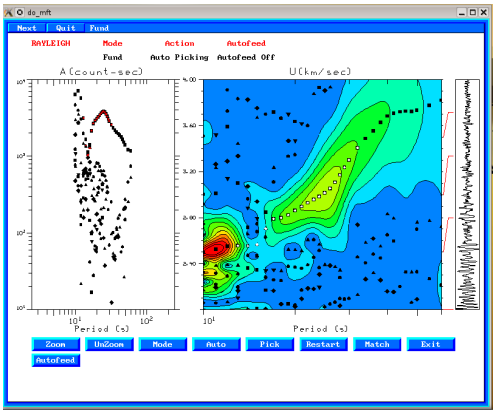

Figure A.22: Aftershock 4

A.5 CPSB Station

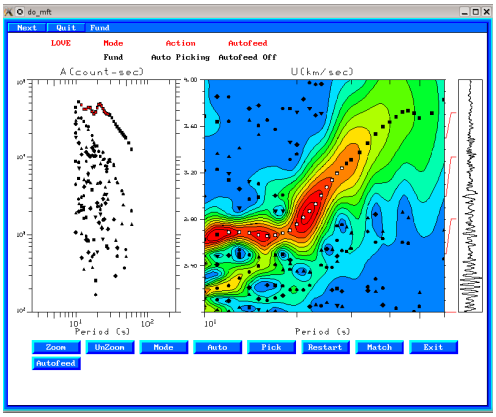

Figure A.23: Mainshock

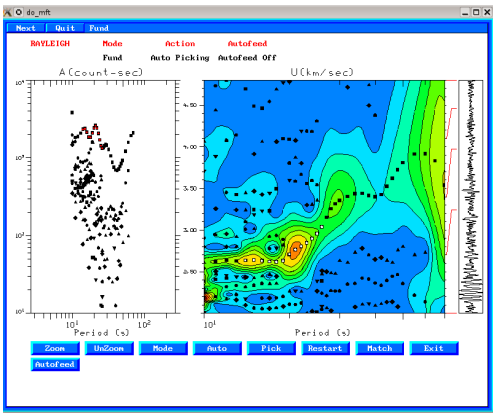

Figure A.24: Aftershock 2

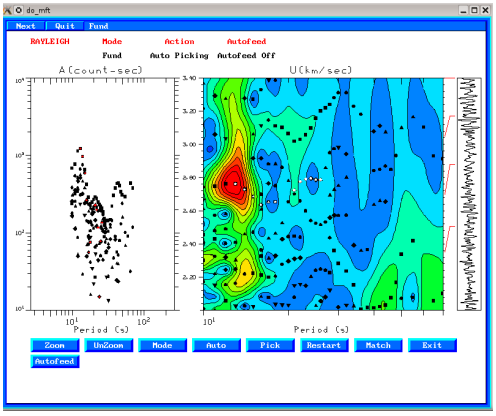

Figure A.25: Aftershock 3

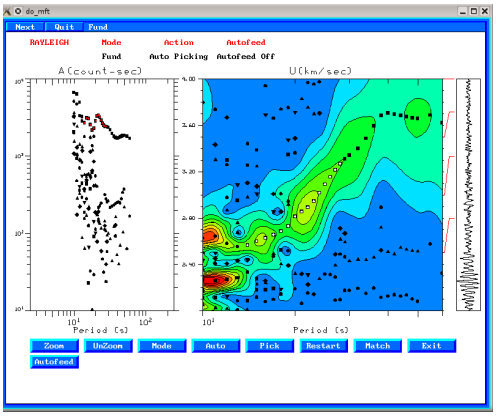

Figure A.26: Aftershock 4

A.6 ITAB Station

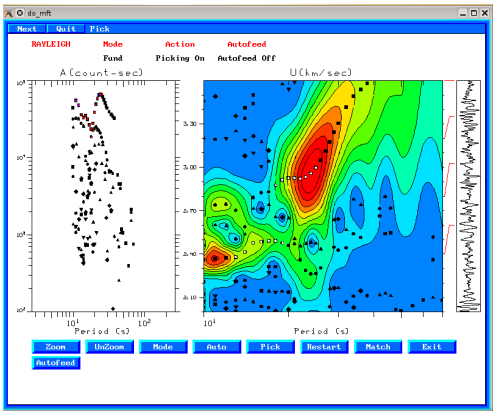

Figure A.27: Mainshock

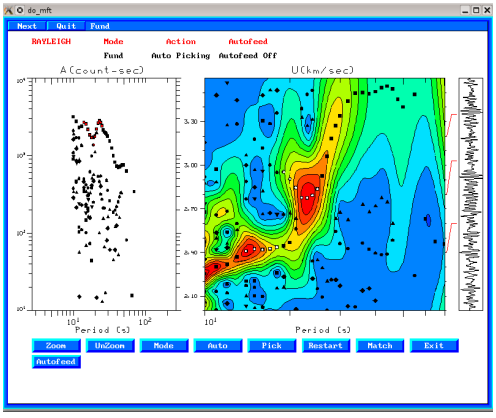

Figure A.28: Aftershock 2

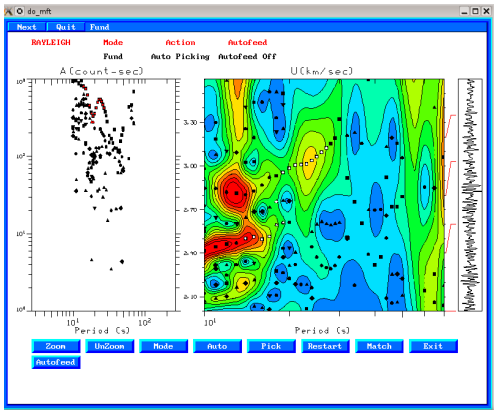

Figure A.29: Aftershock 3

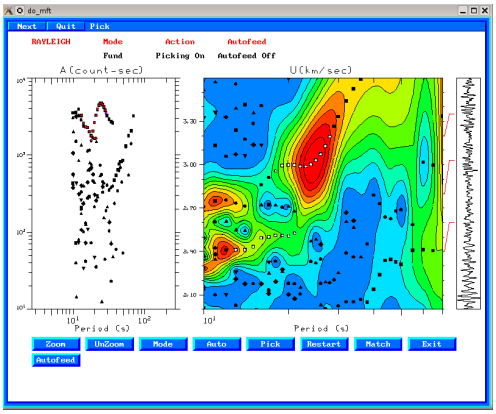

Figure A.30: Aftershock 4

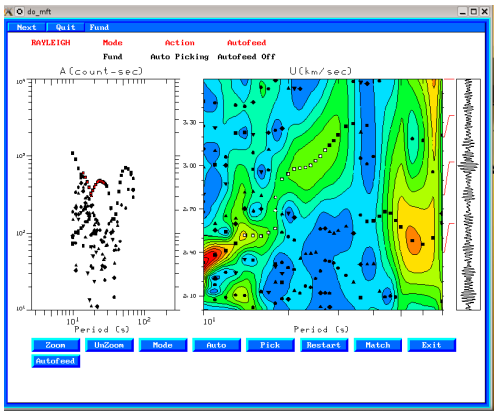

Figure A.31: Aftershock 5

A.7 PEXB Station

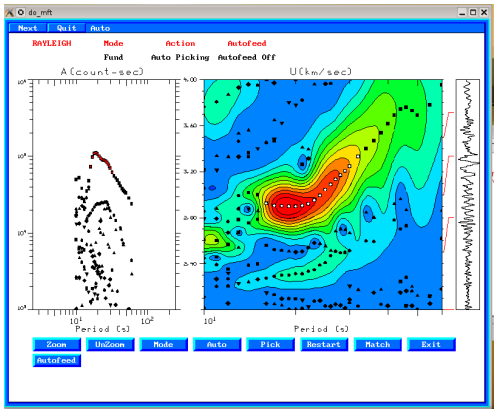

Figure A.32: Mainshock

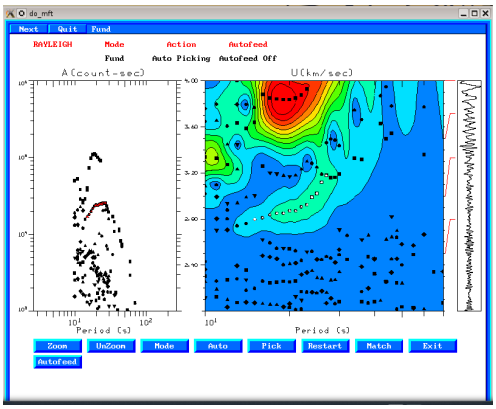

Figure A.33: Aftershock 1

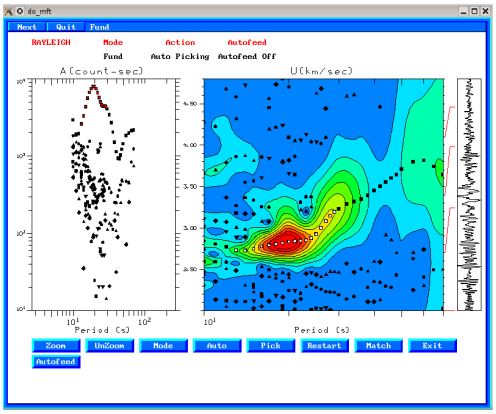

Figure A.34: Aftershock 2

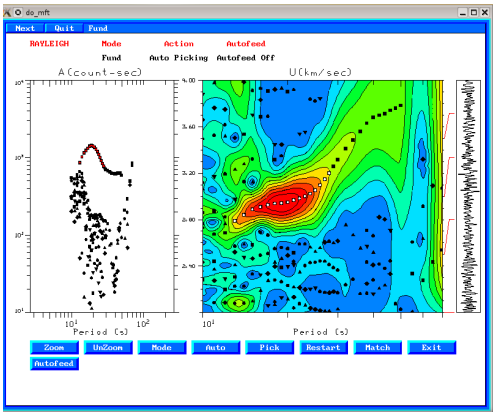

Figure A.35: Aftershock 3

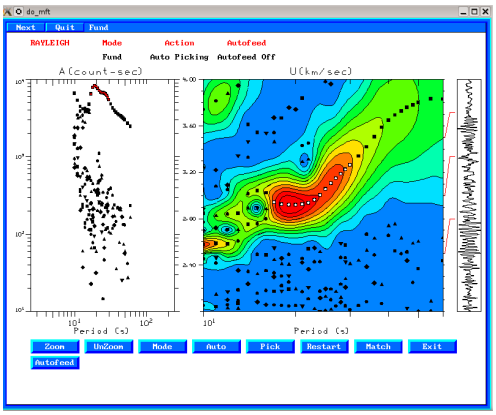

Figure A.36: Aftershock 4

A.8 PLTB Station

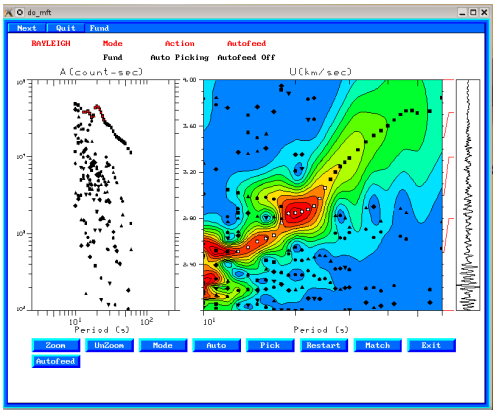

Figure A.37: Mainshock

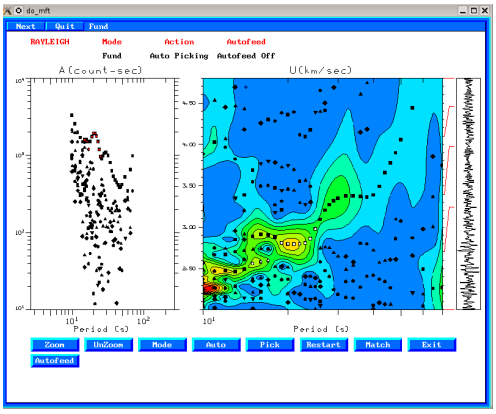

Figure A.38: Aftershock 2

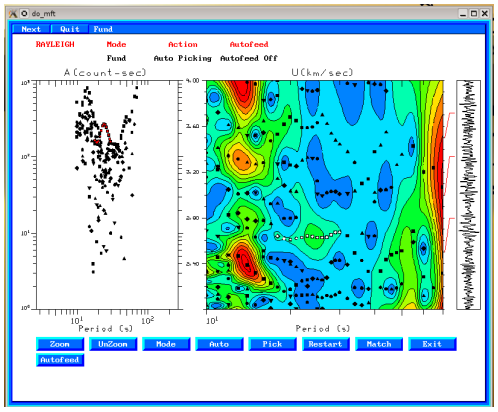

Figure A.39: Aftershock 3

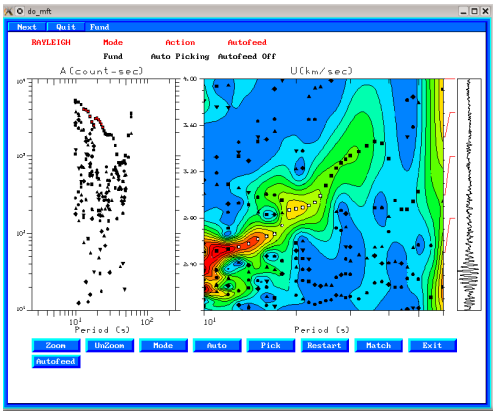

Figure A.40: Aftershock 4

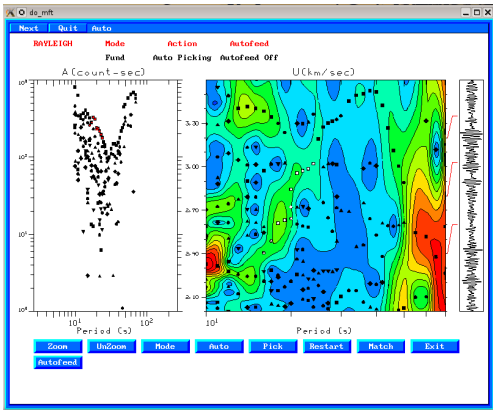

Figure A.41: Aftershock 5

A.9 ARAG Station

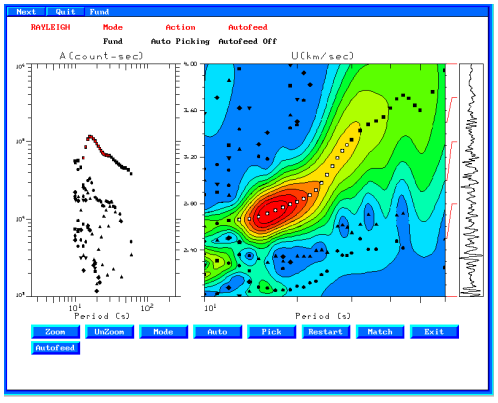

Figure A.42: Mainshock

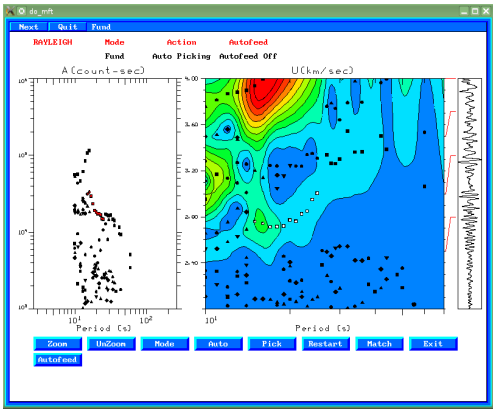

Figure A.43: Aftershock 1

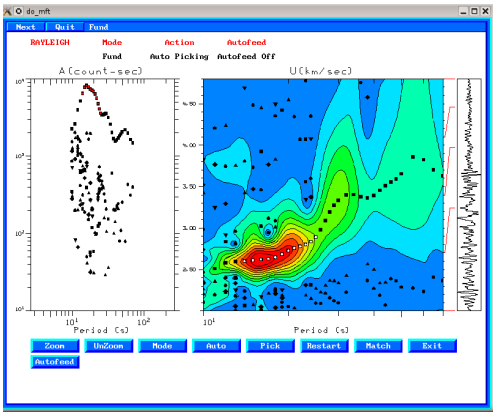

Figure A.44: Aftershock 2

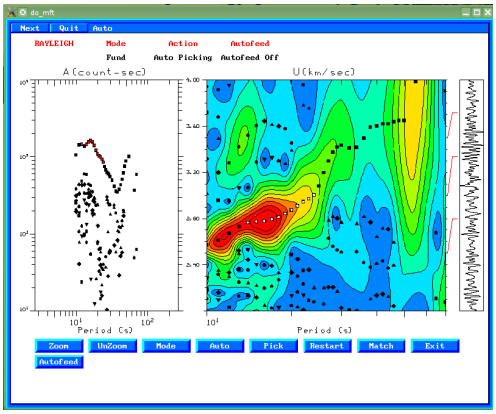

Figure A.45: Aftershock 3

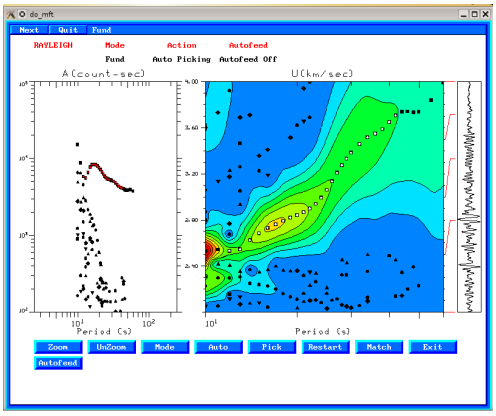

Figure A.46: Aftershock 4

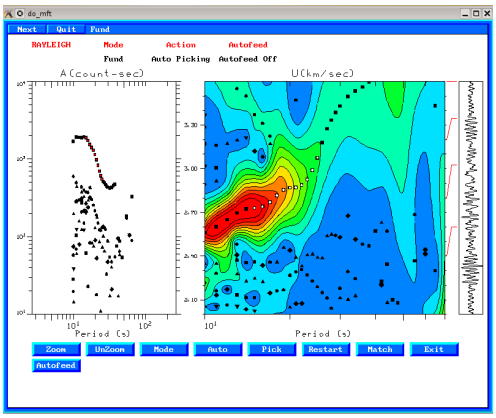

Figure A.47: Aftershock 5

A.10 PEL Station

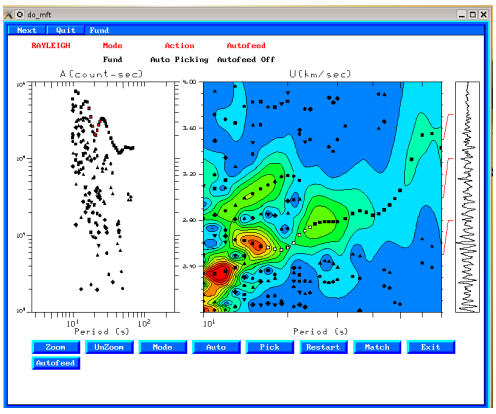

Figure A.48: Mainshock

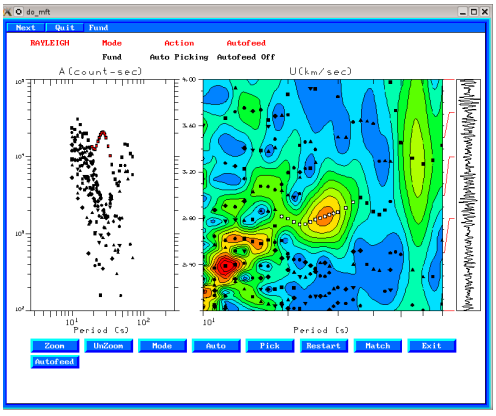

Figure A.49: Aftershock 2

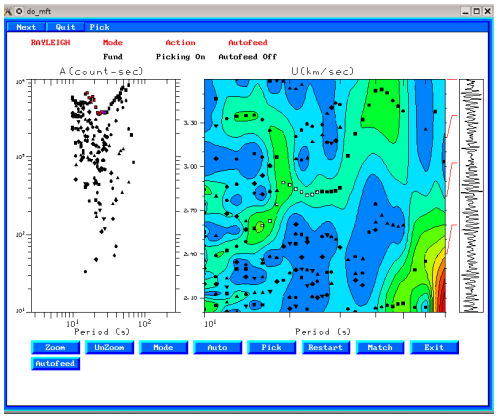

Figure A.50: Aftershock 3

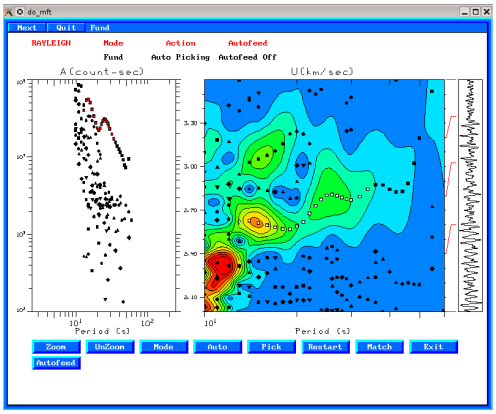

Figure A.51: Aftershock 4

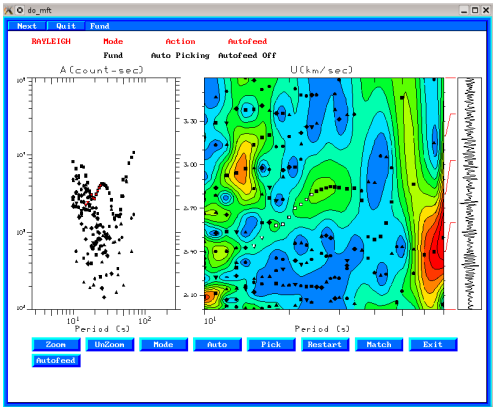

Figure A.52: Aftershock 5

A.11 SPB Station

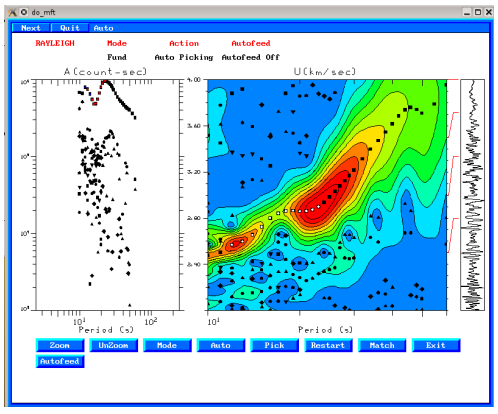

Figure A.53: Mainshock

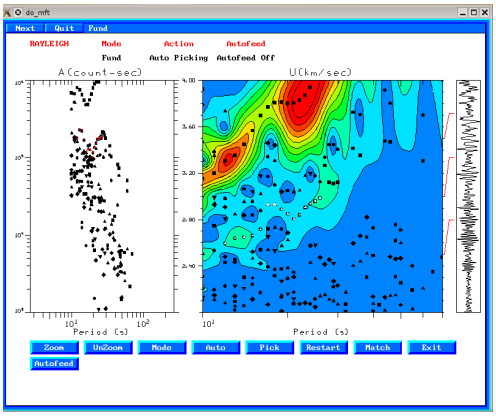

Figure A.54: Aftershock 1

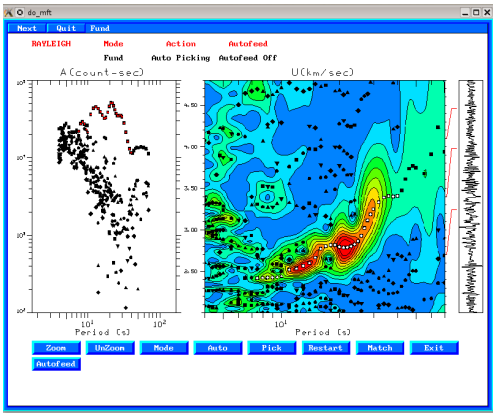

Figure A.55: Aftershock 2

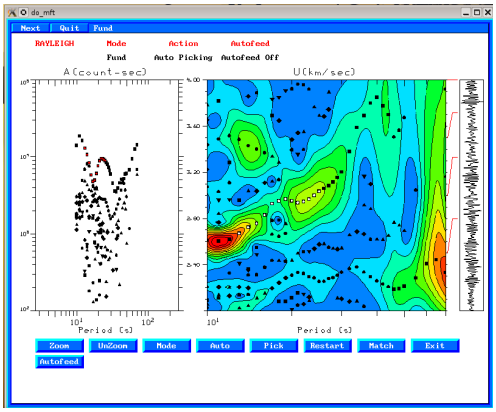

Figure A.56: Aftershock 3

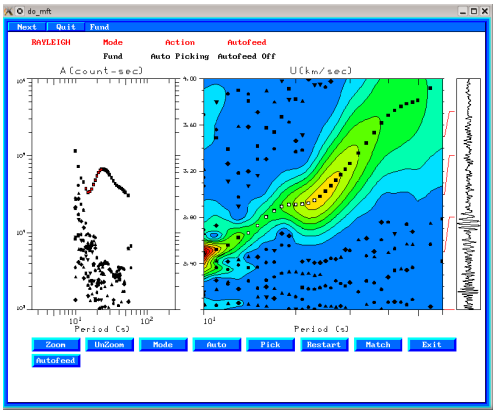

Figure A.57: Aftershock 4

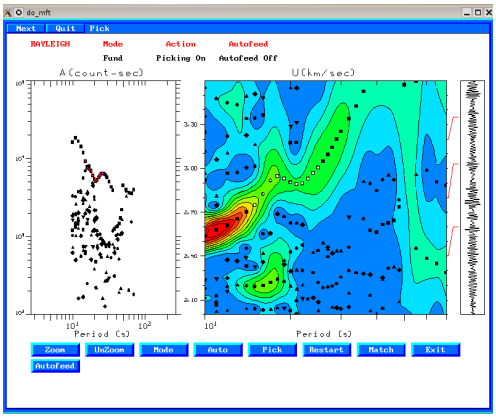

Figure A.58: Aftershock 5

A.12 CPUP Station

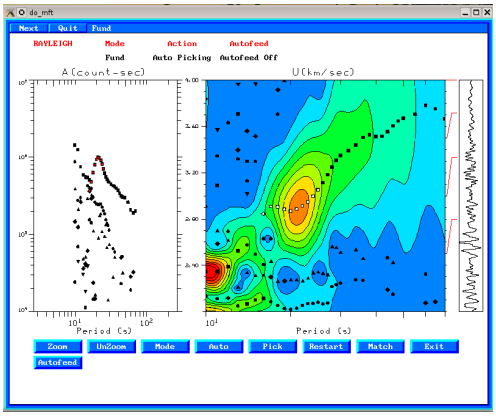

Figure A.59: Mainshock

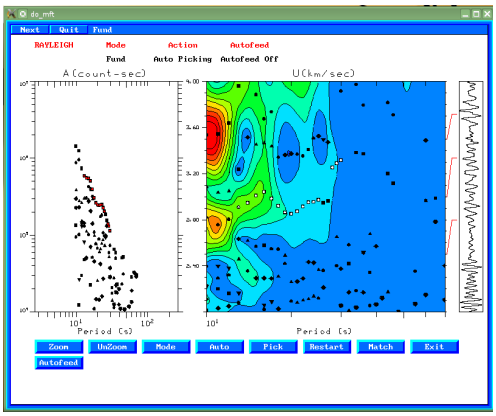

Figure A.60: Aftershock 1

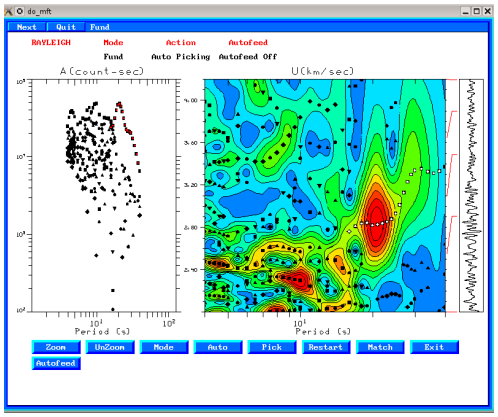

Figure A.61: Aftershock 2

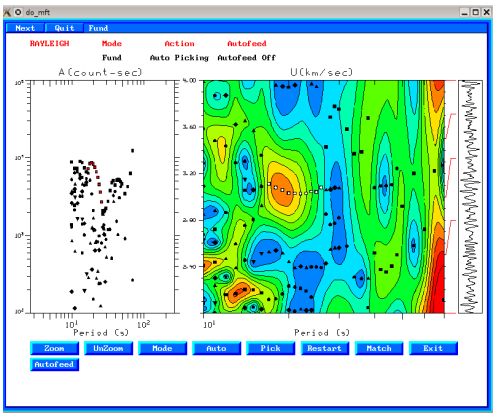

Figure A.62: Aftershock 3

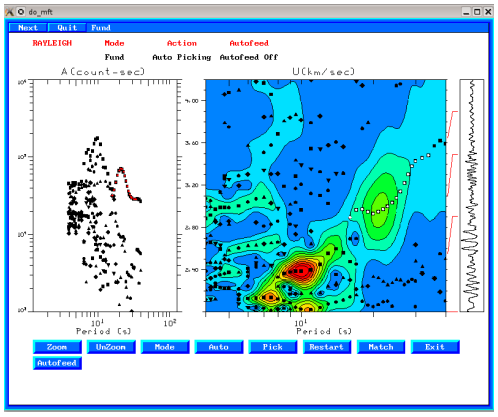

Figure A.63: Aftershock 4

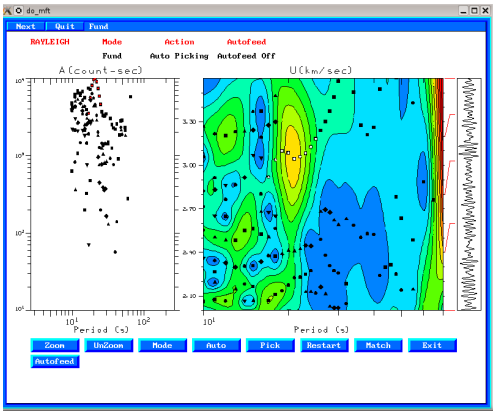

Figure A.64: Aftershock 5

A.13 LPAZ Station

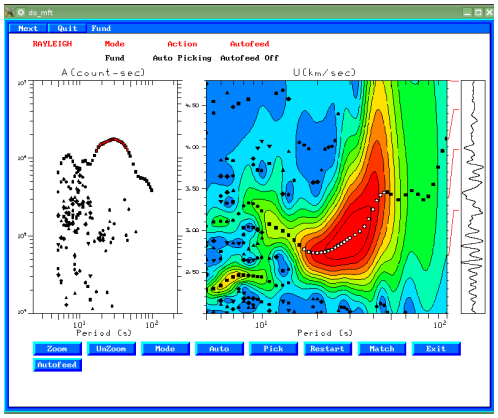

Figure A.65: Mainshock

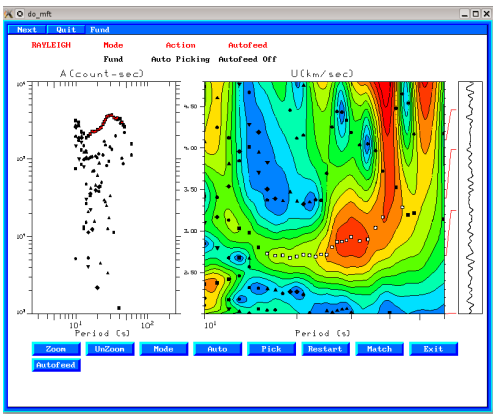

Figure A.66: Aftershock 1

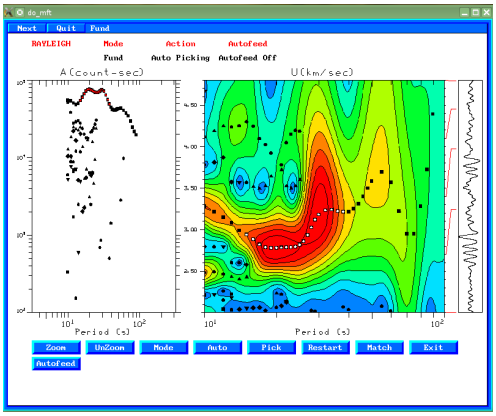

Figure A.67: Aftershock 2

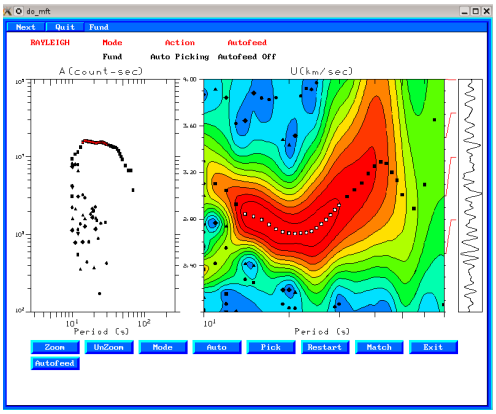

Figure A.68: Aftershock 3

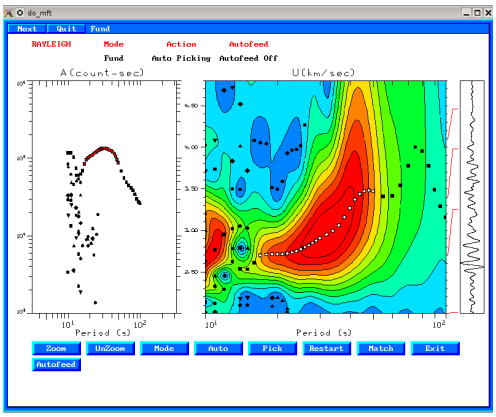

Figure A.69: Aftershock 4

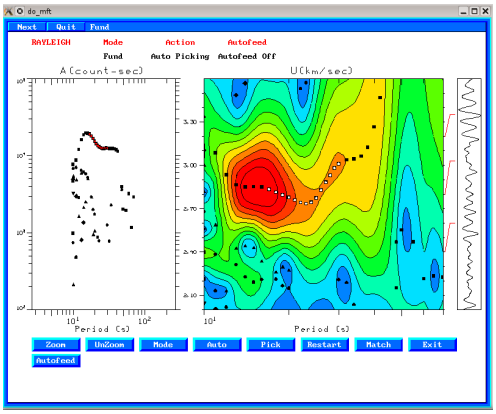

Figure A.70: Aftershock 5

A.14 PLCA Station

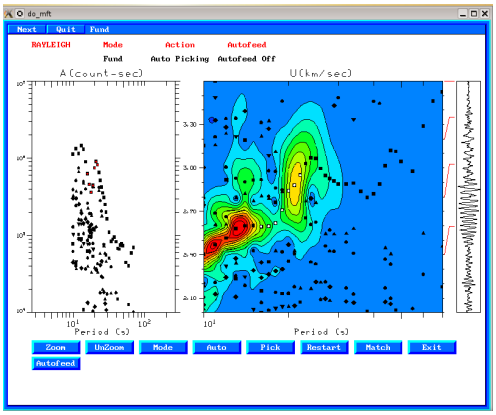

Figure A.71: Mainshock

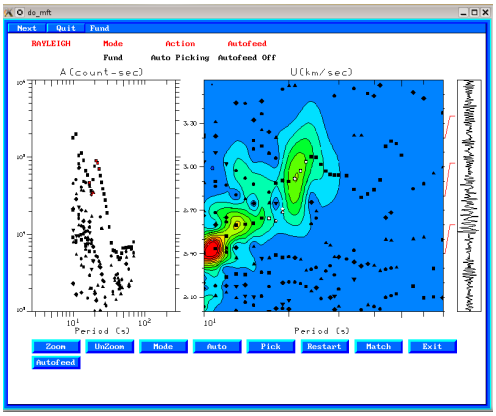

Figure A.72: Aftershock 1

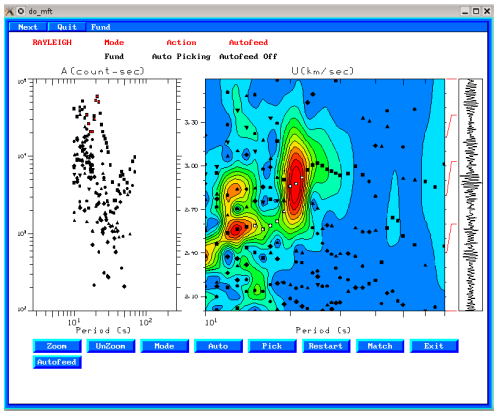

Figure A.73: Aftershock 2

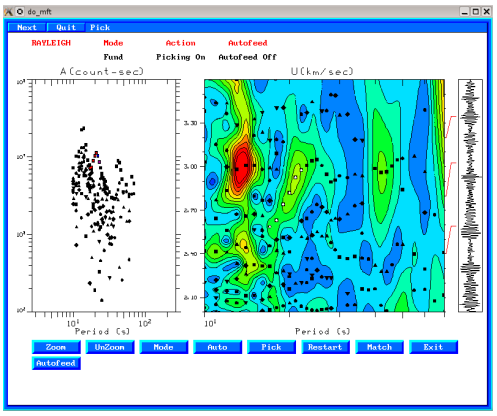

Figure A.74: Aftershock 3

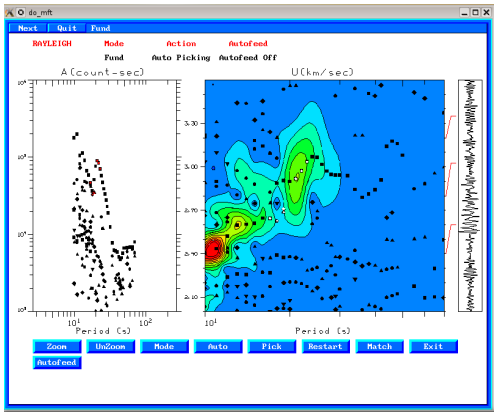

Figure A.75: Aftershock 4

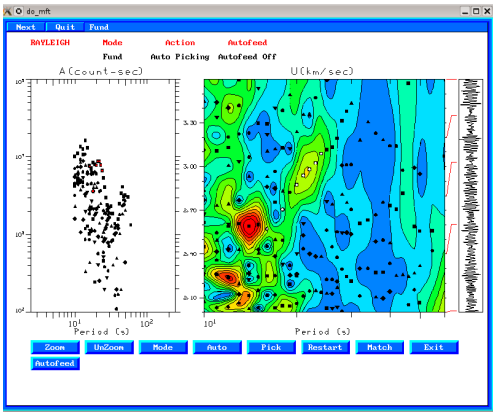

Figure A.76: Aftershock 5

A.15 NNA Station

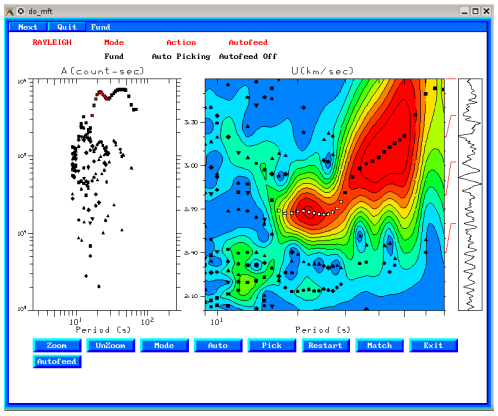

Figure A.77: Mainshock

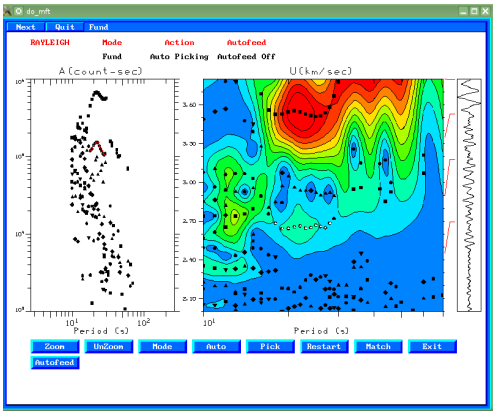

Figure A.78: Aftershock 1

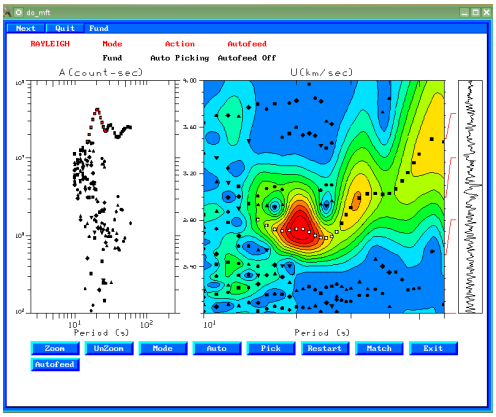

Figure A.79: Aftershock 2

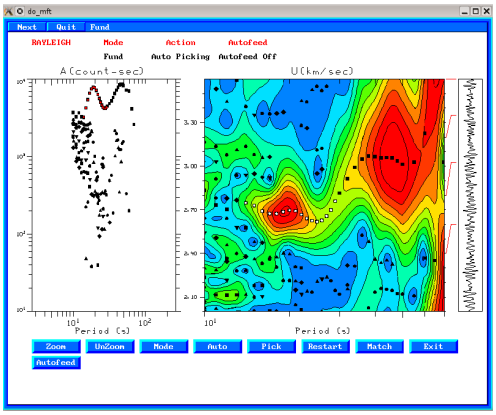

Figure A.80: Aftershock 3

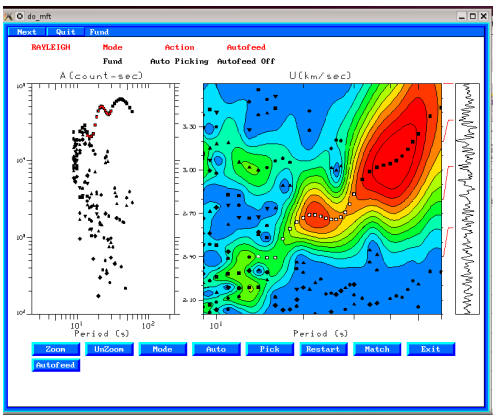

Figure A.81: Aftershock 4

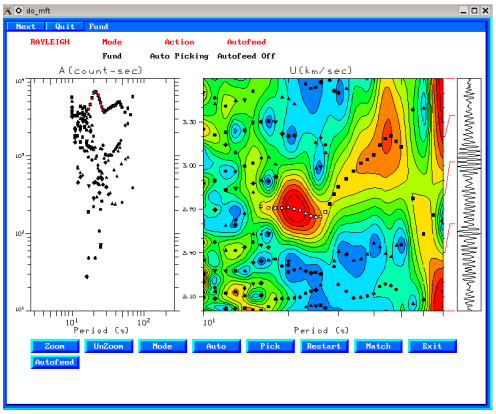

Figure A.82: Aftershock 5

A.16 LVC Station

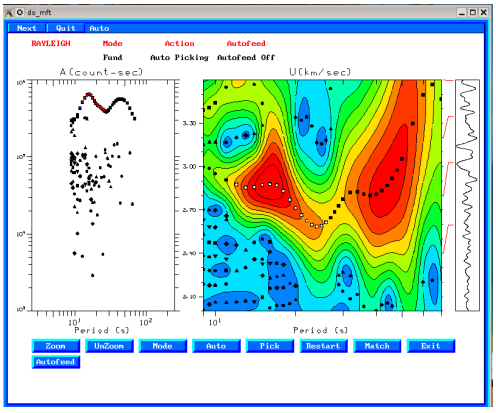

Figure A.83: Mainshock

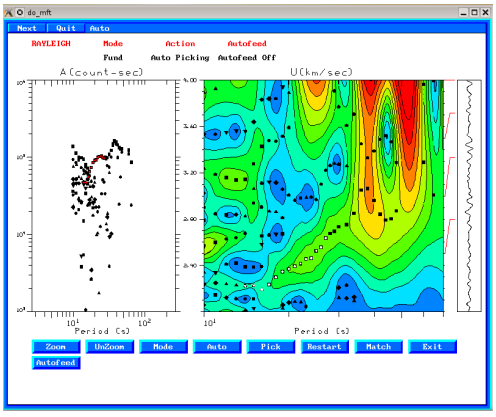

Figure A.84: Aftershock 1

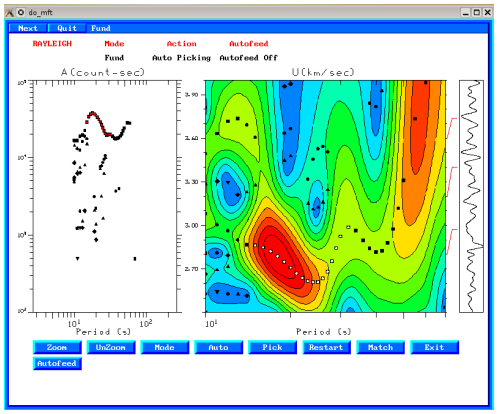

Figure A.85: Aftershock 2

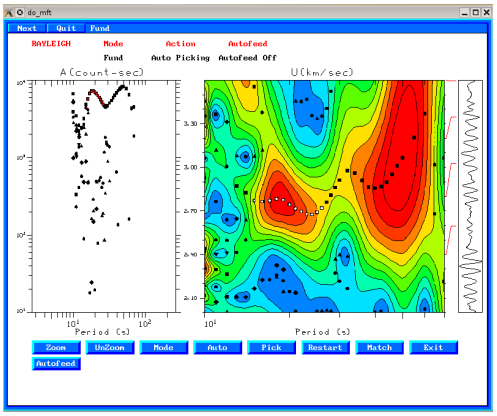

Figure A.86: Aftershock 3

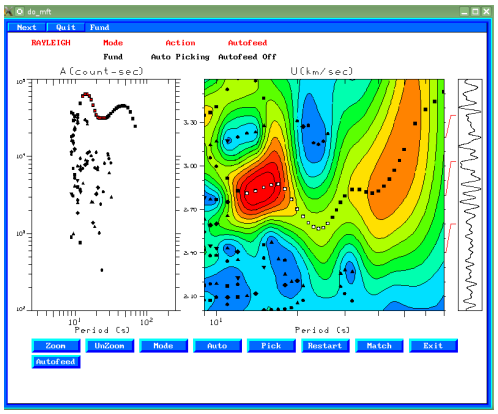

Figure A.87: Aftershock 4

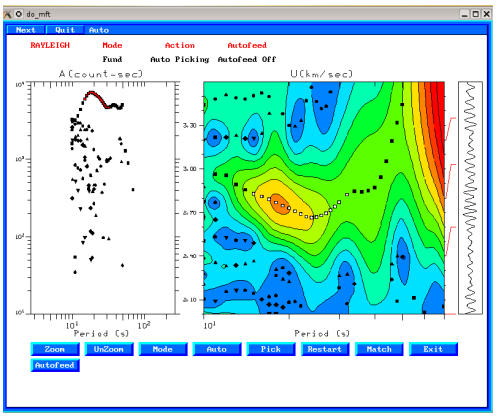

Figure A.88: Aftershock 5

A.17 OTAV Station

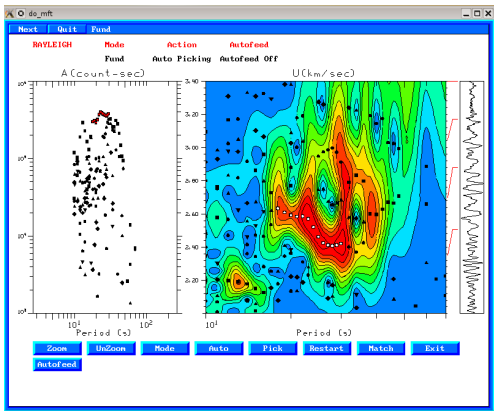

Figure A.89: Mainshock

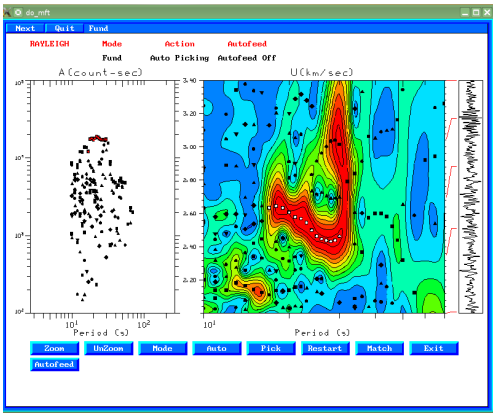

Figure A.90: Aftershock 2

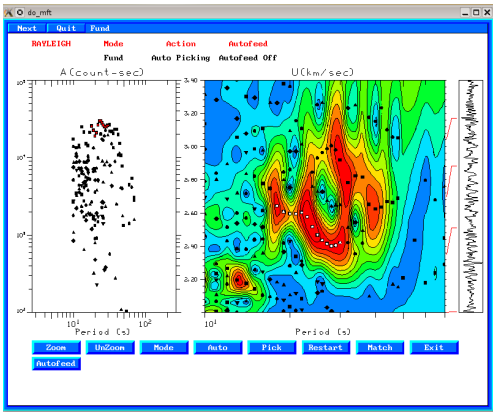

Figure A.91: Aftershock 4

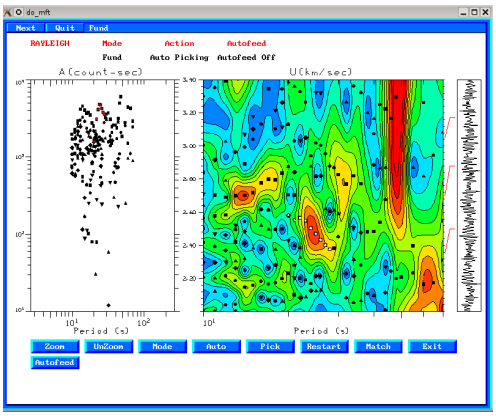

Figure A.92: Aftershock 5

A.18 PAYG Station

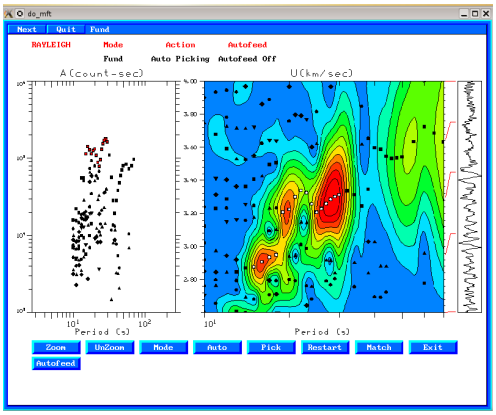

Figure A.93: Mainshock

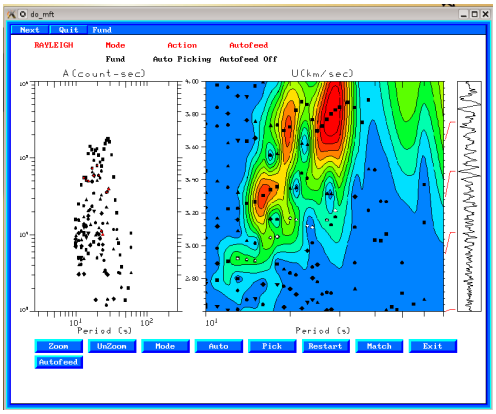

Figure A.94: Aftershock 1

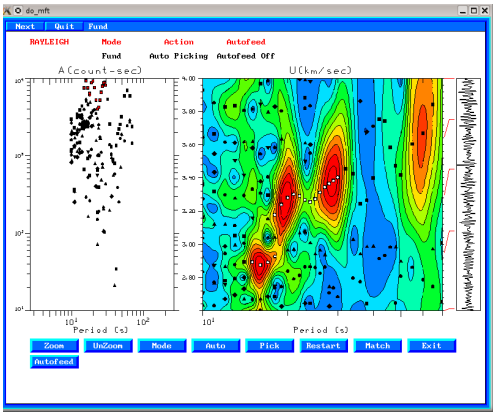

Figure A.95: Aftershock 2

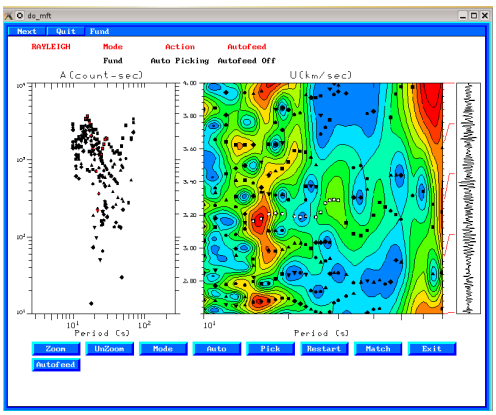

Figure A.96: Aftershock 3

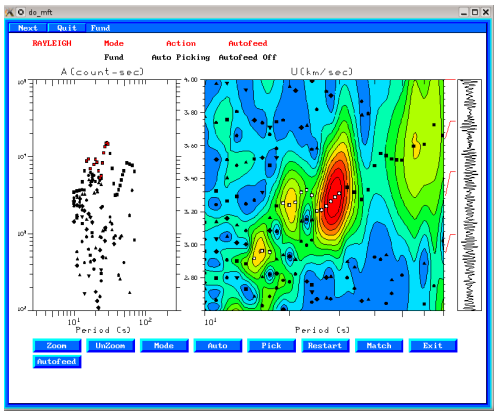

Figure A.97: Aftershock 4

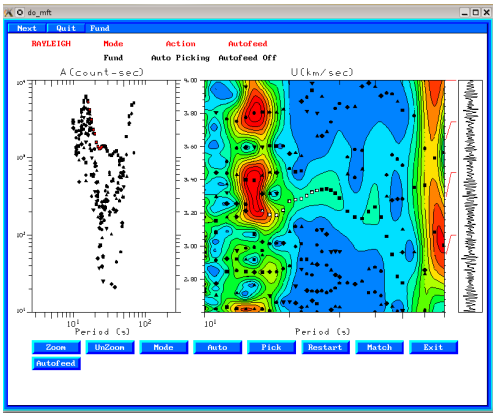

Figure A.98: Aftershock 5

A.19 SAML Station

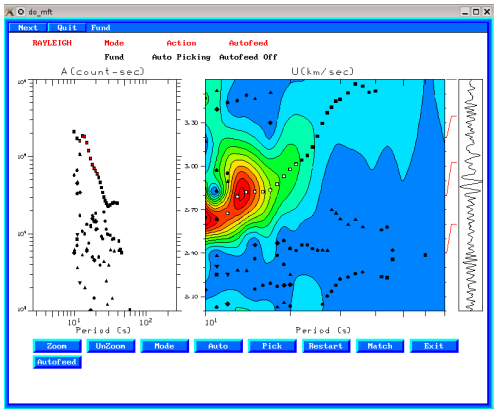

Figure A.99: Mainshock

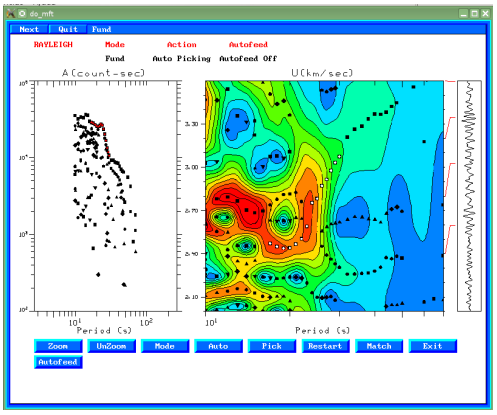

Figure A.100: Aftershock 1

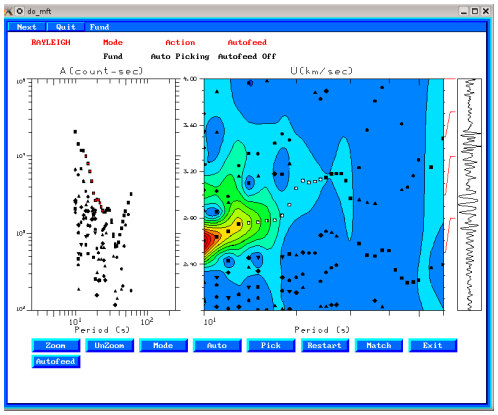

Figure A.101: Aftershock 2

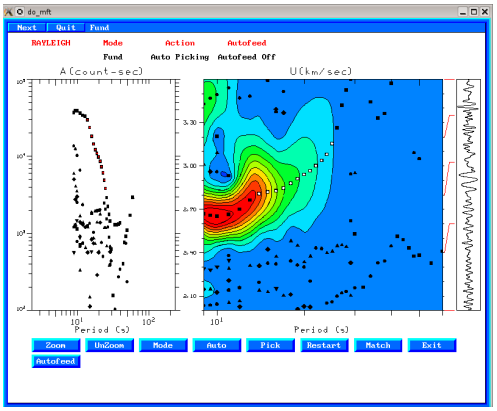

Figure A.102: Aftershock 4